Influence of the extracellular matrix on cellular behaviour – Development and application of a bioengineered 3D cell culture system for cancer research and high resolution microscopy

TECHNISCHE UNIVERSITÄT DARMSTADT

Vom Fachbereich Biologie der Technischen Universität Darmstadt

zur Erlangung des akademischen Grades

eines Doctor rerum naturalium

genehmigte Dissertation von

Dipl.-Biol. Elke Kämmerer

aus Offenbach

1. Referent: PD Dr. Tobias Meckel

2. Referent: Prof. Dr. Gerhard Thiel

Tag der Einreichung: 03.07.2014

Tag der mündlichen Prüfung: 05.09.2014

Darmstadt 2014

D17

Our greatest weakness lies in giving up. The most certain way to succeed is always to try just one more time.

Thomas A. Edision 1847- 1931

Ehrenwörtliche Erklärung

Ich erkläre hiermit ehrenwörtlich, dass ich die vorliegende Arbeit entsprechend den Regeln guter wissenschaftlicher Praxis selbstständig und ohne unzulässige Hilfe Dritter angefertigt habe.
Sämtliche aus fremden Quellen direkt oder indirekt übernommenen Gedanken sowie sämtliche von Anderen direkt oder indirekt übernommenen Daten, Techniken und Materialien sind als solche kenntlich gemacht. Die Arbeit wurde bisher bei keiner anderen Hochschule zu Prüfungszwecken eingereicht.

Darmstadt, den 03. Juli 2014

Dipl. –Biol. Elke Kämmerer

Statement of own work

I have undertaken all experiments, data analysis and writing of the present thesis with exception of the following:

- Images shown in Fig. 36 were provided by PD Dr. Tobias Meckel (Technische Universität Darmstadt, Darmstadt, Germany).

- I have prepared the samples and performed the data acquisition of single molecule detection images shown in Fig. 37. Data were analysed by Dipl.-Phys. Florian Lauer (Technische Universität Darmstadt, Darmstadt, Germany).

- Chapter 2.1, 3.1 and 4.1 (without stated exceptions) are part of the peer-reviewed publication:
  Kaemmerer, Elke; Melchels, Ferry P.W.; Holzapfel, Boris M.; Meckel, Tobias; Hutmacher, Dietmar W. and Loessner, Daniela. (2008) "Gelatine methacrylamide-based hydrogels: An alternative three-dimensional cancer cell culture system." *Acta Biomaterialia* 10(6):2551-2562, 2014.
  I have been highly engaged in the study design of the *in vitro* and *in vivo* experiments, performed all *in vitro* experiments and analyses, prepared all figures of the *in vitro* studies and wrote the complete manuscript. The animal studies were performed by a medical surgeon, Dr. Boris M. Holzapfel and data of the animal studies were analysed by Dr. Daniela Loessner (both: Institute of Health and Biomedical Innovation, Queensland University of Technology, Brisbane, Australia).

Table of Contents

Figures

Supplementary Figures

Tables

Equations

$$\mathrm{E} = 7955 * \mathrm{C}^{2.28}\left(1 - \mathrm{e}^{\left(\frac{4.2-\mathrm{t}}{11.5}\right)}\right) \quad (1)$$

$$D = \frac{kT}{6\pi\eta r_H} \quad (2)$$

$$r_H = 0.015\, M_W^{0.53\ \pm 0.02} \quad (3)$$

List of Abbreviations

2D	Two dimensional
2.5D	On top cell culture onto a soft or coated substrate
3D	Three dimensional
Aminosilane	3-aminopropyltrimethoxysilane
BM	Basement membrane
BSA	Bovine serum albumine
bp	Base pair(s)
CaCO buffer	Cacodylate buffer
cDNA	Complementary DNA
CFM	Confocal fluorescence microscopy
CLSM	Confocal laser scanning microscopy
CRM	Confocal reflection microscopy
C_T	Threshold cycle
CT	Connective tissue
DAPI	4',6-diamidino-2-phenylindole
DMEM	Dulbecco's modified eagle media
DMSO	Dimethyl sulfoxide
dNTP	Deoxynucleotide triphosphate
DTT	Dithiothreitol
E133	Erioglaucine disodium salt
ECM	Extracellular matrix
Em	Emission
EDTA	Ethylenediaminetetraacetic acid
Ex	Excitation
FA	Focal adhesion
F-actin	Filamentous actin
FCS	Foetal calf serum
FD70	Fluoresceinisothiocyanate labelled dextran, 70 kDA
FITC	Fluoresceinisothiocyanate
FRAP	Fluorescence recovery after photobleaching
FS buffer	First strand buffer
G418	Geneticin

GelMA	Gelatine-methacrylamide
GFP	Green fluorescent protein
h	Hour
HA	Hyaluronic acid
HEPES	4-(2-hydroxyethyl)-1-piperazineethanesulfonic acid
hex	Hexamer
HILO	Highly inclined laminated optical sheet
h_r	Hydrodynamic radius
HyD	Hybrid detection system
Hyg	Hygromycin
LN	Laminin
Min	Minute
MMP	Matrix metalloproteinase
NA	Numerical aperture
PAGE	Polyacrylamide gel electrophoresis
PBS	Phosphate buffered saline
PCR	Polymerase chain reaction
PEG	Polyethylene glycol
pen/strep	Penicillin/Streptomycin
PFA	Paraformaldehyde
PMT	Photomultiplier tube
PSF	Point spread function
qRT-PCR	quantitative real time PCR
rFRAP	Rectangular FRAP
RIPA buffer	Radio-immunoprecipitation assay buffer
ROI	Region of interest
rpm	Rounds per minute
RPMI media	Roswell park memorial institute media
RT	Room temperature (20-25 °C)
SDS	Sodium dodecyl sulfate
sec	Second
SEM	Scanning electron microscope
SHG	Second harmonic generation
SMD	Single molecule detection

TIRF	Total internal reflection fluorescence
TRIS	2-Amino-2-(hydroxymethyl)-propan-1,3-diol
TBST buffer	TRIS Tween 20 buffer
U	enzyme unit
UV	Ultraviolet

Amino Acids

A	Ala	Alanine
C	Cys	Cysteine
D	Asp	Aspartic acid
E	Glu	Glutamic acid
F	Phe	Phenylalanine
G	Gly	Glycine
H	His	Histidine
I	Ile	Isoleucine
K	Lys	Lysine
L	Leu	Leucine
M	Met	Methionine
N	Asn	Asparagine
P	Pro	Proline
Q	Gln	Glutamine
R	Arg	Arginine
S	Ser	Serine
T	Thr	Threonine
V	Val	Valine
W	Trp	Tryptophan
Y	Tyr	Tyrosine
	Hyp	Hydroxyproline
X	Xaa	Unspecified or unknown amino acid
	Yaa	Unspecified or unknown amino acid

1 Introduction

1.1 General introduction – The influence of the extracellular matrix on cellular behaviour

Experimental *ex vivo* model systems based on mammalian cells, derived from animal or human donors, are widely used, for general cell biology driven research or clinically relevant studies e.g. in context of drug screenings. Until recently, these model systems, have been utilised mostly by growing cells on two dimensional (2D) surfaces, like tissue culture plastic ware and glass coverslips (Hutmacher 2010). While these culture methods are well established and less complex, they are unable to mimic the physical and chemical characteristics normally present in the natural cellular microenvironment (Gieni and Hendzel 2008; Loessner *et al*. 2010; Yamada and Cukierman 2007). *"The cellular microenvironment is dynamic ..., cells physically transmit the information about their own internal tension in three dimensions ..."*(Gieni and Hendzel 2008).

These properties are not pre-existing in 2D cell cultures, therefore physiologically relevant, three dimensional (3D) cell culture systems have to be applied. In a living organism, cells are surrounded by a substance, namely the extracellular matrix (ECM). The ECM is more than just a mechanically backbone that provides supportive anchorage for a cell (Even-Ram and Yamada 2005; Frantz *et al*. 2010; Hynes 2009; Pizzo *et al*. 2005). Biochemical and mechanical interaction with the microenvironment is an important regulator for a variety of cellular processes, including migration, proliferation and differentiation (Janmey and Miller 2011; Loessner *et al*. 2010; Nguyen-Ngoc *et al*. 2012). Not surprisingly, cellular interaction and exchange with the local microenvironment is also highly engaged in development and progression of various diseases like cancer (Janmey and Miller 2011; Park *et al*. 2000; Wirtz, *et al*. 2011). Cells embedded in a 3D cell culture system, are much closer to cells in a living organism, in having cell-cell contacts and being embedded in a component that mimics the naturally occurring physical and chemical properties of the ECM. The usage of 3D cell culture systems, thereby can bridge the gap between *in vivo* studies and traditionally used 2D cell culture methods, as recognised in studies about the chemo- and radiosensitivity of different cell types (Eke and Cordes 2011; Loessner *et al*. 2010; Pickl and Ries 2009). Particular in cancer research, there is a need for more physiologically relevant 3D cell culture model systems, which allow analyses of matrix-dependent effects on cellular behaviour. To mimic the key characteristics of the natural occurring physiological and patho-physiological ECM for investigations on tumour development, growth, metastasis and reaction to anti-cancer

treatment in a reductionistic experimental model is an ongoing challenge (Griffith and Swartz 2006). Recently promising approaches from the field of tissue engineering, have emerged, thus offering a new toolbox to establish biomaterials for *ex vivo* and *in vivo* models with tailorable physical and chemical key characteristics (Hutmacher *et al*. 2010; Yamada and Cukierman 2007; Zaman 2013)

Of great interest is the communication of a cell with its surrounding neighbourhood which is mediated by plasma membrane located signalling, dynamics of its proteins and lipids, and highly regulated by the ECM (Petroll *et al*. 2003, Kim *et al*. 2011; Kusumi *et al*. 2012; Shibata *et al*. 2012). The cell-ECM contact is mediated via plasma membrane receptors, like integrins. At the extracellular side, integrins bind specifically to ligands presented by the ECM. At the intracellular site, integrins assemble together with other membrane associated and intracellular proteins and form clusters, which are known as focal complexes and focal adhesions (FA) (Geiger *et al*. 2009; Geiger and Yamada 2011). These protein clusters in the plasma membrane are not static, they undergo rapid changes of protein composition upon leaving and entering proteins in the FA zone and a fast remodelling of the whole FA itself (Shibata *et al*. 2012; Tabarin *et al*. 2014; Zamir and Geiger 2001). To study these spatio-temporal plasma membrane dynamics in a living cell, high resolution microscopy has to be applied (Tabarin *et al*. 2014). So far, these studies have been performed mostly on cells cultured on less complex, 2D surfaces (Shibata *et al*. 2012; Tabarin *et al*. 2014). However to analyse membrane dynamics under near native conditions, quantitative assessment also needs to be performed under 3D culture conditions. To perform such complex measurements, microscopy techniques and 3D cell cultures have to be adapted to each other.

1.2 The extracellular matrix – composition and properties

Cells in multi-cellular eukaryotic organisms are surrounded by neighbouring cells and the ECM, a tissue specific substance, secreted from specialised cells (Fig. 1). The ECM is more than a filling substance or an adhesive scaffold, but rather a complex and dynamic structure, consisting of different mechanical and biological characteristics and highly involved in various cellular processes (Janmey and Miller 2011; Park *et al*. 2000; Wirtz *et al*. 2011) (Fig. 1A). Cellular communication within this microenvironment is mediated through the physical and chemical ECM properties, e.g. stiffness, porosity, release of growth factors, via specific interactions directly with the ECM macromolecules (Fig. 1B) or to ECM-presented growth factors (Gattazzo *et al*. 2014). The ECM is a very dynamic structure which is constantly remodelled (Frantz *et al*. 2010; Janmey and Miller 2011; Lu *et al*. 2012). Hence, the ECM is

an integral part in development of functional biological tissue and changes can deeply affect tissue properties (Frantz *et al*. 2010). This view is strengthened by the fact, that one of the characteristic events occurring during cancer development is a loss of tissue organisation and non-natural cellular behaviour, thus resulting in a disorganised much stiffer local tumour microenvironment (Frantz *et al*. 2010). In addition to reorganisation of the local microenvironment, cancer cells secrete soluble factors, which induce morphology changes and differentiation of cells and ultimately lead to a change of the mechanical properties (Chandler *et al*. 2012). The macromolecular organisation found in normal, healthy tissue can be classified into two major forms of ECM architecture (Fig. 2). On the one hand, a compact, less porous, flat cell sheet-like structure is found, which supports and anchors epithelial and endothelial cells, the basement membrane (BM) (Schwarzbauer 1999) (Fig. 2). This thin sheet, with an average thickness of around 50 nm, mostly consists of collagen type-IV, laminins and fibronectin, and is specialised in maintaining tissue integrity and compartmentalisation (Leblond and Inoue 1989; Schwarzbauer 1999). On the other hand, there is a 3D fibrillar heterogeneous network organisation, mainly containing collagen type-I, proteoglycans and various glycoproteins and is found in the interstitial connective tissue (CT) (Wolf *et al*. 2009) (Fig. 2).

One of the main BM proteins is laminin (LN). Members of the LN family are heterotrimeric glycoproteins of high molecular mass (400-800 kDa) and contain three polypeptide chains (α, β, γ) (Domogatskaya *et al*. 2012) (Fig. 3). The LN family is further classified, based on their structure into cross- or T-shaped glycoproteins (Kostourou and Papalazarou 2014). LN is a ligand for cellular membrane receptors, like integrins. A prominent example for a specific laminin-integrin interaction is LN-411/integrin α6β1. This ligand-receptor interaction enhance cellular adhesion, angiogenesis and is essential for blood vessel stabilisation (Ahmed *et al*. 2005; Kostourou and Papalazarou 2014). LN shows a tissue-specific distribution and a development-specific expression pattern (Kostourou and Papalazarou 2014). The total LN level seems to be associated with cancer progression, for example ovarian cancer patients showed an increased level of LN in the tumour fluid (ascites) (Byers *et al*. 1995). Furthermore, LN promotes cellular proliferation and attachment of cancer cells, indicating the role of LN as a modulator in ovarian cancer progression (Ahmed *et al*. 2005).

The main component of the CT is collagen type-I (Fig. 2). It consists of a tight packed helical quaternary structure formed by three parallel α-polypeptide chains, with the repetitive amino acid motif GlyXaaYaa (Shoulders and Raines 2009) (Fig. 4A). The most common naturally occurring triplet in collagen is GlyProHyp (Shoulders and Raines 2009). Individual α-chains

are synthesised as pro-collagen, secreted into the ECM, cleaved into subunits of tropocollagen (around 300 nm in length and 1.5 nm in diameter), which self-assembles into fibrils, to form larger units of fibres and fibre bundles (Cicchi *et al*. 2013) (Fig. 4A-D). The final diameter of a fibre bundle can reach several micrometres (Cicchi *et al*. 2013) (Fig. 4D). This tight hierarchal structure of collagen mediates the tensile strength, the main characteristic of the connective tissue. Thereby, 3D architectural organisation of collagen can vary, depended on the function and type of collagen-rich tissue (Cicchi *et al*. 2013) (Fig. 4E-G).

In addition to fibrous proteins, proteoglycans, another class of macromolecules, are found in the ECM. Proteoglycans are consisting of glycosaminoglycan chains with a protein core, except for hyaluronic acid (HA). They function as buffer and hydration and provide additional binding components (Frantz *et al*. 2010). In general, glycosaminoglycans are very hydrophilic and important components for cell-ECM interactions and protein network stabilisation. An example of a glycosaminoglycan is hyaluronic acid (HA). HA is a linear glycosaminoglycan consisting of 2000-25,000 disaccharides of glucuronic acid and N-acetylglucosamine, and is the ligand of the CD44 receptor (Frantz *et al*. 2010; Toole 2002). HA influences proliferation and migration of various cancer cells, for example increased HA levels are linked to the ovarian tumour-associated stroma and poor prognosis of ovarian cancer patients (Gardner *et al*. 1996; Toole 2002, Anttila *et al*. 2000). The CD44 receptor is also known as major switch associated with tumour growth and metastasis (Gardner *et al*. 1996; Toole 2002; Negi *et al*. 2012). Adhesion of ovarian cancer cells on immobilised HA surfaces is enhanced and correlates with a high CD44 level, indicating a role of HA in peritoneal tumour spread (Toole 2002).

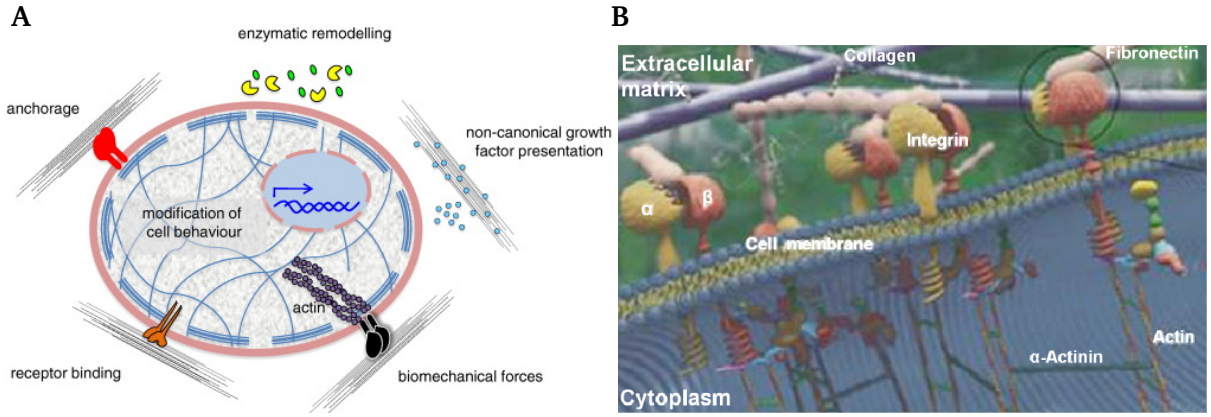

Figure 1: Overview of the cell-ECM crosstalk. Interaction with the local microenvironment and "sensing" of local microenvironmental changes directly influences cellular processes (A), adapted from (Gattazzo *et al*. 2014). A key role in this process play membrane receptors, like integrins, allowing attachment of a cell to the ECM, and mediate the connection between actin

cytoskeleton on the intracellular side to ECM ligands on the extracellular side (B), adapted from (Tirrell *et al*. 2002).

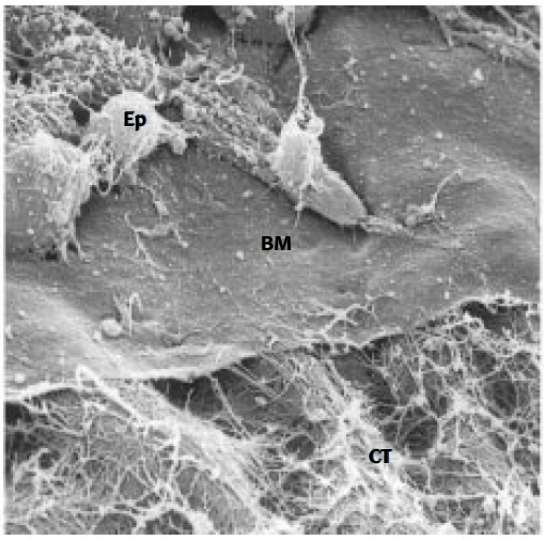

Figure 2: Architecture of corneal epithelium, an example of tissue organisation. The sheet-like structure of the BM allows cellular adhesions of epithelial cells (Ep) on top and separation of this layer from the underlying CT. In contrast to the flat BM structure, the CT is consisting of a fibrillar 3D protein network, mainly collagen type-I, adapted from (Schwarzbauer 1999).

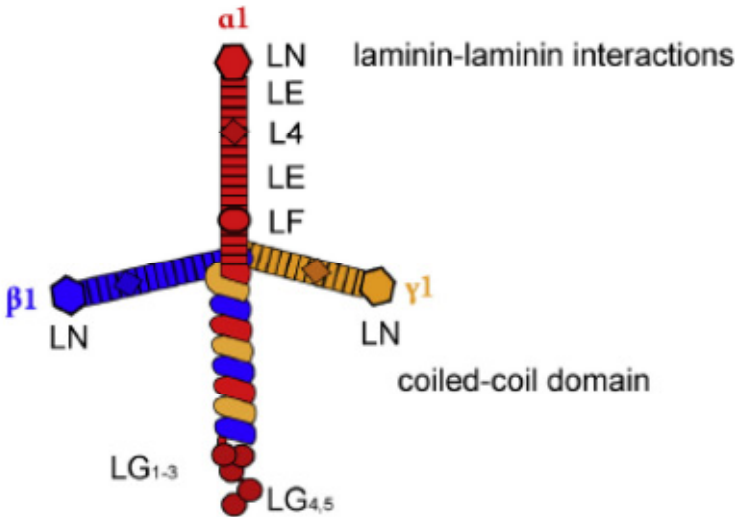

Figure 3: Structure of the LN trimer. LN consists of three polypeptide chains, α, β, γ, indicated in blue, red and yellow, and various globular, rod-like domains. This structure allows binding to ECM proteins, interaction with other LN proteins and incorporation into the BM, adapted from (Kostourou and Papalazarou 2014).

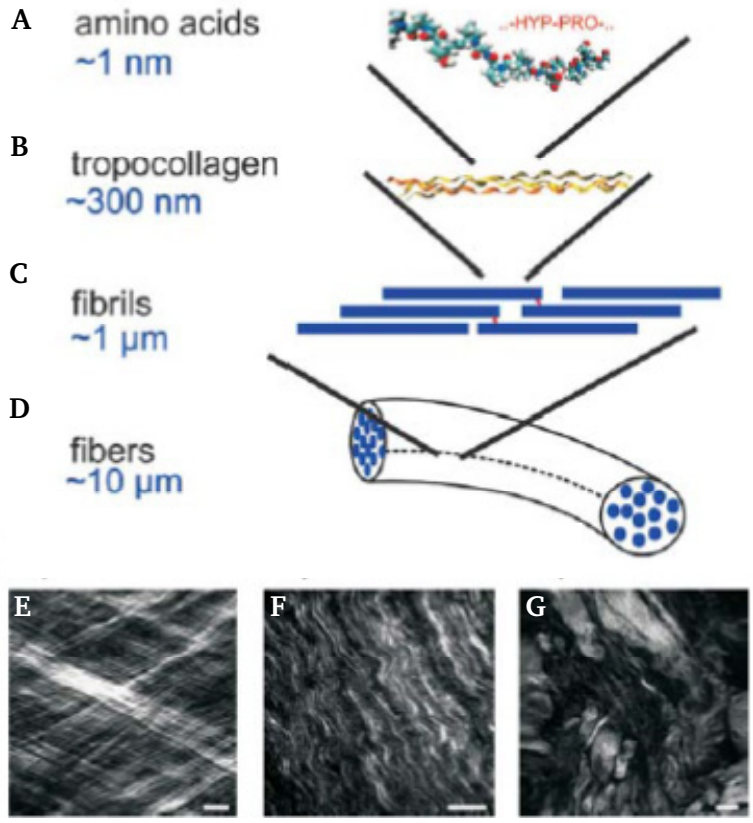

Figure 4: Collagen structure. On the molecular level, a collagen α-chain consists of a repeating amino acid sequence, mostly GlyProHyp (A). A tropocollagen helix is formed by assembling of 3 α-chains (B). Thicker fibrils are generated by assembly of tropocollagen helices (C) which can bundle together into large collagen fibres reaching a diameter of around 10 μm (D). Examples of collagen arrangement in various tissues, tendon (E), cornea (F) and skin (G), adapted from (Cicchi *et al*. 2013). Scale bars: 10 μm.

1.2.1 The extracellular matrix – degradation and remodelling

In a living organism, tissue characteristics, e.g. architecture, strength, and stiffness, are a product of the ECM composition; however, the ECM is not a static, massive structure. It undergoes a dynamic remodelling process during embryonic development, ageing, wound healing, and also in cancer progression and metastasis. The most important proteins causing this constant remodelling are cell-secreted metalloproteinases (MMPs) (Frantz *et al*. 2010; Lu *et al*. 2011). MMPs are zinc-dependent proteases and around 23 different members are expressed in humans (Kessenbrock *et al*. 2010). They are released as zymogens, with a propeptide signal sequence, which is removed during activation (Kessenbrock *et al*. 2010). Proteolytic activity of MMPs in healthy tissue is tightly regulated by tissue inhibitors of metalloproteinases, compartmentalisation and homoeostasis of zymogen and/or active enzyme concentration (Kessenbrock *et al*. 2010). Known substrates for MMPs are structural

ECM proteins, e.g., LN and collagen, which are cleaved by different MMPs, such as MMP2 and MMP9 with varied substrate specificity and efficiency (Knapinska and Fields 2012). MMPs are e.g. frequently expressed in ovarian cancer and contribute to disease progression; MMP-2, MMP-9, and MMP-14 are upregulated in advanced ovarian cancer, tumour fluid and abdominal metastasis and associated with shorter survival times of patients (Karam and Dorigo 2012; Kenny and Lengyel 2009; Kenny *et al*. 2008; Schmalfeldt *et al*. 2001).

1.3 3D cell culture systems

To capture the complex ECM architecture and the ECM-cell crosstalk within an *ex vivo* model, 3D cell culture systems become more and more important. A literature research in PubMed (Online database of biomedical citations from the US national Library of Medicine National Institutes of Health) showed that during the past five years the number of articles containing the key words “3D cell culture” has almost doubled. However, mimicking the natural ECM in an experimental system is an ongoing challenge and so far, there is no “one fits all” approach. The most commonly used 3D cell culture systems are based on multi-cellular spheroids or materials of animal origin, namely, collagen type-I and BM-extract (Pampaloni *et al*. 2007). One important aim in the field of tissue engineering is the generation of 3D models with reduced key ECM characteristics of the original tissue combined with reproducible matrix properties. This aim has led to the design of “new” synthetic and semi-synthetic biomaterials (Hutmacher *et al*. 2010). A 3D cell culture system applicable for cancer research has to include key features of tumour progression and metastasis pattern found in patients and allows its usage for experimental and animal studies. In the following paragraphs, an overview of currently used approaches to meet the terms of these diverse demands is given.
While many of these demands are constantly addressed, requirements of downstream analysis methods are often overlooked. High resolution microscopy is one of these analysis methods, which requires a 3D model system to fulfil an additional layer of properties, such as drift-free investigation, low scattering and axial extension, i.e. thickness. To archive this, 3D cell culture systems have to be optimised for high resolution microscopy methods. However, next to the sample, also microscopy techniques have to be adapted on these more complex samples.

1.3.1 Multi-cellular spheroids – unsupported 3D cell cultures

If cells are grown under conditions that decrease adhesion to a surface and thereby favour adhesion in between cells, multi-cellular spheroids are formed. Such conditions are maintained by growing cells (i) within a hanging drop of media using gravity (Fig. 5A), (ii) on non-adhesive surfaces or (iii) in a rotating bioreactor system using shear force to form

spontaneous multi-cellular spheroids (Fig. 5B). Using these culture conditions multi-cellular spheroids of several micrometres in diameter can be produced (Pampaloni *et al*. 2007; Timmins *et al*. 2004). However, 3D spheroid cultures are prepared without any external support and thus have their limitations. The foremost drawback of these 3D culture methods is that not all cell types form spheroids. If spheroids are formed, micro-tissues with a fairly large cell number and very dense cell distribution are obtained. This can influence e.g. the microscopy analysis of the cellular characteristics. From a bioengineering perspective, the major limitation of isolated multi-cellular spheroids is that they are created without physical contact to an extracellular structural support and grown without solid stress implemented by the ECM (Helmlinger *et al*. 1997). Hence, the properties of the ECM and cell-ECM interaction cannot be externally controlled or modified.

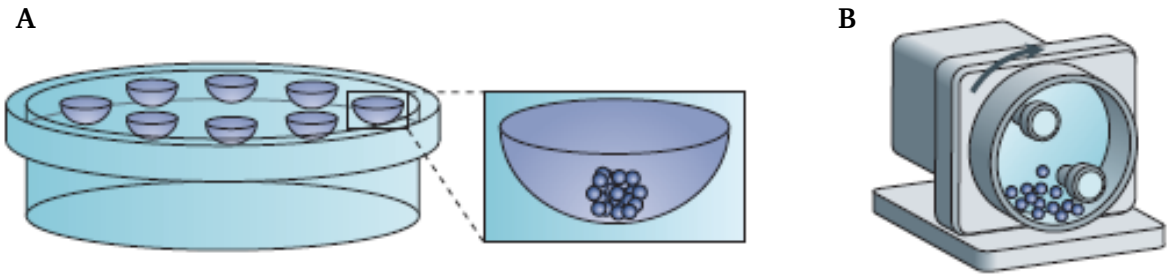

Figure 5: Spheroid preparation using the hanging drop method and within a rotating bioreactor. The principle of spheroid formation is for both methods the same; prohibition of cellular attachment on a surface, either within a drop of media using gravity (A), or by applying a constant shear force within a bioreactor system (B), adapted from (Pampaloni *et al*. 2007).

1.3.2 Matrix-supported 3D cell cultures

An alternative approach for 3D cell culture systems can be gained by introducing external support trough matrices and scaffolds. Based on the definitions used in bioengineering, a matrix is a hydrogel usually formed of a polymer network containing a very high amount of water (up to 99%); scaffolds, on the contrary, are based on cellular solids with larger pore size (Hutmacher *et al*. 2010). In the following chapters, naturally-derived and bioengineered matrices will be further discussed.

1.3.2.1 Naturally derived matrices

Natural-derived matrices are mostly hydrogels based on reconstituted BM-extract, collagen type-I or LN, all of which are of animal origin (Pampaloni *et al.* 2007). These systems have been successfully applied for cancer research and also for microscopy approaches (Booth *et al*. 2013; Fraley *et al*. 2010; Geraldo *et al*. 2012; Szot *et al*. 2011). Animal derived biomaterials

provide a physiological 3D surrounding; containing cellular binding and cleavage sites in their natural occurring distribution and stoichiometry.

Up to now, the gold standard for 3D cell culture systems is based on a reconstructed BM extracted from Engelbreth-Holm-Swarm mouse tumour cells and commercialised as Matrigel (Kleinman and Martin 2005). Matrigel consists of a complex composition including, mainly collagen type-IV, LN and growth factors (Kleinman and Martin 2005). Matrigel shows a high batch-to-batch variation, and the exact composition and concentration of all components remain unknown, which is resulting in an impaired reproducibility (Hutmacher *et al*. 2010). Furthermore, thick layers of Matrigel, which are commonly used for cell-invasion-assays (Nguyen-Ngoc *et al*. 2012), hardly represent the natural cell migration process. Whereas only a thin layer of basement membrane has to be crossed by a cell before further migration progresses into and through the CT.

Less complex and better characterised systems are hydrogels based on collagen type-I. Collagen type-I forms a fibrillar mesh, is the predominant ECM component of the CT and can be used for various biomaterial designs (Frantz *et al* 2010; Szot *et al*. 2011) (Fig. 2, 4E-G). Furthermore collagen type-I can be extracted from different animal sources; is soluble under acidic conditions, can be reconstructed as fibrillar mesh and polymerises into a hydrogel at neutral pH. Fibre diameter and density can be controlled through hydrogel-preparation conditions, such as collagen concentration (Fig. 6A,B), polymerisation time and pH (Fig. 6C,D) (Roeder *et al*. 2002). These properties predestine collagen type-I for usage as 3D cell culture system with near native and modifiable characteristics. As collagen type-I is of natural origin, this can again result in batch-to-batch variation and bear the risk of containing undefined impurities. However, due to the fact, that a lot of processes, including migration and metastasis, take place along collagen fibres in collagen rich tissues, it is the system of choice for investigations of early attachment, detachment and migration events (Frantz *et al*. 2010; Geraldo *et al*. 2012; Wolf *et al*. 2009). To achieve higher reproducibility, collagen source, preparation conditions of hydrogels, including gelation temperature, time and pH-values have to be kept constant (Roeder *et al*. 2002; Walters and Stegemann 2013). Furthermore collagen-based hydrogels offer a system that is profoundly compatible with microscopic techniques. Collagen fibres themselves can be imaged using confocal reflection microscopy (CRM) or second harmonic generation (SHG) and they can be fluorescently labelled and imaged by confocal fluorescence microscopy (CFM). Thus, these hydrogels provide a suitable system to follow cell-collagen binding and detachment-events, and to image collagen fibres simultaneously (Geraldo *et al*. 2012; Pang *et al*. 2011). However, the stiffness

of collagen-based hydrogels can only be manipulated in a small window and incorporation of further ECM components within these hydrogels is rather difficult. To represent a natural, more complex tumour microenvironment during cancer development and progression for *in vitro* and *in vivo* applications, other biomaterials need to be considered.

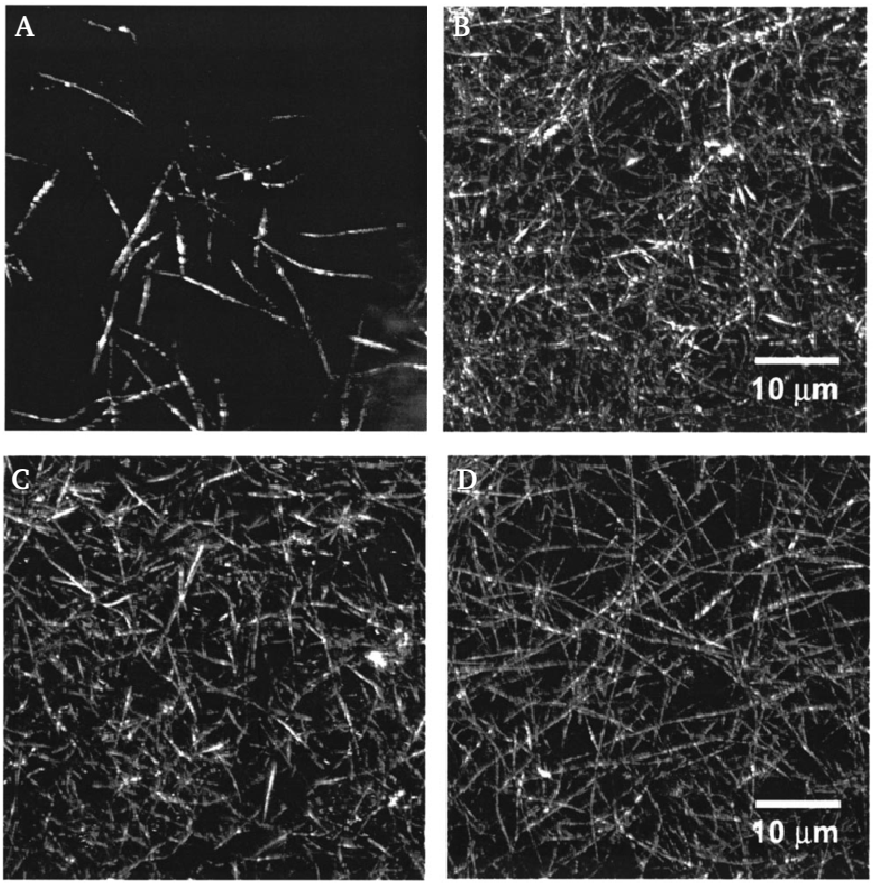

Figure 6: Effect of collagen concentration and pH during gelation on hydrogel structure. CRM images of collagen-based hydrogels prepared with different collagen concentrations, 0.3 mg/mL (A), 3 mg/mL (B); and collagen-based hydrogels (2mg/mL) prepared at different pH, pH 6 (C) and pH 9 (D), adapted from (Roeder *et al*. 2002).

1.3.2.2 Synthetic matrices

Synthetic, 3D systems are an alternative approach in developing new 3D cell culture systems. These bioengineered systems combine key structural ECM features with reproducible and consistent, controllable biomaterial properties, e.g. pore size and degradability (Hutmacher *et al*. 2010). Promising approaches are self-assembling peptide systems, which undergo spontaneous gelation due to altered pH or salt concentration (Zhang *et al*. 2005). Such biomaterials have successfully been used for e.g. ovarian cancer spheroid cultures (Yang and Zhao 2011). Alternatively polyethylene glycol (PEG)-based hydrogels and modified PEG-

derivates are becoming more popular for cancer research (Loessner *et al*. 2010; Sieh *et al*. 2012). In general, synthetic biomaterials offer the advantage that physical and chemical properties can be adjusted independent from each other, but have the disadvantage of lacking native bioactive ECM ligands. This can, in part, be overcome by incorporation of protease cleavage sites and integrin cell-binding sites (Loessner *et al*. 2010; Sieh *et al*. 2012) (Fig. 7).

Figure 7: Preparation of PEG-based hydrogels. Prostate cancer LNCaP cells, are directly mixed with the precursor PEG solution, which contains various binding (RGD) and (MMP)-cleavage sites resulting in hydrogels by a Factor XIII and Ca^{2+} induced polymerisation, adapted from (Sieh *et al*. 2012).

1.3.2.3 Semi-synthetic matrices

Semi-synthetic matrices are a combination of natural ECM components and synthetic components, resulting in a system presenting natural binding sites and tuneable properties. These matrices are usually easier to handle and less cost-intensive, for example gelatine-methacrylamide (GelMA) (Van Den Bulcke *et al*. 2000). GelMA consists of gelatine, an inexpensive component prepared from an industry level degeneration of collagen, mainly type-I (Van Den Bulcke *et al*. 2000). Functionalisation with methacrylamide-groups results in a photo-crosslinkable hydrogel system (Van Den Bulcke *et al*. 2000). The crosslinking reaction of methacrylamide side groups is catalysed by a photo-initiator and UV light (Fig. 8). Compared to the original components collagen and gelatine, GelMA provides very stable and reproducible properties, which can be externally controlled by gelation conditions and in addition shows a low antigenicity (Van den Bulcke *et al*. 2000; Schuurman *et al*. 2013). Mechanical hydrogel properties, stiffness and pore size can be controlled by varying the polymer dry mass, degree of functionalisation, photo-initiator concentration, UV intensity and exposure time (Van den Bulcke *et al*. 2000; Schuurman *et al*. 2013). GelMA vinyl side groups interfere with the helix formation that prohibits physical gelation before and after chemical crosslinking (Schuurman *et al*. 2013). As a starter for the photo-reaction, Irgacure 2959 is chosen, which is widely used for cell encapsulation within hydrogels, and its minimal toxicity at the used concentration has independently been proven in several studies (Nicodemus and

Bryant 2008; Williams *et al*. 2005). As many other hydrogel systems, GelMA-based hydrogels show a high transparency permitting microscopic analysis of cells embedded within these matrices. Providing a more complex, tuneable microenvironment, it is a 3D cell culture system for *in vitro* and *in vivo* experiments on cancer development, progression and reaction to anti-cancer treatment.

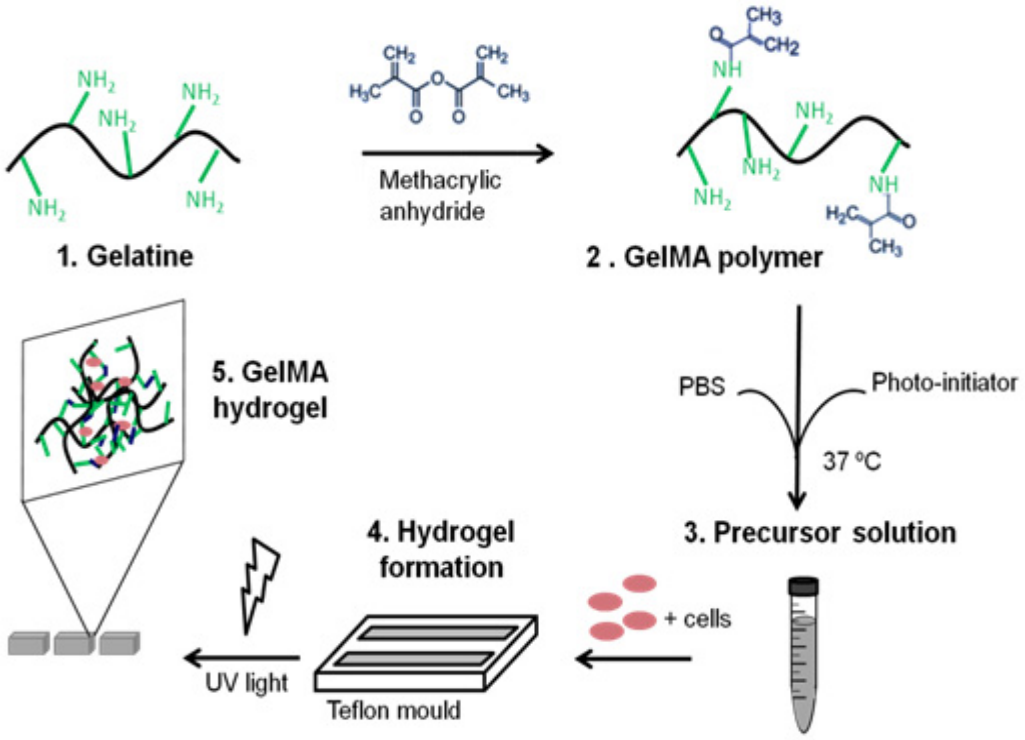

Figure 8: Preparation of GelMA-based hydrogels. Critical steps of GelMA-based hydrogel preparation are depicted. Gelatine (1) and methacrylic anhydride (ratio 1:0.6 w/w) reacted to gelatine methacrylamide (GelMA; 2). The GelMA polymer is dissolved in PBS at 37 °C and mixed with the photo-initiator, cells, and optionally with other ECM components (3). The presence of photo-initiator allowed hydrogel formation during a radical crosslinking reaction induced by UV light (4). Polymerisation within the Teflon mould produced a hydrogel that was cut into smaller units, adapted from (Kaemmerer *et al*. 2014).

1.3.3 Commonly used 3D cell culture model systems – an overview

Mimicking the surrounding ECM *ex vivo*, in these 3D platforms improve medical-orientated research and allows the assessment of protein dynamics in a near native microenvironment. In the following, a summary of the previous described 3D cell culture model systems of various origins, their key features and main advantages and disadvantages is shown (Tab. 1). It highlights parameters, why GelMA is used as a 3D cancer cell model system for *ex vivo* and *in vivo* approaches and a 3D collagen-based hydrogel for analysis of native membrane properties with high resolution microscopy, rather than other commonly used methods.

Table 1: Overview of commonly used 3D cell culture model systems

Model system	ECM morphology	ECM composition and architecture	ECM properties	Advantages	Disadvantages	References
Without external support						
Multi-cellular spheroids	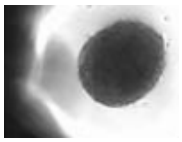 Multi-cellular spheroid, adapted from (Timmins *et al.* 2004).	• No external ECM support	-	• Cell-cell contacts • Tumour-like phenotype • Nutrition and oxygen gradient	• No contact to external ECM support • Less strength • High cell density • Spheroid and matrix properties are not controllable	(Pampaloni *et al.* 2007; Timmins *et al.* 2004)
Natural ECM						
Basement membrane extract (Matrigel)	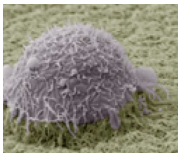 Breast cancer cell invading into Matrigel, adapted from (Poincloux *et al.* 2011).	• Non-fibrillar • Mainly: Collagen type-IV, laminin, proteoglycans	• Soft • ~ 450 Pa (elastic modulus) • Small pores	• Cell-cell and cell-ECM contacts • Natural ECM binding motifs • Basal lamina properties	• Undefined, complex composition • Batch-to-batch variation	(Kleinman and Martin 2005; Soofi *et al.* 2009)
Collagen based hydrogels	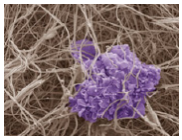 Macrophages in a collagen-based hydrogel, adapted from (Van Goethem *et al.* 2010)	• Fibrillar, random aligned • Collagen type-I	• Soft-medium stiffness, dependent on preparation conditions • Large pores, 1-5 μm	• Cell-cell and cell-ECM contacts • Fibrillar network • Properties are controllable by pH, collagen source/ concentration • Connective tissue properties	• Risk of natural impureness • Small range of stiffness modification • Incorporating further ECM components is difficult	(Franke *et al.* 2014; Geraldo *et al.* 2012; Jayo and Parsons 2012; Walters and Stegemann 2013)

Synthetic ECM						
PEG-based hydrogels	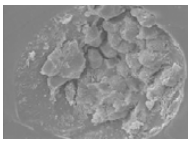 Multi-cellular spheroid in PEG-based hydrogels, adapted from (Hutmacher *et al*. 2010)	• Pocket like structure • Polyehtylene glycol (PEG) • ECM proteins of choice can be incorporated	• Adjustable stiffness • Adjustable pore size	• Cell-cell and cell-ECM contacts • Controllable stiffness • Controllable pore size • Controllable ligand density	• Non-fibrillar structure • ECM ligands have to be externally incorporated • Preparation of precursor components is cost and time-intensive	(Loessner *et al*. 2010; Sieh *et al*. 2012)
Semi-synthetic ECM						
GelMA-based hydrogels	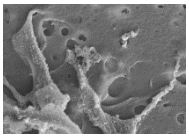 Cell-laden GelMA-based hydrogel. Image provided by Dr. Christina Theodoropoulos	• Pocket-like structure • Gelatine-methacrylamide • ECM proteins of choice can be incorporated	• Stiffness adjustable by polymer concentration and crosslinking time • Pore size adjustable by polymer concentration	• Cell-cell and cell-ECM contacts • Controllable stiffness • Natural ligand distribution/ concentration • cost-effective preparation	• Non-fibrillar structure • UV light needed for crosslinking	(Nichol *et al*. 2010; Schuurman *et al*. 2013)

1.4 The plasma membrane

1.4.1 The fluid membrane - Structure and composition

The crosstalk between a cell and the ECM takes place at the plasma membrane, a cellular barrier and location of energy- and information transfer. The plasma membrane, representing the interface between the intracellular and the extracellular compartment, is of outmost interest in cell physiology, but far from being fully understood.

The thickness of the plasma membrane is about 10 nm and therefore optical and fluorescent microscopy methods are difficult to apply. These techniques fail to resolve structures below 200 nm due to the Rayleigh limit (Rayleigh 1903), which exceeds the membrane thickness (Singer and Nicolson 1971). However, over the past 15 years, new developments in microscopy techniques have overcome this resolution limit, providing a toolbox for new

insights into membrane structure and dynamics (Kusumi *et al*. 2012; Marguet *et al*. 2006; Schermelleh *et al*. 2010). The plasma membrane consists of a cell-type specific composition, which directly influences the membrane properties. Despite that, all membranes follow a common basic structural-functional principle. The predominant, well accepted model used for over 40 years to describe the structure of the plasma membrane is known as the fluid mosaic model (Singer and Nicolson 1972) (Fig. 9A). The plasma membrane is a natural bilayer formed by amphipathic phospholipids, glycolipids and sterols in various concentrations, where lipid molecules facing each other with their hydrophobic tails (Singer and Nicolson 1972). Embedded in or attached to this bilayer are integral and peripheral proteins, respectively (Singer and Nicolson 1972). According to the Singer and Nicolson model all proteins and lipids exhibit free lateral motion within the plasma membrane, which gives the membrane its character of a 2D fluid. Hence, this motion leads to an even and random distribution of proteins and lipids (Singer and Nicolson 1972) (Fig. 9A). However, this model does not include or represent newer experimental data from the last decades (Goñi 2014). An updated model shows a membrane full of transmembrane proteins, resulting in a protein-packed membrane structure and rarely protein-free parts (Goñi 2014) (Fig. 9B). This model furthermore includes occasionally binding proteins and concludes that proteins must not be either membrane bound or cytosolic, some of them can change their properties (Goñi 2014). The membrane bilayer itself is not static; it is heterogenic in composition and degrees of freedom for lipids are increased, allowing spontaneous and transiently, local non-bilayer structures and flip flop movements of lipids (Goñi 2014).

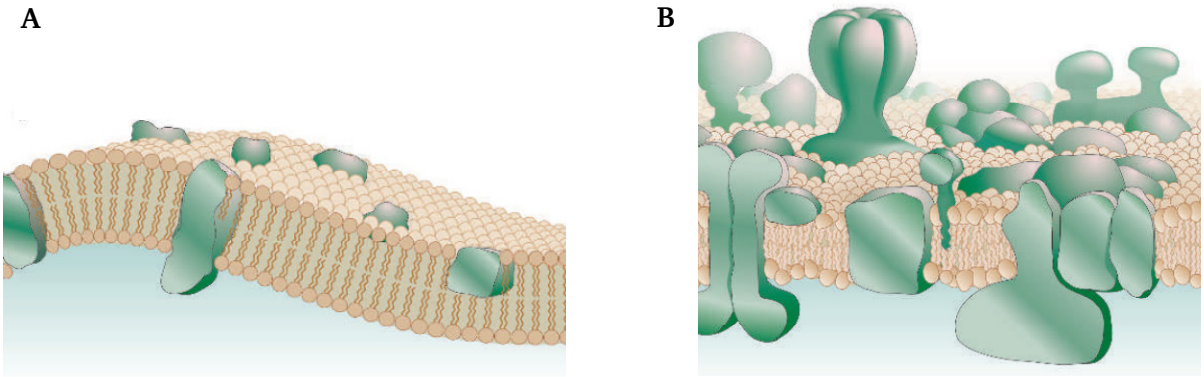

Figure 9: Fluid models of the plasma membrane. The plasma membrane model developed 1972 (A) and an updated version from 2014 (B). The Fluid mosaic model developed by Singer and Nicolson shows the plasma membrane as natural bilayer, with integrated proteins at low concentration (A). These integrated proteins and lipids can diffuse lateral trough the plasma membrane (A). The updated model shows a different structure, including newer experimental results (B). This revised model includes a high protein density and proteins those bind only

occasionally to the membrane (B). In addition non-lamellar intermediates and curvature of the membrane is integrated (B). Overall, it shows that membrane organisation is much more heterogeneous, which allows protein assembling within discrete patches and also spontaneous flip flop movement of the lipids within certain membrane areas, adapted from (Goñi 2014).

1.4.2 The patterned membrane

However, it is more complex and membrane properties are highly affected by another component, the actin cytoskeleton. In addition to the updated membrane model, the patterned membrane includes the structure of the actin cytoskeleton and its effect on membrane properties e.g. protein diffusion within the plasma membrane (Kusumi *et al*. 2012) (Fig. 10). The plasma membrane is assumed to be structured in compartments, consisting of a membrane-associated actin-based skeleton and transmembrane proteins anchored in this network (Kusumi *et al*. 2012). This model shows that the diffusion properties of the plasma membrane are dependent on the cytoplasm-plasma membrane-cytoskeleton continuum (Kusumi *et al*. 2012). Furthermore, this model integrates the presence of lipid rafts, micro-domains of the plasma membrane rich in cholesterol, glycosphingolipids and glycosylphosphatidylinositol anchored proteins, and dynamic multi-protein complexes (Kusumi *et al*. 2012). The result is a model of the plasma membrane, whose components are irregularly distributed both in space and time. Hence, the plasma membrane is characterised by high spatio-temporal dynamics of its components. The updated Singer and Nicolson model and the patterned membrane model can explain some of the observed membrane properties. However applied to focal adhesions, the protein complexes mediating the cell-ECM crosstalk, and their dynamics within the membrane, a lot of processes are still unclear

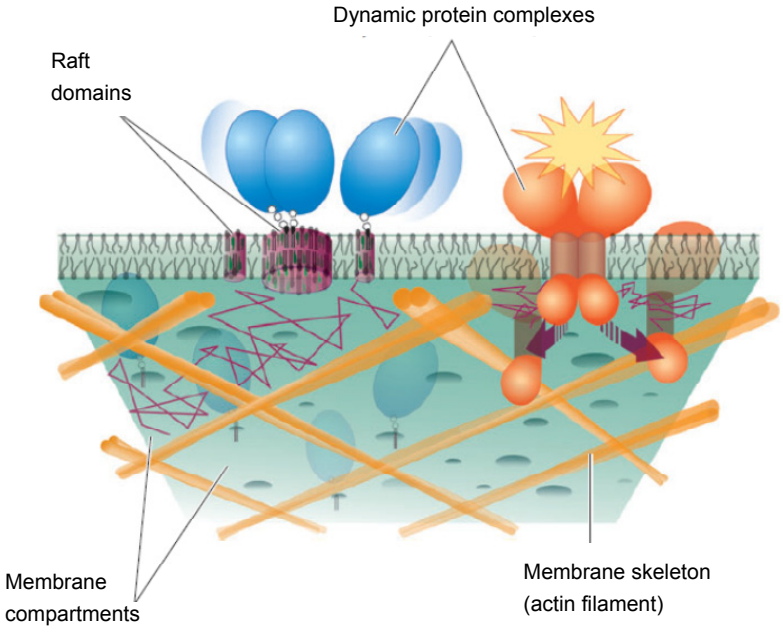

Figure 10: The patterned plasma membrane. This enhanced model describes the plasma membrane as a highly compartmented structure. These compartments are result of membrane-associated actin-based membrane skeleton and transmembrane proteins connected to this network. It includes raft domains and transiently existing large membrane protein complexes. Protein diffusion is thereby regulated by the cytoplasm-plasma membrane-cytoskeleton continuum, adapted from (Kusumi *et al*. 2012).

1.4.3 The attached membrane – Integrins and focal adhesions

The attachment and communication of a cell to the ECM, is mediated via plasma membrane receptors, like integrins which recognise on the extracellular side ligands and highly conserved binding motives of the ECM (Geiger and Yamada 2011; Humphries *et al*. 2006). Integrins are a family of αβ-heterodimeric plasma membrane proteins (Humphries *et al*. 2006). In mammals, 18 α-subunits and 8 β-subunits are found, resulting in 24 different integrin heterodimers (Humphries *et al*. 2006). Integrins bind to ligands, containing mostly RGD-amino acid motifs and non-RGD ligands, such as collagen and LN (Humphries *et al*. 2006). Activated integrins, i.e. ligand bound, assemble together with many more membrane and cytosolic proteins, e.g. paxillin and talin and form large and complex, integrin-mediated surface adhesion complexes, namely FA (Geiger and Yamada 2011)(Fig. 11). A FA model, resolving its static architecture was presented by Kanchanawong and colleagues 2010 using superresolution fluorescence microscopy (Kanchanawong *et al*. 2010). They showed a FA as a very organised structure, which can be divided into different layers in axial direction, directly and indirectly involved in various cellular signalling pathways (Kanchanawong *et al*. 2010) (Fig. 11).

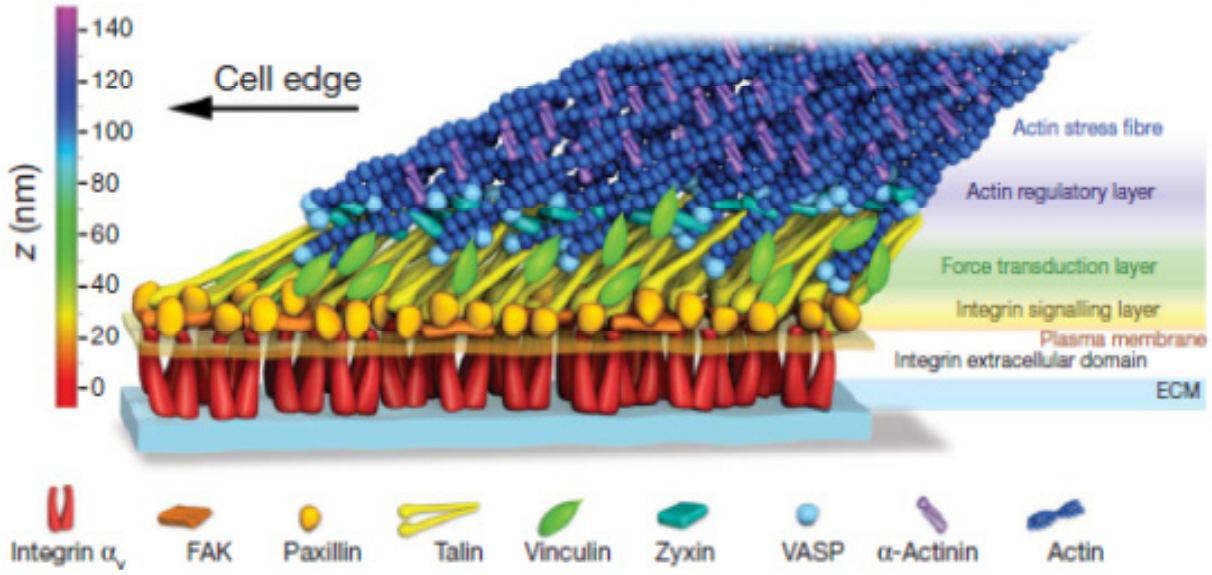

Figure 11: Schematic model of static FA organisation. Integrins, cytosolic and membrane proteins form large cellular adhesion clusters, namely FA. These clusters showed a profoundly axial organisation consisting of different protein layers. Integrins, together with other adaptor proteins form a tight connection of the actin cytoskeleton on the intracellular side and ECM ligands on the extracellular side, which is mediating the cell-ECM crosstalk, adapted from (Kanchanawong *et al*. 2010).

1.4.4 The dynamic architecture of focal adhesions

Over the last decades, FA were viewed as large, compact and very organised static protein clusters within the plasma membrane (Fig. 11, 12A). However, FA can also undergo rapid assembly and/or disassembly within one minute, allowing for fast migration along a substrate (Zamir and Geiger 2001). This process allows the recognition and a fast response to extracellular changes. The extracellular substrate itself is a regulator of FA size, distribution and dynamics in a substrate dependent manner (Geiger *et al*. 2009).

The development of new microscopic techniques, in overcoming the resolution limit with high spatio-temporal solutions provided also new insights into this topic and resulted in an updated FA model, including the dynamic structural FA organisation (Shibata *et al*. 2012) (Fig. 12B). According to this model a FA is no longer a compact assembly of FA protein (Fig. 12A), but rather an archipelago, as described by Shibata and colleagues (Fig. 12B). According to this model, a FA consists of many integrin islands and membrane molecules enter the inter-island areas rather frequently (Shibata *et al*. 2012). Evidence for this model is found as proteins that do not belong to a focal adhesion, can enter, cross and leave a FA zone, without displaying a marked slowdown (Shibata *et al*. 2012). A complete different pattern occurs for proteins which are associated with the FA complexes, e.g. integrin β3 (Shibata *et al*. 2012).. This protein also enters the FA zone easily, but it frequently stops and stays longer within the focal adhesion zone, which is most likely due to transient binding events with FA proteins (Shibata *et al*. 2012). The observation that proteins can enter and escape FA, provided means for a fast assembly and disassembly of a FA (Shibata *et al*. 2012).

Over the past decade, cellular adhesions became more in focus of cancer research. Given that most of the knowledge has resulted from 2D or 2.5D (on top culture onto a soft or coated substrate) experiments and is often investigated on fixed cells, less is known about their detailed architecture and dynamics under 3D culture conditions or even *in vivo*. In a pioneering attempt, Fraley and colleagues were unable to detect FA in cells grown in a 3D microenvironment, implementing that their size or their lifetime is completely different compared to FA in 2D (Fraley *et al*. 2010) (Fig. 13). However, using the same 3D cell culture

system and the same cell line, Kubow and Horwitz were able to identify that a simple contrast problem induced by the overexpression of a cytosolic FA protein, but not a different architecture or lifetime caused the differential appearance of FA in the work of Fraley and colleagues (Kubow and Horwitz 2011) (Fig. 14).

This example demonstrates that both physiological and imaging conditions change in a 3D cell culture system. Hence, a thorough understanding of the imaging method is required, to clearly separate both aspects from one and another. In addition, the depth of the cell position within a 3D system affects the distribution and size of FA, which might result in different FA detection in a 3D microenvironment (Fraley *et al*. 2011). Observations of FA in cells cultured in a 3D systems are much more complex and various parameters have to be kept in mind when analysing these data and setting up an experiment. These findings demonstrated the need for the optimisation of 3D cell culture systems suitable for high resolution microscopy to overcome limitations of commonly used analysis methods.

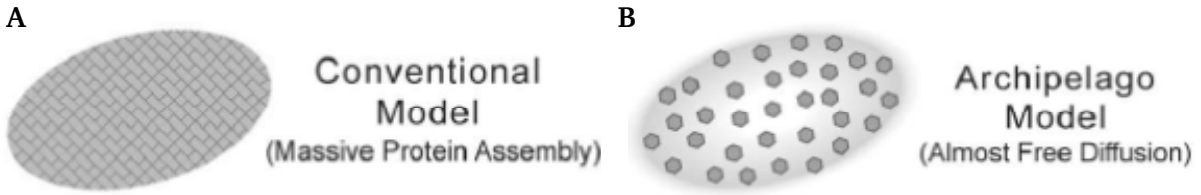

Figure 12: Schematic model of static and dynamic FA organisation. FA, as classically defined are tight, compact protein complexes (A). Including newer experimental results, FA are organised in an archipelago structure (B). This FA archipelago model allows free protein diffusion within the FA zone, which is slowed down only by interaction with the island-like assembled FA proteins (B), adapted from (Shibata *et al*. 2012).

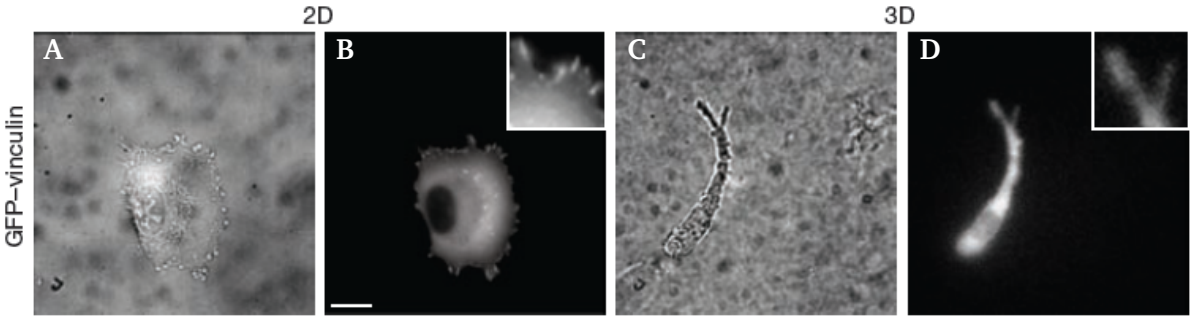

Figure 13: Cell-ECM adhesions within a 2D and 3D microenvironment. Distribution of EFGP -labelled vinculin, as FA marker in cells cultured on a 2D substrate (A, B) and within a 3D collagen-based hydrogel (C, D). In 2D, FA were seen on the cell periphery (bright dots, B). However, in 3D no discrete FA were detectable (D), adapted from (Fraley *et al*. 2010). Scale bar: 10 μm.

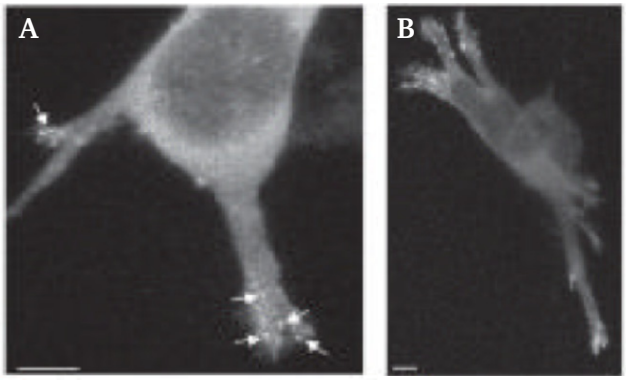

Figure 14: Cell-ECM adhesions within a 3D microenvironment. Distribution of EGFP-labelled paxillin (indicated by arrows) (A); and vinculin clusters (dot like structures) (B), as FA marker, expressed under the control of a truncated promotor in human osteosarcoma U2OS cells, cultured within a collagen-based hydrogel. The usage of a truncated promotor reduced the fluorescent background in the cytosol and allowed detection of FA, also within a 3D microenvironment, adapted from (Kubow and Horwitz 2011). Scale bar: 5 μm.

1.5 Ovarian cancer – an example of cell-ECM interactions with clinical relevance

Interaction with the ECM, binding and/or detaching events and ECM remodelling are critical steps in initiating progression and invasion of tumours (Ahmed *et al*. 2002; Pupa *et al*. 2002; Ricciardelli and Rodgers 2006). Thereby, dysregulation of the ECM is highly involved in the development of epithelial carcinoma, like breast or ovarian cancer and in the anti-cancer treatment-response of these cancer cells (Ahmed *et al*. 2002; Loessner *et al*. 2013; Vasaturo *et al*. 2005). This evidence suggests that mimicking more physiological conditions in a 3D cell culture model is a promising tool to deepen the understanding of fundamental steps in cancer development and reaction to anti-cancer treatment. As cancer model system, ovarian cancer was chosen. The metastatic pattern of ovarian cancer patients shows a unique path (Shield *et al*. 2009), which is challenging to model in an experimental *ex vivo* system. Ovarian cancer is the main cause of death of gynaecological cancers worldwide (Shield *et al*. 2009), with more than 1,000 Australian (Australian Institute of Health and Welfare) and 5,500 German (Robert Koch Institute (ed) and Gesellschaft der epidemiologischen Krebsregister in Deutschland e.V) women die every year from this disease. It is a very aggressive cancer type and patients are typically diagnosed in an advanced state of the disease, when chemo-resistance occurs, resulting in a high mortality rate and poor outcome (Agarwal and Kaye 2003; Shield *et al*. 2009). The survival rates for ovarian cancer patients have not been increased over the past five decades (Auersperg 2013). Therefore a suitable 3D cell culture system can form a basis for a better cellular understanding of the disease and provide means for an improved drug

screening. Single ovarian cancer cells separate from the primary tumour, and form larger multi-cellular spheroids within the abdominal cavity (Shield *et al*. 2009) (Fig. 15). These spheroids then attach to the surface of the peritoneum, resulting in spheroid disassembly and metastasis to distant organs (Fig. 15). During this process, building and losing of cell-cell and cell-surface contacts via cellular adhesion receptors, such as integrins, play a key role (Shield *et al*. 2009). Within synthetic PEG-based 3D hydrogels spheroid formation of ovarian cancer cells OV-MZ-6 cells occurred, but not in 2D. In 3D, the proliferation rates were depend on RGD binding sites within the matrix (Loessner *et al*. 2010). These results again underline the importance, and often underestimated influence, of the cell-ECM interaction on cellular behaviour and cellular responses to the extracellular microenvironment.

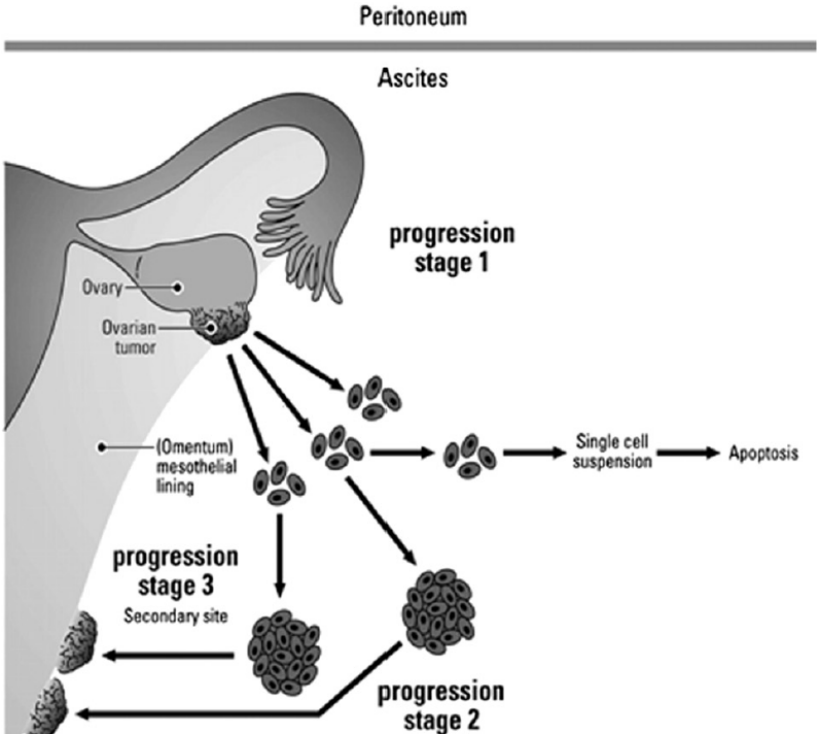

Figure 15: Progression of ovarian cancer at various stages. Single cells detach from the primary tumour (progression stage 1) into the peritoneal fluid, where spheroid formation occurs (progression stage 2). These spheroids can then adhere onto the mesothelial layer and invade into distant tissue (progression state 3), adapted from (Shield *et al*. 2009).

1.6 Microscopy

1.6.1 High resolution imaging of cells cultured within a 3D system

With normal, wide-field, epi- illumination, fluorescence microscopy a resolution of ~220 nm in lateral (x) and~ 520 nm in axial (z) direction can be achieved (Fig. 16A), provided an objective with a high numerical aperture (NA) is used. These values are driven from the limits

imposed by the diffraction of light (Abbe 1873; Rayleigh 1903). Especially in the last decade, many imaging techniques and procedures have been developed, which are able to overcome the diffraction limit of resolution, achieving so called superresolution (Farsiu *et al*. 2004; Schermelleh *et al*. 2010).

All too often, as already mentioned on the results carried out by Fraley and colleagues, not resolution, but contrast limits the outcome of a microscopic investigation. This is especially the case, if detectability is concerned. An often used technique for increasing the contrast is the total internal reflection fluorescence microscopy (TIRF) (Axelrod 1984). The laser beam undergoes a total internal reflection, which occurs at the interface between an optically dense medium, i.e. the coverslip and a medium with a lower refractive index, i.e. phosphate buffered saline (PBS) in which the sample is embedded (Axelrod 1981) (Fig. 16B). At the reflection zone, an evanescent field with a depth of around 100 nm forms above the coverslip (Fig. 16B). Hence, TIRF excitation is ideally suited for selective observation of objects close to the coverslip, like the plasma membrane of adherent 2D-cultured cells. As illustrated this approach however, cannot be used to image deeper in 3D cell cultures (Fig. 16C). To overcome these limitations, the so called highly inclined laminated optical sheet (HILO) illumination is used to achieve the excitation of a selective plane within the hydrogel (Tokunaga *et al*. 2008) (Fig. 16D). Here, the laser beam is tilted by refraction and produces a thin light sheet (Tokunaga *et al*. 2008). Confined illumination allows imaging with high temporal resolution, as the fluorescence of molecules illuminated within the evanescent field or by the light sheet is directly recorded as an image. In contrast, confocal microscopy requires a scanning motion of the laser, to form an image out of individual point detections, which results in a much lower “frame-rate” than “frame-wise” detection of the first approach.

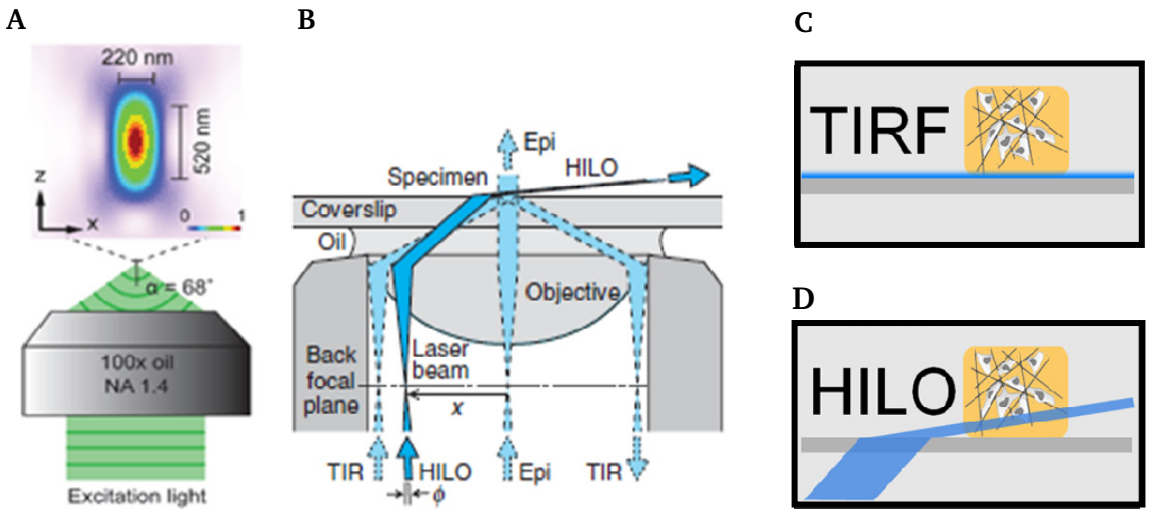

Figure 16: Limitations of fluorescence microscopy and how to overcome these. The point spread function (PSF) of a commonly used high NA oil immersion objective, showed the limitations of epi-fluorescence microscopy, a maximum resolution of 220 nm and 520 nm in xy and xz direction, respectively (A), adapted from (Huang *et al.* 2009). To overcome these limitations, TIRF and HILO illumination are applied (B). This confined illumination increases the contrast, as only molecules within this area are excited (Tokunaga *et al*. 2008). The area of confined excitation is illustrated in (C) and (D). As TIRF provides selective illumination close to the coverslip surface only (C), HILO allows selective illumination deeper within the sample (D), which is compatible with imaging of cells embedded in a hydrogel, images provided by PD. Dr. Tobias Meckel.

1.7 Project aims

Exchange and interaction with the microenvironment is highly engaged in influencing and controlling of cellular behaviour, including cellular processes, such as cellular morphology, proliferation and migration. Unsurprisingly, ECM composition and its physical/chemical properties have a high impact on tumourigenesis and cellular reactions to anti-cancer treatment. Although the importance of a more physiological three-dimensional microenvironment is well reported, it is still not applied routinely in experimental pre-clinical and pre-animal models in cancer research. Cellular interactions with the microenvironment are mediated via the interface of the plasma membrane. Thereby the spatio-temporal dynamic heterogeneity of proteins and lipids seem to encode the information passed outside-in and inside-out a cell. To capture this cell-ECM crosstalk in time and space in living cells, high resolution microscopy techniques have to be applied. To gain results into native dynamics, also these high resolution measurements have to be performed in a more physiological, 3D microenvironment.

First aim of this project is the application of a semi-synthetic biomaterial, GelMA, to establish an alternative 3D cell culture system for ovarian cancer. GelMA-based hydrogels combine natural binding motifs with reproducible and tuneable properties of synthetic materials. This results in a physiological relevant, reproducible and cost-effective approach for 3D cell cultures. GelMA-based hydrogels will be tested *ex vivo,* in an experimental model and *in vivo,* in an animal study as spheroid-based model system for ovarian cancer. In these studies, fundamental hydrogel and spheroid properties will be characterised. This 3D approach will deepen the understanding of ovarian cancer spheroid formation and progression in an experimental model system and will provide a screening tool for the efficacy of therapeutics targeting multi-cellular spheroids of advanced ovarian cancer.

Second aim of this project is the optimisation of a collagen-based hydrogel as 3D cell culture model which is compatible with high resolution microscopy. Therefore a small-volume collagen-based hydrogel will be applied. Essential hydrogel and cellular parameters will be analysed, and single molecule microscopy measurements will be performed in the plasma membrane of embedded cells. This system will provide a tool to capture dynamics of cellular processes on the molecular level with high spatio-temporal resolution in a physiological relevant 3D microenvironment.

The approach to these aims and the outcome are summarised in the following layout:

GelMA-based hydrogels – a bioengineered 3D cell culture system for cancer research

I. Characterisation of hydrogel structure and hydrogel properties
II. Characterisation of ovarian cancer spheroids (*ex vivo*)
III. Tumour growth and reaction to anti-cancer treatment in an animal study (*in vivo*)

Collagen-based hydrogels – a bioengineered 3D cell culture system for high resolution microscopy

I. Preparation of small volume 3D collagen-based hydrogels
II. Characterisation of hydrogel structure and hydrogel properties
III. Characterisation of single cells and multi-cellular aggregates
IV. Single molecule microscopy in the plasma membrane of hydrogel-embedded cells

2 Material and Methods

2.1 GelMA-based hydrogels – a bioengineered 3D cell culture system suitable for cancer research

All methods described in 2.1, with exception of chapter 2.1.4.5, were published in a peer reviewed publication in Acta Biomaterialia 10(6):2551-2562, 2014.

2.1.1 Cell culture

The human epithelial ovarian cancer cell line OV-MZ-6 was derived from a 70-year old patient with advanced cystadeno ovarian cancer and cultured as reported (Loessner *et al*. 2010; Möbus *et al*. 1992). Their potential to form multi-cellular spheroids in hydrogels has been shown previously (Loessner *et al*. 2010). For animal experiments, OV-MZ-6 cells were transfected with a lentiviral luciferase expression system (pLenti6/V5-D-TOPO; Invitrogen) using blasticidin-selection (Loessner *et al*. 2013). Briefly, OV-MZ-6 cells were cultured in Dulbecco's modified eagle media (DMEM high glucose, GlutaMAX containing, 4,500 mg/mL glucose and pyridoxine, without sodium pyruvate (Invitrogen). Media was supplemented with 10 mM 4-(2-hydroxyethyl)-1-piperazineethanesulfonic acid (HEPES) buffer (Invitrogen), 0.55 mM L-arginine (Sigma Aldrich), 0.272 mM L-asparagine (Sigma Aldrich, Australia), 20 μg/mL Gentamycin (Invitrogen), 1% penicillin/streptomycin (pen/strep) (Gibco, Australia) and 10% foetal calf serum (FCS)(Gibco, Invitrogen). Cells were cultured for 3 to 4 days at 37 °C/ 5% CO_2 till reaching 60-80% confluence. Cells were detached using 0.2 g/L Ethylendiaminotetraacetic tetrasoidum (EDTA(Na_4)/PBS (Versene, Invitrogen), washed with PBS and centrifuged for 5 min at 1200 rpm. Cell pellet was carefully resuspended in fresh media and required amount of cell suspension was transferred into a new cell culture flask.

2.1.2 Preparation of GelMA-based hydrogels

Gelatine methacrylamide (GelMA) was synthesised from gelatine (isolated from porcine skin, type A; Sigma Aldrich, St. Louis, MO, USA) and methacrylic anhydride (Sigma Aldrich) following a previously published procedure, resulting in GelMA with a high degree of functionalisation with 70-80% of all lysine groups (Van den Bulcke *et a*l. 2000; Schuurman *et al*. 2013). GelMA-based hydrogels were crosslinked by UV irradiation in the presence of 0.5 mg/mL of a water soluble photo-initiator (Irgacure, IC2959; BASF, Germany). GelMA solution was prepared in PBS to a final concentration ranging from 2.5 to 10%, with polymer concentrations in percentages of weight per volume of PBS (w/v). The precursor GelMA

solution was transferred into a custom-made, rectangular Teflon mould, covered with a glass slide and crosslinked using a CL-1000 UV crosslinker (UVP; Upland California, USA) with 365 nm wavelength tubes for 10 min (exposed intensity of 2.7 mW/cm^2 on hydrogel surface). After polymerisation, hydrogels were removed from the mould and cut into 2 x 4 x 5 mm pieces. For cell-laden hydrogels, 2.8 x 10^5 cells/mL cells were resuspended in GelMA solution before crosslinking. After cutting, each hydrogel containing 1.12 x 10^4 cells was cultured at 37 °C/ 5% CO_2 for up to 21 days, with media changes every 3-4 days. The ECM components LN-411 (20 μg/mL; Biolamina, Stockholm, Sweden) and HA (0.1%; Lifecore Biomedical, USA) were incorporated, separately or combined, by mixing into the precursor GelMA solution prior to (addition of cells and) crosslinking.

2.1.3 Characterisation of GelMA-based hydrogels

2.1.3.1 Analysis of mechanical properties - Compression tests

Compression tests were performed using a micro-tester 5848 system (Instron, Norwood, MA USA), with a 5 N load cell, immersed in PBS at 37°C. Hydrogels were prepared 1-2 days before testing and incubated at 37 °C/ 5% CO_2 in PBS. Sample height was derived from the force-displacement data, while cross-sectional area was calculated using the height and weight of the rectangular sample (ρ = 1.05 g/mL). The slope of the stress-strain curve from 10-15% strain was taken as the compressive modulus.

2.1.3.2 Analysis of diffusion properties within a hydrogel – Fluorescence recovery after photobleaching

Fluorescence recovery after photobleaching (FRAP) measurements were performed using confocal laser scanning microscopy (CLSM; SP5, Leica) to analyse diffusion properties of solutes within the hydrogel. Hydrogels were incubated with fluorescein isothiocyanate (FITC)-labelled 70 kDa dextran (FD70), which was prepared as described previously (De Belder and Granath 1973). Hydrogels were pre-incubated with FD70 solution in the dark on a shaker to ensure uniform distribution within the hydrogel. To allow measurements in the linear concentration range (< 4 mg/mL) of the fluorophore intensity over concentration, a 3 mg/mL FD70/PBS solution was used (Deschout *et al*. 2010). Hydrogels remained in FD70 solution throughout the measurements, and FRAP experiments were performed at least 100 μm above the coverslip to ensure measurements within the hydrogel and to avoid artefacts from the glass/hydrogel and solution/hydrogel interfaces. For imaging and bleaching a 488 nm line from an inbuilt Argon-ion laser, a zoom factor of 3 and a scan frequency of 1000 Hz were used. Images were taken using a 10x low NA objective (0.45) to yield a beam profile with

high axial extension, which allows modelling of the fluorescence recovery as two-dimensional diffusion process (Deschout *et al*. 2010). Diffusion coefficients and mobile fractions were determined from the FRAP image sequences by an analysis method that includes spatial and temporal intensity changes, rectangular FRAP (rFRAP) (Deschout *et al*. 2010). All FRAP analyses were performed with Matlab2011a (Mathworks; Natick, MA, USA). A rectangular bleach area of 50 μm x 50 μm was used throughout all FRAP recordings.

2.1.4 Characterisation of ovarian cancer spheroids *in vitro*

2.1.4.1 Spheroid morphology of fixed cells – Nuclei and cytoskeleton staining

Spheroid morphology over the duration of 3D cultures was assessed with 4´,6-diamidino-2-phenylindole (DAPI) to visualise nuclei and rhodamine415-conjugated phalloidin to stain the cytoskeleton. Hydrogels were washed with PBS, fixed in 4% paraformaldehyde (PFA)/PBS for 20 min and permeabilised in 0.2% Triton X-100/PBS for 30 min at room temperature. Samples were washed with 0.1 M glycine/PBS followed by two washing steps in PBS. Hydrogels were stained with 0.8 U/mL rhodamine415-conjugated phalloidin/1% bovine serum albumin (BSA)/PBS and 2.5 μg/mL DAPI/PBS and stored in PBS at 4°C until imaged by CLSM. (Ex: 405/561 nm, Em: 430-490/620-740 nm). Z-stacks were acquired with a constant slice thickness of 2 μm and a depth of 80-200 μm to reconstruct maximal projections that were processed with Fiji image analysis software (Schindelin *et al*. 2012).

2.1.4.2 Protein expression – Immunohistochemistry

For immunohistological analyses, hydrogels were processed as described earlier (Loessner *et al*. 2013). Briefly, samples were incubated in TissueTek embedding media (ProSciTech), shock-frozen in liquid nitrogen and stored at -80°C until cryo-sectioned (5-7 μm). Then, samples were permeabilised with 0.2% Triton X-100/PBS for 30 min, washed with PBS and incubated with primary [cytokeratin-8 (1/100; Abcam); integrin α6 (1/50; Chemicon); MMP-9 (1/200; Abcam)] and secondary [Alexa488/568-conjugated anti-mouse/rabbit IgG (1/1,000; Invitrogen)] antibodies in 1% BSA/PBS for 1 h at room temperature. Cytoskeleton and nuclei were stained as above and fluorescence signals detected via CLSM. Hematoxylin and eosin staining was performed using standard procedures (Loessner *et al*. 2013).

2.1.4.3 Cell proliferation –Metabolic activity and DNA content

Proliferation assays, AlamarBlue® (Invitrogen) to quantify metabolic activity and CyQuant® (Invitrogen) to measure the DNA content, were conducted as described earlier (Loessner *et al*. 2010). Briefly, spheroid growth was detected at several time points (1, 7, 14 and 21 days)

after cell encapsulation. To determine the metabolic activity, hydrogels were incubated in media contained 8% (v/v) AlamarBlue® reagent for 2 h at 37°C/ 5% CO_2. Media without cell-laden hydrogels with AlamarBlue® reagent served as negative control. The AlamarBlue® solution was transferred into a black 96-well plate (Corning) and fluorescent signals (Ex: 544 nm, Em: 590 nm) detected using a POLARStar OPTIMA plate reader (BMG LABTECH). The signal of the control media was subtracted from all samples. To determine the DNA content, hydrogels were digested with proteinase K (0.5 mg/mL; Invitrogen) overnight. Then, samples were treated with RNaseA (1.4 U/mL; Invitrogen) for 1 h at room temperature (RT) in cell lysis buffer supplemented with NaCl (180 mM) and EDTA (1 mM). CyQuant® dye solution was added and fluorescent signals (Ex: 485 nm, Em: 520 nm) detected using a plate reader. A λ-DNA standard (10 ng/mL to 2 μg/mL) was used to calculate the change of DNA content for each time point. Each condition was measured in biological triplicates/quadruplicates (unless stated otherwise) in technical replicates.

2.1.4.4 MMP Inhibition

Inhibition of cell-secreted MMPs and their effect on spheroid morphology and proliferation was examined using media supplemented with a broad-band MMP-inhibitor (GM6001; 20 μM; Chemicon). Cells were encapsulated within hydrogels as described above, and MMP inhibition started on day 1 of 3D culture for up to 21 days. Dimethyl sulfoxide (DMSO) served as control treatment. The media was replaced every third day. Each condition was measured in biological triplicates.

2.1.4.5 RNA and protein expression

2.1.4.5.1 Cell lysate preparation and RNA extraction

For RNA extraction, GelMA-based hydrogels were pooled (4-5 hydrogels) in a 2 mL reaction tube in 350 μL lysis buffer, supplemented with 1% Mercaptoethanol (Lysis buffer, RNeasy Micro Kit, QUIAGEN, Hilden, Germany) and stored at -80°C until further usage. Hydrogels were homogenised using silica beads and a tissue homogeniser and RNA extraction was performed following the RNeasy Micro kit protocol. Briefly, samples were centrifuged for 3 min at 10,000 rpm at RT and the supernatant was transferred into a new collection tube. Then 70% ethanol was added and samples were transferred onto RNeasy minElute spin columns and centrifuged for 15 sec at 10,000 rpm, washed with RW1 washing buffer and centrifuged for 15 sec at 10,000 rpm. DNase I/RDD buffer (27.3 U/sample) solution was added directly onto the column membranes and incubated for 15 min at RT. Columns were washed again with RW1 buffer, RPE buffer and centrifuged for 2 min at 10,000 rpm with

80% ethanol. Columns were placed in new collection tubes, centrifuged for 5 min with an open lid at 10,000 rpm and RNA was extracted from the membrane using 11 μL RNase free water. RNA quality was analysed using a Nanodrop ND-1000 spectrophotometer, measuring the absorption at 230 nm, 260 nm and 280 nm in order to determine the ratios A_{260}/A_{280} and A_{230}/A_{260} and the RNA concentration of each sample.

2.1.4.5.2 Complementary DNA synthesis

Equal amounts of total RNA (1 μg) extracted as described above were used for reverse transcription, to synthesise complementary DNA (cDNA). Briefly, RNA was dissolved in water and diluted with DNase reaction buffer and treated with DNase I (0.5 U, Invitrogen) to degrade remaining DNA. After incubation at 15 min at 37 °C, DNase was inactivated for 2 min at 95 °C, samples were centrifuged and kept on ice. Then random hexamer (hex) primers (250 ng) were added, incubated for 5 min at 65 °C, to denaturate the secondary RNA structure, samples were centrifuged and cooled on ice (less than 5 min), to allow annealing of the hex primers to the RNA. Lastly, cDNA was synthesised using First strand (FS) buffer, Dithiothreitol (DTT, 5 mM, Invitrogen), SuperScript III Reverse Transcriptase (Invitrogen, 200 U) and desoxynucleotids (dNTPs,Roche, 0.5 mM). This reaction was incubated for 5 min at RT, followed by 60 min at 55 °C and 15 min at 70 °C. The concentration of each cDNA sample was determined using a NanoDrop spectrophotometer. Samples were stored at -80 °C until further usage.

2.1.4.5.3 Real time quantitative polymerase chain reaction

For Real time quantitative polymerase chain reaction (RT-qPCR), diluted cDNA samples (1:10) generated as described above and specific primers (1 μM, Tab. 2) were used, following a previously described protocol (Loessner *et al*. 2010). PCR samples without template cDNA for each primer were used as negative control. RT-qPCR was performed in duplicates with SYBR Green chemistry (Roche, Australia), according to manufacturer's instructions (all PCR reagents were from Invitrogen) with an ABI7300 thermal cycler (Applied Biosystems). The RT-qPCR reaction was carried out using the following protocol: 50 °C, 2 min; 95 °C, 10 min for initial polymerase activation and 95 °C, 15 sec, denaturation and 60°C for 1 min primer annealing and elongation (40 cycles). Additionally to confirm specificity of PCR-reaction, a melting curve was generated consisting of the following steps: 95 °C, 15 sec; 60 °C, 30 sec; 95 °C, 15 sec. Results of fluorescence intensity were analysed with the sequence detection system software (Applied Biosystems) using the relative standard curve method to quantify gene expression levels. The standard curve was obtained from serial dilutions (10^{-2}-10^{-6}) of

PCR products. Linear template standards were synthesised using TaqDNA polymerase (Invitrogen) and the following thermal profile, 94 °C for 2 min, PCR initialisation; 94 °C, 30 sec, denaturation; 60 °C, 30 sec, primer annealing; 72 °C, 1 min, elongation (35 cycles) and a final elongation step 72 °C, 15 min. Linear template standards for RT-qPCR were run on a 2% (w/v) agarose gel and visualised by ethidium bromide staining using a gel documentation system (Syngene). Samples and template standards were analysed and quantified in the same RT-qPCR run. Cycle threshold (C_T) values for all samples were fitted onto a standard curve generated from specific standard templates to obtain respective expression level. Finally all expression levels were normalised to the house keeping gene 18S.

Table 2: Specific primer for RT-qPCR

Gene	Forward primer	Reverse primer	Size [bp]
ITGB1	5'-AGGTGGTTTCGATGCCATCAT-3'	5'-AAGTGAAACCCGGCATCTGTG-3'	105
18S	5'-GATCCATTGGAGGGCAAGTCT-3'	5'-CCAAGATCCAACTACGAGCTTTTT-3'	103

2.1.4.5.4 Cell lysate preparation and Western blotting

For Western blotting, three cell-laden GelMA/HA-based hydrogels after 14 days of 3D cell culture were harvested, pooled and digested for 1-1.5 h in 0.15% collagenase II (ScimaR) in DMEM media, centrifuged for 5 min, at 1200 rpm and pellet was resuspend in Radio immunoprecipitation assay (RIPA) buffer, supplemented with 0.1% protease inhibitor cocktail (Roche Diagnostic, Australia). Samples were homogenised using a syringe and thin needle, denaturated under reducing conditions (5% mercaptoethanol) for 10 min at 70 °C and loaded onto a 5% sodium dodecyl sulphate (SDS) polyacrylamide gel and separated by electrophoresis for 30 min 90 V and 75 V for 200 min at 4 °C in Towbin SDS-polyacrylamidegelelectrophoresis running buffer (25 mM 2-Amino-2-hydroxymethyl-propane-1,3-diol (TRIS), 192 mM glycine, 0.1% SDS). Proteins were transferred onto a nitrocellulose membrane (25 mM TRIS, 192 mM glycine, 20% methanol) for 2 h at 350 mA at 4 °C. The membrane was blocked for 1.5 h with Odyssey® blocking buffer (LI-COR Biosciences, Australia) and subsequently incubated with primary anti GAPDH (Abcam, 1:10,000 in Odyssey® buffer) and secondary Alexa680 conjugated rabbit IgG (1:5000, LI-COR, Biosciences in Odyssey® buffer) over night and 1.5 h at RT, respectively. Signals were detected using the Odyssey® system (LI-COR-Biosciences).

2.1.5 Tumour growth and the effect of anti-cancer treatment *in vivo*

The spheroid-based ovarian cancer animal model was conducted as reported before (Loessner *et al*. 2013). All animal experiments were performed in compliance with the *Australian Code of Practice for the Care and Use of Animals for Scientific Purposes* and approved by the University Animal Ethics Committee (QUT-0900001170, UQ-287-11). 3D cultures were prepared as above, and spheroids were grown for 10 days within GelMA-based hydrogels before implantation into 6 weeks old female NOD/SCID mice. Animals received spheroid-containing hydrogel implants adjacent to both ovaries after opening the ventral abdominal wall and the peritoneum (6 animals per group) and were monitored until the predetermined endpoint of 8 weeks was reached. After 4 weeks of tumour growth, animals were treated with paclitaxel (10 mg/kg; twice per week; Sigma-Aldrich) or ATN-161 (10 mg/kg; thrice per week; Peptisyntha, Belgium) or a combination of both anti-cancer drugs intraperitoneally over 4 weeks. DMSO and/or water served as control treatment. Tumour growth was assessed fortnightly via bioluminescence imaging (7.5 mg/mL D-luciferin, Caliper Life Sciences, US; Living Image® software v.4.3.1, Perkin Elmer). Images were obtained for each group of 3 mice per image with a 13 cm field of view, binning (resolution factor) of 8 (medium), f-stop = 1 and exposure time 0.5-15 sec. Data were analysed using a threshold set at 10% around each bioluminescent source to determine the amount of photons emitted within a given time and presented as radiance (photons/sec/cm^2/steridian) from a constant sized region of interest drawn over the murine abdomen. After 8 weeks, animals were sacrificed, and the tumour tissues were removed. Tumours were weighed, and their volume determined according to Tomayko and colleagues (Tomayko and Reynolds 1989).

2.2 Collagen-based hydrogels as 3D cell culture model system for high resolution microscopy

2.2.1 Cell culture

2.2.1.1 2D Cell cultures – Passages and media

COS7, a fibroblast cell line generated from a cell line derived from the African green monkey (*Cercopithecus aethiops*) (CV-1) by transforming cells with an origin defective SV-40 mutant virus (Gluzman 1981). Cells were cultured in DMEM media (Biochrom AG, Berlin, Germany), supplemented with 1% pen/strep (Sigma Aldrich, Munich, Germany) and 10% FCS (Sigma Aldrich, Munich, Germany) for 3-4 days at 37 °C/ 5% CO_2 till reaching 80% confluence. Cells were washed with PBS (PBS, 8 g/L sodium chloride, 0.2 g/L potassium chloride, 1.42 g/L

disodium hydrogen phosphate, 0.24 g/L potassium hydrogen phosphate; pH was adjusted with 1M sodium hydroxide to 7.4) and detached using Accutase solution (PAA, GE Healthcare, Freiburg, Germany). Reaction was stopped by diluting cells in media and required amount of cell suspension was transferred to a new cell culture flask. As selection marker for stable transfected cells, G418 (300 μg/mL) was used. Wild type cells were supplied from the Leibniz Institute DSMZ German Collection of Microorganisms and Cell cultures, Germany. Stable and transient transfected cells were generated using a lipid nanoparticle-based system (Lipofectamine®2000, Lifetechnologies, Darmstadt).

LNCaPs, a human prostate carcinoma cell line, was derived from the supraclavicular lymph node metastasis from a 50 year old prostate cancer patient (Horoszewicz *et al*. 1980). Cells are androgen sensitive and formation of multi-cellular aggregation in 3D was described previously (Sieh *et al*. 2012). Cells were cultured in Roswell Park Memorial Institute 1640 (RPMI) media (Biochrom AG, Berlin, Germany), supplemented with 10% FCS (Sigma Aldrich, Munich, Germany) and 1% pen/strep (Sigma Aldrich, Munich, Germany) for 3-4 days at 37 °C/ 5% CO_2 till reaching 60-80% confluence. Cells were detached using Trypsin (Sigma Aldrich, Munich, Germany), reaction was stopped by diluting cells in media and required amount of cell suspension was transferred into a new flask. Cells were supplied from Leibniz Institute DSMZ German Collection of Microorganisms and Cell cultures, Germany.

K562, a human erythroleukemic cell line was established from a 53 years old Female with chronic myelogenous leukemia (Lozzio and Lozzio 1977). This non-adherent cell line was cultured as suspension in RPMI media (Biochrom AG, Berlin, Germany) with 2% L-glutamine, 50 μg/mL Gentamycin (Sigma Aldrich, Munich, Germany) and 10% FCS (Sigma Aldrich, Munich, Germany) at 37 °C/ 5% CO_2. After 7 days, required amount of cell suspension was transferred into a new flask. Cells were a generous gift from Dr. J. Lausen, Georg Speyer Haus, Institute for Biomedical Research, Frankfurt a.M., Germany.

U2OS, originally named T2, a human osteosarcoma cell line was derived from a 15 year old girl in 1964. Cells were cultured in DMEM (Biochrom AG, Berlin, Germany), supplemented with 1% pen/strep (Sigma Aldrich, Munich, Germany), 1% non-essential amino acids (Invitrogen) and 10% FCS (Sigma Aldrich, Munich, Germany). U2OS wild type cells were cultured for 3-4 days at 37 °C/ 5% CO_2 till reaching 80% confluence. Cells were detached using Accutase (PAA, GE Healthcare, Freiburg, Germany) reaction was stopped by diluting cells in media and required amount of cell suspension was transferred into a new cell culture flask. Cells were a generous gift from Prof. Dr. Löbrich's group, TU Darmstadt, Darmstadt, Germany.

2.2.2 Preparation of small volume collagen-based hydrogels

Collagen-based hydrogels were prepared after the following:

Protocol I:

Hydrogels were prepared using rat tail collagen type-I (stock concentration: 5 mg/mL) (ibidi, Martinsried, Germany). Hydrogels containing 4 mg/mL were prepared by diluting collagen solution in 1x PBS and neutralised with 10x PBS and NaOH (0.1M). For on top cultures, cell-free hydrogels were prepared as mentioned above. After hydrogel formation occurred, cells were seeded on top of each collagen-based hydrogel.

Protocol II:

All other collagen-based hydrogels were prepared with rat tail collagen type-I (stock concentration: 3 mg/mL or 5 mg/mL, ibidi). Collagen solution was diluted to final concentration in 1x PBS, or cell suspension in media, neutralised with 10x PBS and 7.5% $NaHCO_3$. Final collagen concentrations in hydrogels ranged from 1.6-2.8 mg/mL.

All components were kept at 4 °C until hydrogel preparation, to apply equal gelation conditions for all experiments. To provide hydrogels with homogenous structures, all components were mixed carefully; to avoid formation of air bubbles. This precursor-solution was then immediately pipetted, at volumes of 5-100 μL drops, on glass coverslips and coverslips were placed into the incubator 37 °C/ 5% CO_2 for 30-45 min. Hydrogel formation was visible by a shift of hydrogel transparency to opaque when polymerisation occurred. All hydrogels were cultured at 37 °C/ 5% CO_2 for up to 21 days, with media change every 3-4 days.

2.2.2.1 Aminosilane coated coverslips - An adhesive surface for collagen-based hydrogels

Round coverslips (Ø 25 mm, Type 1/1.5; Hecht-Assisstent, Sondheim, Germany) were carefully washed in acetone (technical grade, 99%) for 15 min and dried afterwards for 15 min at RT. Aminosilane solution, (3-aminopropyl)trimethoxysilane (aminosilane; Sigma Aldrich) was prepared freshly; containing 2% (v/v) aminosilane in acetone and spincoated onto the dried, pre-cleaned coverslip. Coverslips were coated with 40 μL of the prepared aminosilane solution in a two-step process (step 1: 30 sec, 500 rpm, step 2: 30 sec, 3000 rpm), using a spincoater (PIN150, SPS Europe Spincoating, Putten, Netherlands) followed by two washing steps in H_2O each of 3 min. The coverslips were dried afterwards at RT and stored on a dry, dark, dust-free place until usage. Reaction is shown in Fig. 17.

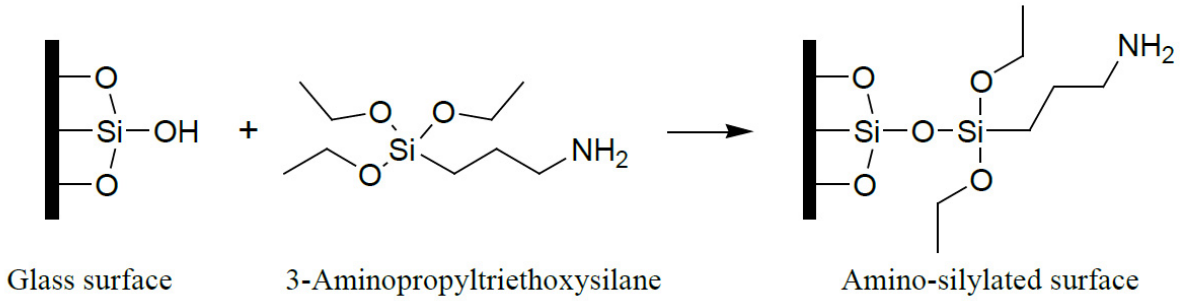

Figure 17: Preparation of aminosilane coated coverslips. NH_2 groups of 3-Aminopropyltriethoxysilane react with free hydroxyl groups of the glass surface, resulting in a stable coated surface. This coated surface provided binding sites for proteins, for example collagen, the reaction mechanism was adapted from (https://www.piercenet.com/instructions/2160905.pdf, 21/06/2014).

2.2.3 Characterisation of collagen-based hydrogels

2.2.3.1 Analysis of hydrogel structure– Confocal reflection microscopy

Unstained hydrogels were used for CRM on a CLSM (SP5, Leica Microsystems GmbH, Mannheim, Germany) thereby the back-scattered or reflected light, of structures with a different refractive index than their surroundings was collected. Samples were imaged with a HCX PL APO 63.0x1.20 W CORR UV or a PL APO 100.0x1.40 OIL UV objective. Samples were illuminated using a continuous wave argon laser, with a wavelength of 458 nm, 476 nm or 488 nm, respectively. The reflected light was detected with a photomultiplier tube (PMT) or a hybrid detection system (HyD).

2.2.3.2 Analysis of hydrogel structure – Confocal fluorescence microscopy

CFM analyses of hydrogel architecture were performed with fluorescently labelled hydrogels, after polymerisation. Hydrogels were incubated in Erioglaucine disodium salt (E133, Sigma Aldrich) or Sirius Red solution. E133 is an intensive blue dye used for various cosmetic and pharmaceutical application and consist of several aromatic groups with π–electrons (Fig. 18A), indicating its possible usage for fluorescence microscopic applications. Hydrogels were incubated for at least 10 min in E133 (100 μg/mL) and imaged using Em: 633 nm, Ex: 650-750 nm (CLSM, SP5, Leica).

Sirius red is an anionic light polarising dye, which binds specifically to collagen and is widely used for collagen labelling in tissue sections for histology approaches. Also this molecule consists of a large number of aromatic groups and several π electrons, indicating its possible usage for fluorescence imaging (Fig. 18B). Hydrogels were incubated for 60 min in Sirius Red solution (1mg/mL) before imaging using Em: 514 nm, Ex: 580-670 nm (CLSM, SP5, Leica).

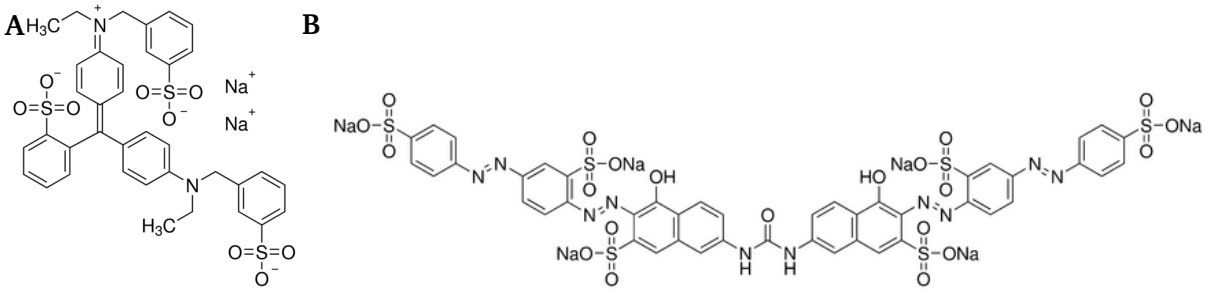

Figure 18: Molecular structure of E133 and Sirius Red. Shown is the molecular structure of E133 (A) and Sirius red (B). Molecular structures were adapted from (http://www.Sigmaaldrich.com, 25/06/2014).

2.2.3.3 Analysis of diffusion properties – Carboxylated microspheres

To model protein diffusion within a hydrogel, yellow-green carboxylated microspheres (Ø 20 nm, Life technologies) were used. The size of these microspheres were in the range of hydrodynamic radii of growth factors (Erickson 2009). Collagen-based hydrogels (2.8 mg/mL) were placed on top of a coverslip within a coverslip holder fitted to the motorised stage of a CLSM (SP5, Leica) and covered with a metal grid, to keep the hydrogel in place during imaging. Single microsphere suspension was prepared in PBS and added from the side to the hydrogel. Images of the same position were taken at various time points, during a time-span of 30 min, using CRM (collagen fibres) and CFM (microspheres), simultaneously. After 30 min, the hydrogel was placed back into microsphere solution and was fully immersed with microspheres suspension for further 72 h. The hydrogel was imaged afterwards again. Microspheres were exited at 488 nm and emission was detected at 505-540 nm and CRM signal was detected using illumination with 458 nm and detection of the CRM signals at 453-463 nm. Samples were imaged using a TCS SP5 CLSM (Leica) or a TCS SP (Leica), respectively.

2.2.1 Characterisation of single cells and multi-cellular aggregations

2.2.1.1 Analysis of cellular morphology in living cells – Plasma membrane staining

The plasma membrane was labelled using the membrane staining Cellmask™ Orange (Life technologies). This probe is based on amphipathic molecules. Thereby a combination of a lipophilic and a negatively charged, hydrophilic part results in optimal properties for plasma membrane loading and stable attachment to the plasma membrane in most cell lines (Rossignol *et al*. 2009). For membrane staining, cells were stained with Cellmask™ Orange in PBS (1-5 μg/mL) for 10-15 min, washed and imaged in PBS. CellmaskOrange™ was excited at

561 nm and emission was detected at 575-620 nm. Samples were imaged using a TCS SP5 CLSM or a TCS SP (Leica), respectively.

2.2.1.2 Analysis of cellular compartments – Fusion proteins

Cells were seeded on top of a coverslip or directly on the bottom of a well plate. Cells were cultured till reaching 70-90% confluence at time of transfection. For transfection Lipofectamine®2000 (Life technologies) was used, followed the protocol provided by the company. Briefly, DNA and Lipofectamine®2000 were mixed separately with serum free media. Both solutions were mixed independently, incubated for 5 min, combined, mixed, incubated for 20 min and added to media of cultured cells. Media, containing Lipofectamine®2000 and DNA was removed after 6-8 h and replaced with standard media. Stable transfected COS7 cells, were cultured in media supplemented with 300 μg/mL G418 as selective marker, treatment started 7 days after transfection.

Green fluorescent protein (GFP) variants and homologues are widely used as fusion protein for investigations on living cells (Chudakov *et al*. 2010). Here, the plasma membrane was stained, using a fusion protein consisting of the minimal anchor domain of the human H-Ras protein family (CAAX-motif) (Wright and Philips 2006), and enhanced GFP (EGFP). This resulted in plasma membrane staining from the cytosolic side, by anchoring in the inner leaflet of the plasma membrane and has been used successfully in living cells (Schaaf *et al*. 2009). The CAAX construct in the vector pCDNA3.1 tagged with enhanced GFP (EGFP) was a generous gift of Prof. Thomas Schmidt (Universiteit Leiden, Leiden, The Netherlands). Fluorescence images were generated using Ex: 488 nm/Em: 505-540 nm.

The actin cytoskeleton (F-actin) was stained using a 17-amino-acid peptide (Lifeact), with specific F-actin binding properties. This peptide-sequence was heterologous expressed as C-terminal GFP2 fusion protein (ibidi GmbH, Planegg/Martinsried, Germany)(Riedl *et al*. 2008). Samples were imaged using a TCS SP5 CLSM or a TCS SP (Leica), respectively. Fluorescence images were generated using Ex: 488 nm, Em: 505-540 nm.

2.2.1.3 Analysis of cell viability - Fluorescent-based life dead assay

Samples were incubated in staining solution (10 μM Calcein AM /10 μM Ethidiumhomodimer1, in PBS) for 10 min, washed with PBS and imaged on a Leica SP5 CLSM using Ex: 488 nm/ Em: 505-550nm, 555-625 nm.

2.2.1.4 Analysis of cellular morphology and compartments – Transmissions electron microscopy

COS7 cells were grown up to 80% confluence in a T75 cell culture flask; cell pellet was washed twice with PBS and resuspended in PBS (2D sample). COS7 cell-laden collagen-based hydrogels were prepared as described earlier and hydrogels, 2 h after preparation, were used further (3D sample). Briefly samples were fixed with 2% glutaraldehyde in 0.1 M cacodylate buffer (CaCo-buffer, pH 7.4) overnight. Samples were washed in CaCo-buffer and postfixed in CaCo-buffer containing 1% osmium and 1.5% potassium ferricyanide. After additional washing steps in CaCo buffer and H_2O, sample contrast was enhanced using 2%.uranylacetate in H_2O overnight. Samples were washed with H_2O, followed by graded acetone dehydration and embedded in Spurr's medium (Spurr 1969). Samples were transferred in fresh Spurr's medium and suspension was poured in small capsules and polymerised at 74 °C for 24 h. Ultrathin sections were obtained using an ultra-microtome with diamond knives (Ultracut R, Leica) and imaged using an TEM109 (Zeiss) at 80000 kV with the BioScan 792 camera (Gatan).

2.2.2 Single molecule microscopy

2.2.2.1 Single molecule acquisition

The microscopic analysis of the membrane patches was performed on a Nikon Eclipse Ti microscope (Nikon GmbH, Düsseldorf, Germany) equipped with an AndoriXon+ camera (Andor Technology Belfast, United Kingdom). CellMask™orange was excited with a 561 nm laser (Coherent, Dieburg, Germany) with an intensity of 2 kW/cm^2 for a duration of 5 ms. Images were acquired with a Nikon APO TIRF 100x/1.49 oil object lens. The open source software Micro Manager in Version 1.4.11 (www.micro-manager.org) in combination with a custom LabVIEW VI (virtual instrument; National Instruments Corporation, Austin, TX, USA), written by Sylvain Tchani, was used for controlling the Andor iXon+ camera and for acquiring the images with a frame rate of 20 Hz. Cells were cultured within hydrogels stably attached onto aminosilane coated coverslips. Samples were incubated in 0.1-5 ng/mL of CellMask™Orange for 10 min and imaged afterwards.

2.2.2.2 Single molecule detection and tracking analysis

Single molecules signals were detected and tracked using custom written image analysis software developed by Florian Lauer. Tracking routines within this analysis software were adapted from u-track routines developed in the Danuser lab (Jaqaman et al. 2008).

2.3 Software and Statistical analysis

- ImageJ (Schneider *et al*. 2012)
- Fiji (Schindelin *et al*. 2012)
    - Primary confocal datasets were processed using the ImageJ plugin "*Pure denoise*" (Luisier *et al*. 2010), where noted.
- Matlab2011a, Mathworks; Natick, MA, USA
- PASW Statistics v18, Quarry Bay, Hong Kong
- Statistical analyses were carried out using a two-way ANOVA including a Tukey test in the software package 'PASW Statistics' (v. 18). Results for all analyses with '*p*' value less than 0.05 were considered to indicate statistically significant differences.
- Mendeley, Mendeley Ltd., London, United Kingdom

3 Results

3.1 GelMA based hydrogels – a bioengineered 3D cell culture system suitable for cancer research

The following chapter describes the successful application of GelMA, a bioengineered semi-synthetic biomaterial, to establish a spheroid based ovarian cancer model system; providing a controllable 3D microenvironment for investigations on ovarian cancer cells *ex vivo* and *in vivo*. All results described in 3.1, except chapter 3.1.2.4, were published in a peer reviewed publication in Acta Biomaterialia 10(6):2551-2562, 2014.

3.1.1 Characterisation of GelMA-based hydrogels

3.1.1.1 GelMA concentration altered hydrogel stiffness but not diffusion properties

A major drawback of commonly used hydrogel systems is often that they are not well characterised and properties are less reproducible. To overcome these limitations a validation protocol for GelMA-based hydrogels was established, which allowed reproducible hydrogel properties followed by a standardised step by step hydrogel preparation protocol. A bioengineered 3D cell culture model system must provide mechanical support for cells but also providing stiffness and diffusion properties within a physiological range. Therefore stiffness and diffusion properties in dependency of GelMA concentration were analysed.

To characterise the hydrogel preparation, two parameters of biological relevance, namely stiffness and solute diffusion within the matrix, were assessed using unconfined compression tests and FRAP measurements. A previously reported results showed that hydrogel stiffness was a function of GelMA concentration, c, and UV-crosslinking time, t (equation 1) (Schuurman *et al*. 2013). The dry weight of the GelMA polymer within the hydrogel had only a minor influence on hydrogel swelling (Schuurman *et al*. 2013). For the used UV source, photo-initiator and mould, the empirical compression modulus (E, kPa) of hydrogels was based on the polymer concentration (c, 5-20% w/v) and UV exposure time (t, min):

$$E = 7955 * C^{2.28}\left(1 - e^{\left(\frac{4.2-t}{11.5}\right)}\right). \quad (1)$$

The compression moduli clearly revealed a positive correlation between polymer concentration and stiffness for the two different batches tested (Fig. 19A), which is in line with the reported empirical model (Schuurman *et al*. 2013). The compression modulus for

2.5% hydrogels was 0.5 ± 0.2 kPa (empirical model: 0.7 kPa), for 5% hydrogels 3.7 ± 0.5 kPa (empirical model: 3.4 kPa) and for 7% hydrogels 8.9 ± 1.8 kPa (empirical model: 7.3 kPa). Variability with respect to metabolic activity (no significant difference; $p = 0.2$), spheroid distribution and size was low, as indicated for 5% hydrogels of different batches for different time points (Sup. Fig. 1).

Solute diffusion was measured using FD70 representing relevant biomolecules, such as growth factors. The diffusion coefficients were determined by rFRAP, a method which allows quantitatively correct diffusion values in 3D samples (Deschout *et al*. 2010). In addition to a rectangular bleach area (red box), a rectangular fitting region (green box) and background region (blue box) was defined (Fig. 19B). Within the fitting area, the spatial intensity distribution was mathematically described for each time point of the recovery sequence (Fig. 19C). In addition to the intensity, this spatial information of the bleach profile was used to obtain the recovery curve (Fig. 19D). In the last analysis step, a fit to the recovery curve yielded in the diffusion coefficient, which is a measure of the mobility of the diffusing components and the mobile fraction of the diffusing molecule, including molecules that contribute to the recovery within the FRAP region of interest (ROI) (Fig. 19E). The mobile fraction was quantified by the percentage of total fluorescence recovery (plateau of the fitted recovery curve) of initial fluorescence intensity in images taken prior to bleaching. As a control for the accuracy of the FRAP method, FD70 was measured in water, as the expected diffusion coefficient for this sample was calculated using the Stokes-Einstein Equation:

$$D = \frac{kT}{6\pi\eta r_H}. \qquad (2)$$

Hydrodynamic radii (r_H) were calculated according to the empirical formula for dextran (Braeckmans *et al*. 2003):

$$r_H = 0.015\, M_W^{0.53\,\pm 0.02}. \qquad (3)$$

Equation 3 gives a hydrodynamic radius for FD70 of 5.55 nm. The shaded blue area denoted the range of possible diffusion coefficients that resulted from the molecular mass distribution of FD70. According to the manufacturer, the mean molecular mass of FD70 was 63-77 kDa as measured by size exclusion chromatography. This yielded hydrodynamic radii for FD70 ranging from 5.25-5.83 nm. Assuming a 10% error in the hydrodynamic radius for FD70, a range of expected diffusion coefficients in the FRAP calibration experiment across a range of

temperatures were plotted (Fig. 19F). The mobile fraction of FD70 in water was 1. For hydrogels, values were close to 1, indicating that the majority of FD70 was mobile within the hydrogel. For the concentration range from 0% (water calibration) to 7% GelMA a linear decrease in the diffusion coefficient was observed. However, diffusion into hydrogels was a fast process, and FD70 did not interact with GelMA structures, indicated by mobile fractions close to 1 in all samples tested (Fig. 19F). These findings suggest that the polymer concentration was linked to the hydrogel stiffness but only marginally to the diffusive properties.

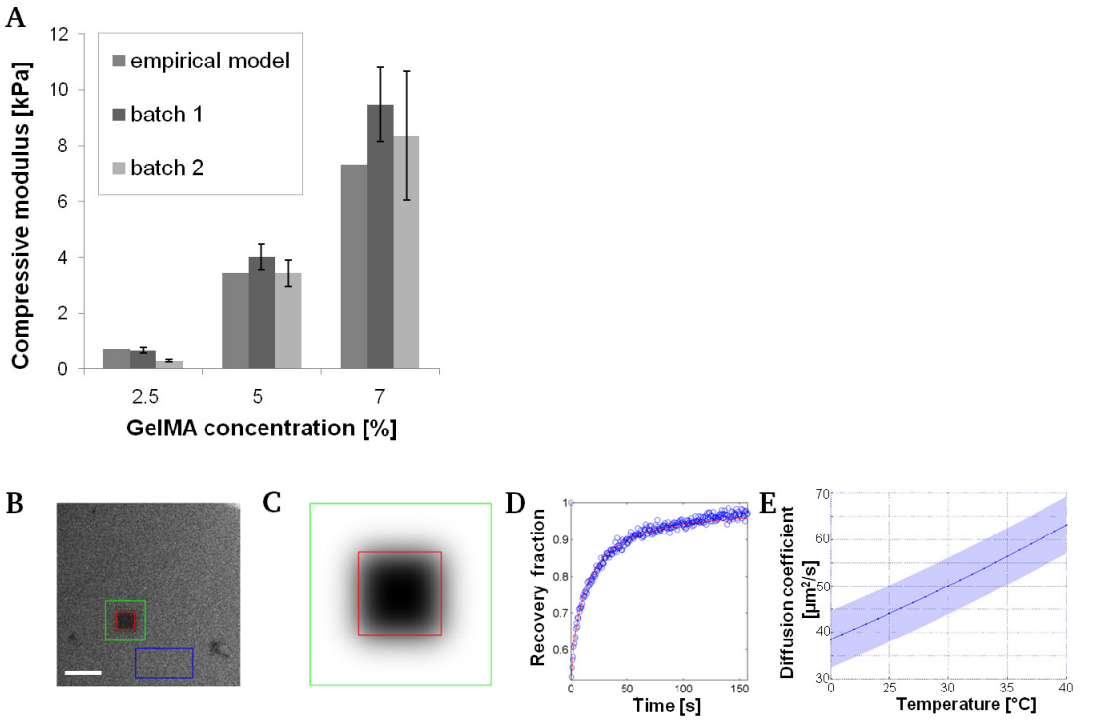

F

GelMA concentration [%]	0 (water)	2.5	5	7
Diffusion coefficient ± SD [µm²/s]	39.2 ± 2.8	29.9 ± 3.3	23.4 ± 4.8	16.9*
Mobile fraction ± SD	1.01 ± 0.01	0.97 ± 0.01	1.01 ± 0.01	0.95*

* Average out of two values

Figure 19: Compressive moduli indicated that increasing polymer concentrations resulted in stiffer hydrogels, but only minor influenced diffusion properties. Hydrogels of two independent batches were tested (n = 5-8 hydrogels for each batch, error bars denoted SD) (A). The measured compressive moduli were in accordance with the reported empirical model (Schuurman *et al.* 2013a). Diffusion coefficients were determined by FRAP measurements on fluorescent dextran (FD70) absorbed in GelMA-based hydrogels (B-E). Within a rectangular ROI (red box), FD70 was bleached, and the recovery of fluorescent intensity was monitored in an additional fitting (green box) and background (blue box) region. Scale bar, 100 μm (B). The spatial intensity distribution

within the fitting area was determined for each time point of the recovery sequence (C). In addition to the intensity, the spatial information of the bleach profile was used to obtain the recovery curve (D), which yielded in the diffusion coefficient and mobile fraction of the diffusing biomolecules. The method was validated against measurements of FD70 in water. Calculations following equations 2 and 3 predict the theoretical diffusion coefficient of FD70 in water (straight line) and upper and lower boundaries for an error in the hydrodynamic radius (r_H) of 10% (E). Diffusion coefficients and mobile fractions indicated a decreasing diffusion rate upon increasing polymer concentrations, while the mobile fraction was unchanged and close to 1 for all experiments (F).

3.1.1.2 Cell encapsulation did not alter diffusion properties

Local microenvironmental changes play a key role in tumour growth and are limiting factors in 3D cell culture systems (Cushing and Anseth 2007; Park *et al*. 2000). Hence, FRAP measurements within cell-laden hydrogels at various time points were performed to determine potential cell-related changes to the diffusive properties of the hydrogels. Therefore, ovarian cancer cells were embedded within GelMA-based hydrogels and FRAP measurements using FD70 were performed on day 1, 7, 14 and 21 of 3D culture. Cell-free hydrogels incubated for the same time in culture media served as controls. As spheroids were formed out of single cells after 7 days, the bleaching ROI was placed next to a single cell on day 1 and next to a spheroid on day 7, 14, and 21 of 3D culture (Fig. 20A-B). Cell-free hydrogels showed a slightly increase in diffusion coefficients over time. Higher diffusion coefficients were detected in cell-laden hydrogels compared to cell-free hydrogels, in particular on day 7. However, a comparison between diffusion coefficients over all time points showed diffusion values for FD70 without significant difference comparing cell-laden with cell-free hydrogels ($p = 0.8$) and each day ($p = 0.3$). The measured average of the diffusion coefficient for cell-free hydrogels was 27.1 ± 4.8 and for cell-laden hydrogels 30.2 ± 4.6; the values scattered around the mutual mean of 28.5 ± 4.9 $\mu m^2/s$ in all conditions tested (Fig. 20C-D). These findings suggest that diffusion was not influenced by the culture time or presence of cells or spheroids indicating that the structural hydrogel properties were not altered outside the spheroid volumes.

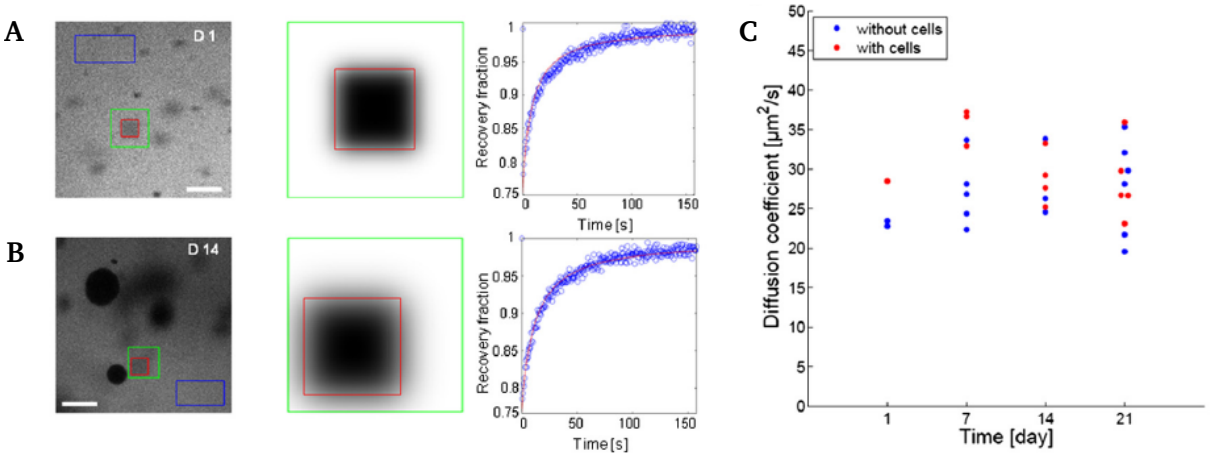

D

	condition	Day 1	Day 7	Day 14	Day 21
Diffusion coefficient ± SD [µm²/s]	with cells	28.5	35.6 ± 2.3	28.8 ± 3.4	28.5 ± 4.8
	without cells	23.1*	27.1 ± 4.3	28.2 ± 4.9	27.8 ± 6.1
Mobile fraction ± SD	with cells	1.03	1.02 ± 0.01	1.02 ± 0.02	1.00 ± 0.01
	without cells	1.02*	1.02 ± 0.01	1.01 ± 0.02	1.02 ± 0.03

* Average of two values

Figure 20: Diffusion properties were not influenced by growing spheroids. A representative image of a cell-laden hydrogel at day 1 is shown (left panel) (A). Diffusion coefficients were measured, as described earlier, within the rectangular bleached ROI next to a single cell (red box), the data were analysed within the fitting area (green box) and the determined background area (blue box; middle panel), and a recovery curve was obtained (right panel). Scale bar, 100 μm. A representative image of a FRAP measurement at day 14 of spheroid formation is shown (B). The bleached area was chosen next to a growing spheroid (red box). All measurements were performed at several time points (day 1, 7, 14 and 21) of 3D culture. Scale bar, 100 μm. The diffusion coefficients were determined for cell-free and cell-laden hydrogels that were prepared on the same day and cultured at the same conditions (C). Diffusion coefficients were relatively constant over the incubation period of 21 days (D). A comparison between diffusion coefficients showed no significant difference between cell-laden and cell-free hydrogels (p = 0.8) at each time point (p = 0.3) (D). The mobile fraction was close to 1 for all experiments (D).

3.1.2 Characterisation of ovarian cancer spheroids *in vitro*

3.1.2.1 Spheroid formation and morphology was a function of hydrogel stiffness

A previous study demonstrated that the biomaterial stiffness has a high impact on cell behaviour; spheroid morphology was dependent on matrix stiffness, and proliferation decreased with increasing hydrogel stiffness (Loessner *et al.* 2010). The stiffness of GelMA-

based hydrogels was a function of polymer concentration as shown above, which allows the modification of the stiffness by changing the amount of polymer dry weight. Hence, hydrogels with 2.5, 5, 7 and 10% GelMA concentration, with - according to the empirical model (Schuurman *et al*. 2013) (equation 1) - stiffnesses of 0.7, 3.4, 7.3 and 16.5 kPa were examined. Maximal projections of CLSM images showed a single cell distribution on day 1 for all conditions tested (Fig. 21A, top panel). Already at early time points, differences of cell morphology in dependency of the hydrogel stiffness were observed. On day 7 of 3D culture, low stiffness (2.5%, 0.7 kPa) resulted in loose cell aggregation and cell migration out of these aggregates, while in stiff (7%, 7.3 kPa; 10%, 16.5 kPa) hydrogels smaller and inhomogeneous-shaped spheroids were formed. In contrast, in medium stiff (5%, 3.4 kPa) hydrogels, distinctive round and compact spheroids were formed (Fig. 21A, middle panel). The spheroid size increased from day 7 to day 14 of 3D culture (Fig. 21A, bottom panel), which was also observed using bright field microscopy (Fig. 21B).

An increase in metabolic activity, indicative of cell proliferation, from day 1 to day 7 was observed across all conditions tested. While the metabolic activity from day 7 to day 14 was constant or increased in soft and medium stiff (2.5%, 0.7 kPa; 5%, 3.4 kPa) hydrogels, stiff (7%, 7.3 kPa; 10%, 16.5 kPa) hydrogels resulted in a constant or decreased metabolic activity (Fig. 21C). The same effect was observed for the DNA content, indicative of cell proliferation, in 3D cultures up to 21 days (Fig. 21D).

In replicate experiments, a high variation of the metabolic activity and DNA content, and the formation of cell monolayers on the surface of the plastic culture dishes used for 3D cultures, was noticed, in particular for hydrogels cultured over 14 and 21 days. However, the highest reproducibility over time in metabolic activity, DNA content and morphology was detected in 5% hydrogels. Consequently, for all further experiments, a 5% GelMA concentration was chosen as it promoted a consistent spheroid growth and reproducible cell behaviours (Sup. Fig. 1). Overall, these findings suggest that a high polymer concentration inhibited spheroid growth, while low concentrations stimulated migration showing a high dependence of cell proliferation and spheroid formation on the mechanical properties of the extracellular microenvironment.

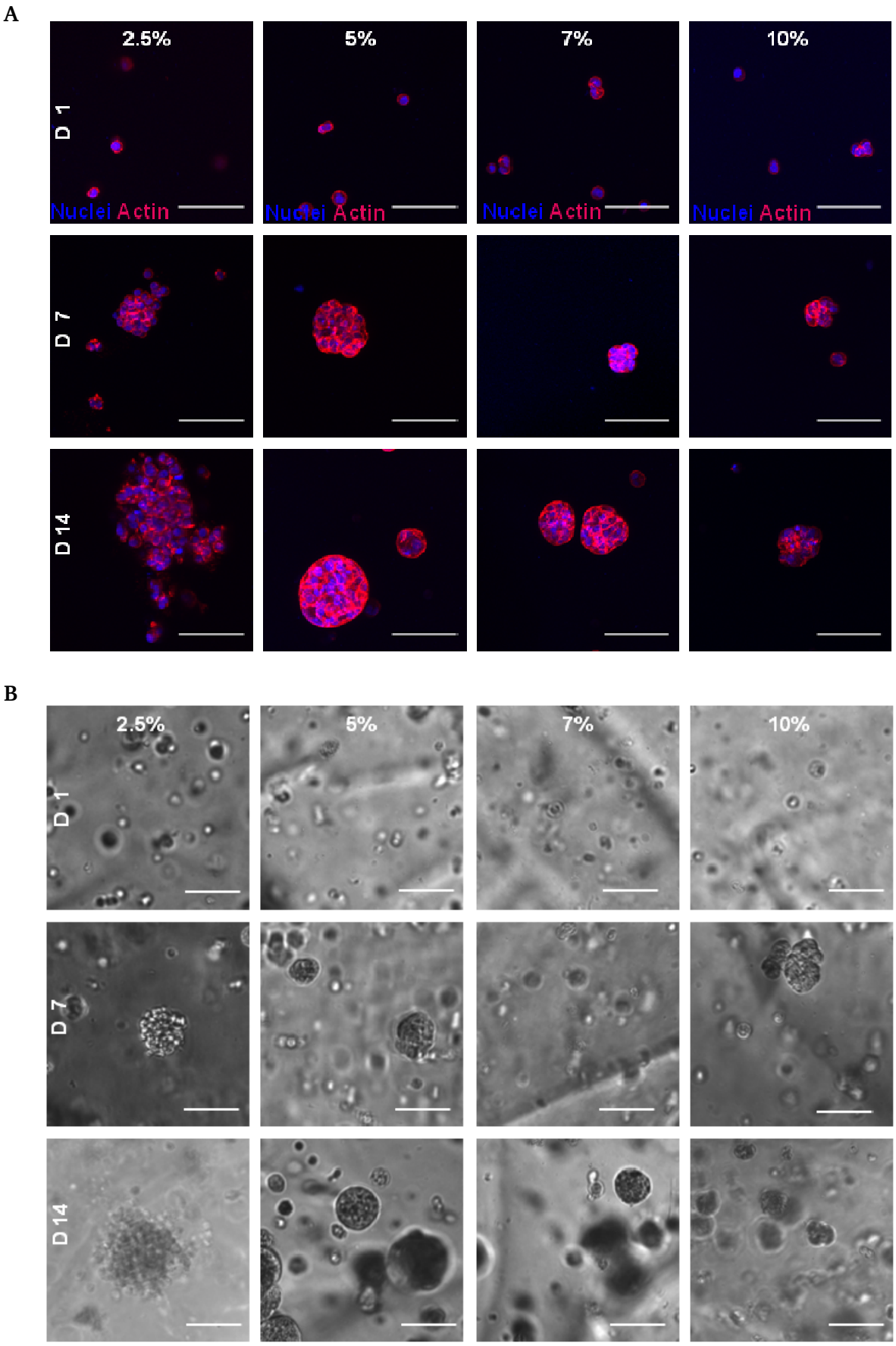
A
2.5%
5%
7%
10%
D 1
D 7
D 14
Nuclei Actin
B
2.5%
5%
7%
10%
D 1
D 7
D 14

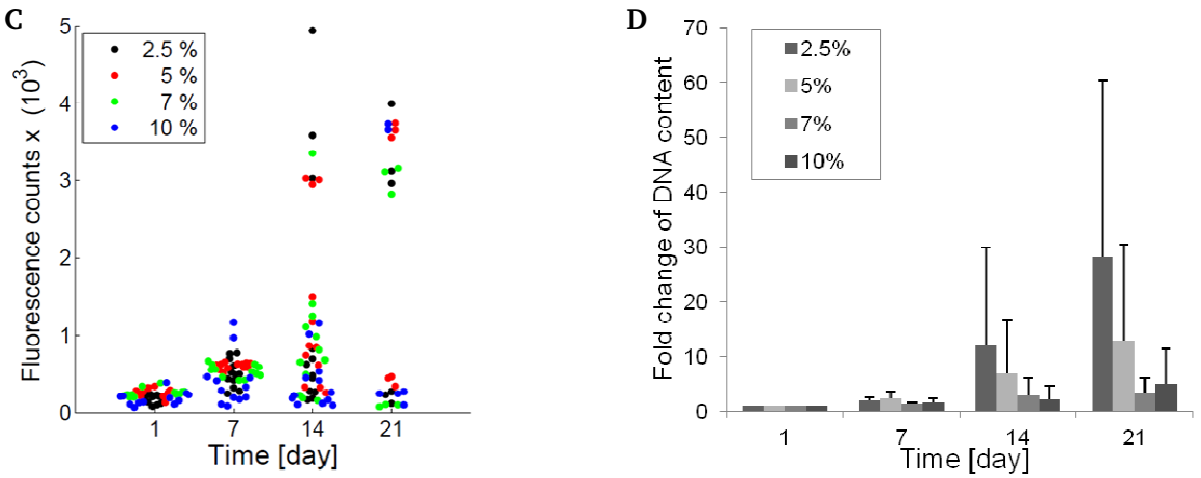

Figure 21: Spheroid morphology, metabolic activity and proliferation were depended on GelMA concentration. Representative maximal projections of CLSM images of cells embedded within hydrogels of various polymer concentrations (2.5%, 0.7 kPa; 5%, 3.4 kPa; 7%, 7.3 kPa and 10%, 16.5 kPa) are shown, with nuclei stained in blue and actin cytoskeleton in red (A). A single cell distribution was present on day 1 in all conditions of 3D culture (top panel). A low GelMA concentration (2.5%, 0.7 kPa) resulted in loose cell aggregates, whereas high GelMA concentrations (7%, 7.3 kPa; 10%, 16.5 kPa) caused smaller spheroids after 7 days (middle panel) and 14 days (bottom panel). The medium GelMA concentration (5%, 3.4 kPa) led to well defined and round-shaped spheroids. Scale bars, 100 μm. Representative bright field images of cells embedded within hydrogels of various polymer concentrations (as above) are shown (B). Scale bars, 100 μm. An increase in metabolic activity, indicative of spheroid proliferation, from day 1 to day 7 was observed in all conditions tested (C). An enhanced metabolic activity was detected in soft hydrogels compared to stiff hydrogels (n = 4 for day 1-14; n = 2 for day 21). The DNA content increased from day 1 to day 7 (D). From day 7 to day 21 of 3D culture, a higher DNA content was detected in soft hydrogels compared to stiff hydrogels (D). Shown are mean values, normalised to day 1 (n = 4 for day 1-14; n = 2 for day 21) (D).

3.1.2.2 MMP inhibition decreased spheroid growth and metabolic activity

Changes of the local microenvironment mediated by cell-secreted proteases, such as MMPs, play a key function in cell growth and matrix remodelling (Loessner *et al.* 2010). Therefore, spheroid-containing hydrogels (5%, 3.4 kPa) were treated with culture media supplemented with a broad-band MMP-inhibitor (20 μM). MMP inhibition resulted in smaller spheroids compared to controls as indicated by maximal projections of CLSM images and H/E staining (Fig. 22A). Immunostaining of cytokeratin-8, an epithelial marker, MMP-9 and integrin α6 revealed the expression of these proteins in the presence and absence of the MMP-inhibitor (Fig. 22B). Inhibition of MMPs resulted not only in smaller spheroid size, but also decreased

proliferation rates significantly indicated as metabolic activity ($p < 0.001$; Fig. 22C) and DNA content ($p < 0.001$; Fig. 22D). These findings suggest that cell growth and spheroid size were a function of biomaterial degradability.

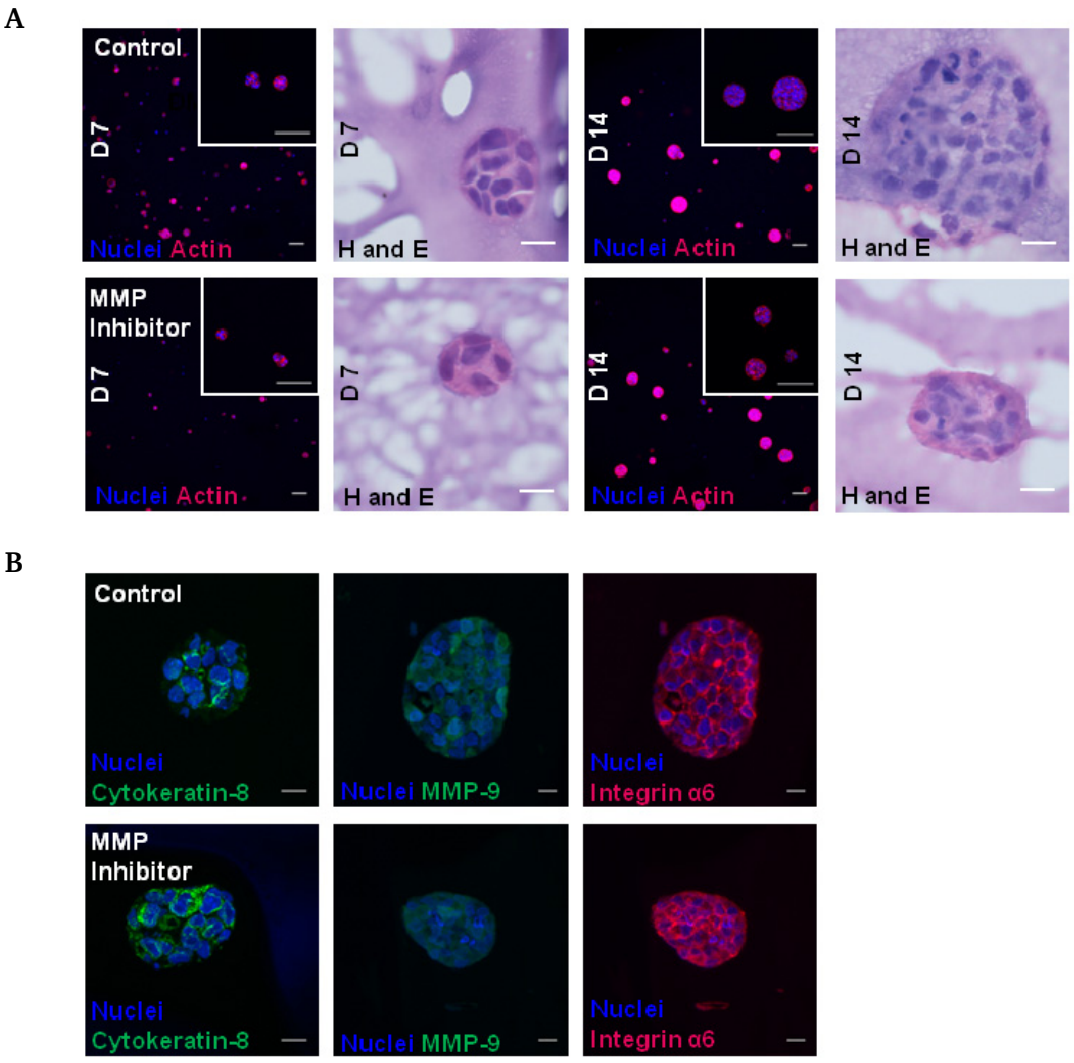

Figure 22: MMP inhibition resulted in smaller spheroids, reduced metabolic activity and proliferation of spheroids. Maximal projections of CLSM images, with nuclei stained in blue and actin cytoskeleton in red, and H/E staining of hydrogels are shown on day 7 and day 14 with and without MMP inhibition (A). MMP inhibition resulted in smaller spheroids compared to non-treated controls. Scale bars, 100 μm, H/E staining 10 μm. Immunostaining of cytokeratin-8, MMP-9 and integrin α6 is shown with and without MMP inhibition; proteins stained in green or red and nuclei in blue (B). Protein expression was detected independent of MMP inhibition. Scale bars, 10 μm. The metabolic activity upon MMP inhibition was reduced compared to controls after 21 days of 3D culture (n = 3, $p < 0.001$) (C). MMP inhibition resulted in a reduced DNA content on day 7 up to day 21 compared to controls. Shown are mean values, normalised to day 1 (n = 3, $p < 0.001$) (D).

3.1.2.3 Additional ECM components altered spheroid behaviour

The biomaterial GelMA offers the opportunity to modify its cell functional features by additional cell binding sites by mixing natural ECM components to the polymer solution. Here, the effects of LN-411 (20 μg/mL) and/or HA (0.1%) on hydrogel stiffness, diffusion and spheroid proliferation were examined. Maximal projections of CLSM images of spheroid growth within hydrogels containing additional components, separately or in combination, showed a single cell distribution on day 1 and spheroid growth by day 14 of 3D culture (Fig. 23A). Bright field images indicated a different hydrogel structure by addition of HA to GelMA, resulting in larger macro-pores and a heterogeneous polymer-network within the hydrogels (Sup. Fig. 2). Compression moduli of hydrogels containing LN-411, HA or the combination of both were increased compared to controls (5%, 4.0 ± 0.5 kPa). The incorporation of HA increased the hydrogel stiffness by 77% (7.1 ± 0.7 kPa) compared to controls, while the combination of HA and LN-411 by 58% (6.4 ± 0.5 kPa), and LN-411 alone by 31% (5.3 ± 0.7 kPa; Fig. 23B). The metabolic activity increased from day 1 to day 7 in all conditions tested. The metabolic activity changed over time and a significant difference between 5% GelMA controls compared to LN-411- ($p = 0.02$), HA- ($p < 0.001$)) and LN-411/HA-containing hydrogels ($p < 0.001$) was observed. However, after 21 days of 3D culture, the metabolic activity was reduced in LN-411- and HA-containing hydrogels. Control hydrogels showed an increase in metabolic activity from day 1 to day 21 of 3D culture, but with an overall decreased activity compared to hydrogels containing LN-411 and HA (Fig. 23C). The same effect was visible in the DNA content, which was increased in hydrogels with additional components after 14 days of 3D culture compared to controls. An increase in the DNA content was observed in all conditions from day 1 to day 7. The comparison over time showed a significant difference in DNA content between 5% GelMA controls and

hydrogels with the additional components HA (p = 0.001) and LN-411/HA (p = 0.003). There was no difference between controls and LN-411-containing hydrogels (p = 0.49). However, there was a decreased DNA content after 21 days of 3D culture in LN-411- and HA-containing hydrogels compared to controls (Fig. 23D). The positive effect of the addition of ECM components on spheroid proliferation was more pronounced upon HA incorporation compared to LN-411 (Fig. 23C-D). Diffusion properties were not influenced by the addition of these ECM components (Fig. 23E). These findings suggest that spheroid growth is a function of the ECM components LN-411 and HA, with HA displaying a greater spheroid growth-promoting effect.

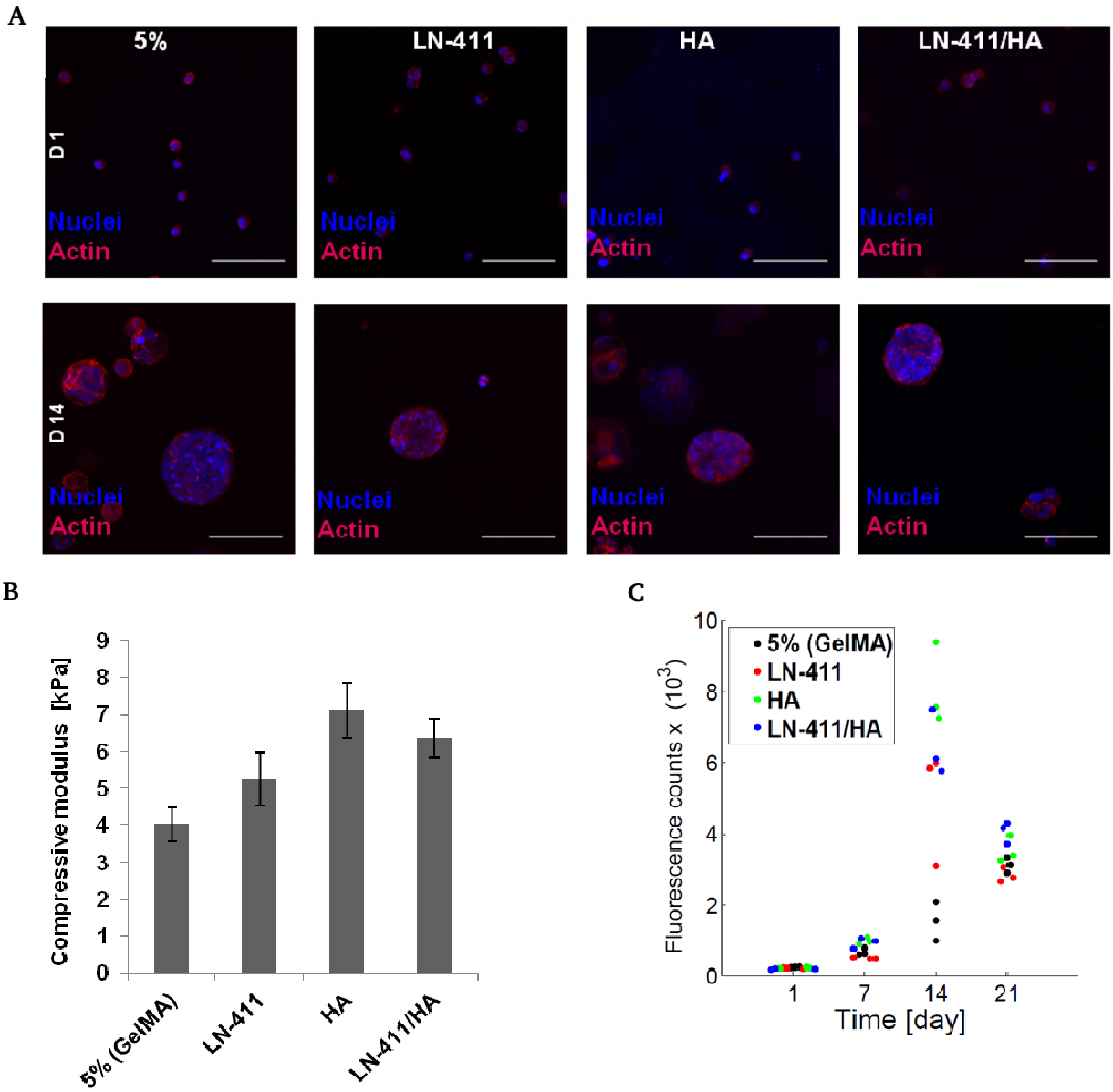

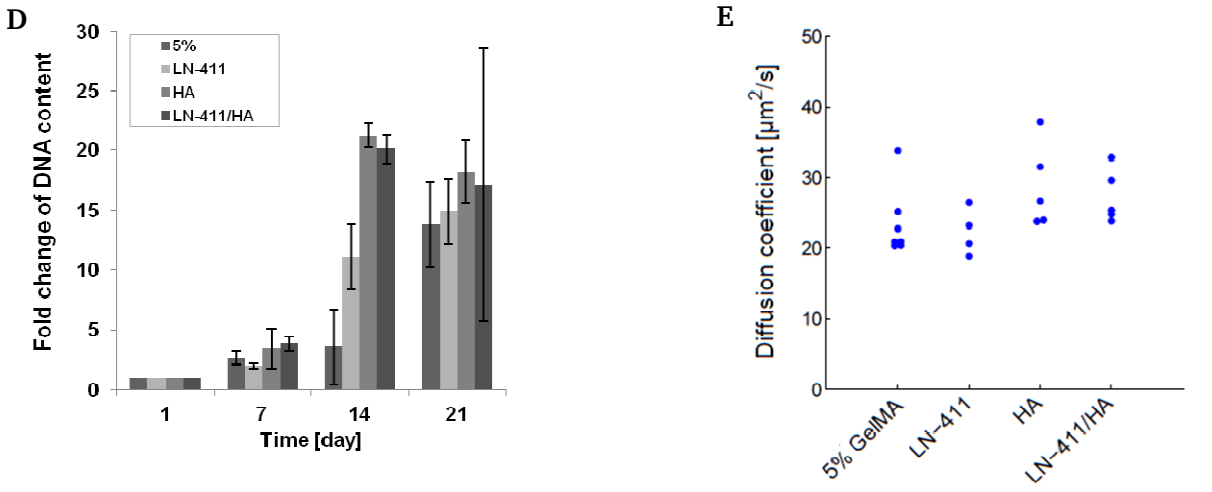

Figure 23: LN-411 and HA increased hydrogel stiffness, metabolic activity and proliferation of spheroids. Maximal projections of CLSM images indicated spheroid formation upon LN-411 and HA incorporation into hydrogels on day 1 (top panel) and day 14 (bottom panel); nuclei stained in blue and actin cytoskeleton in red (A). Scale bars, 100 μm. The addition of the ECM components LN-411 and HA into hydrogels increased stiffness compared to 5% GelMA controls (4.0 ± 0.5 kPa) (B). The metabolic activity was significantly different in hydrogels containing LN-411 (p = 0.02), HA (p < 0.001) and LN-411/HA (p < 0.001) over time compared to controls (C). The incorporation of LN-411 and HA into hydrogels increased the DNA content compared to controls. Shown are mean values, normalised to day 1 (n = 3). The DNA content was significantly different in hydrogels containing HA (p = 0.001) and LN-411/HA (p = 0.003) over time compared to controls (D). There was no significant difference between LN-411-containing and control hydrogels (p = 0.49). The diffusion properties were not influenced by addition of LN-411 and HA and were in the range of solute diffusion of FD70 measured in 5% GelMA controls (E).

3.1.2.4 RNA and protein extraction of GelMA-embedded ovarian cancer cells was possible

Cellular reaction to microenvironmental changes, often go along with up- and down regulation in gene expression and protein levels. For the analysis of differentially gene expression and protein levels, RNA and proteins have to be extracted from cells. This can be challenging using a 3D cell culture system. RNA extraction from 3D cultured cells within GelMA-based hydrogels has been established for cartilage cells (Levett *et al*. 2014); however not for cancer spheroids grown in this hydrogel system. Here the expression level of integrin β1 in ovarian cancer cells grown in 2D and 3D was analysed. Increased integrin β1 expression and integrin β1-mediated signalling is highly involved in cancer cell growth, metastatic progression and cellular resistance to anti-cancer treatment (Cordes and Park 2007; Desgrosellier and Cheresh 2010; Nam *et al*. 2009). Therefore as reported previously mRNA

was isolated from cell-laden GelMA/HA-based hydrogels, using the micro column extraction method (Loessner *et al*. 2010), after 14 days of 3D culture. The extracted mRNA was of high purity and concentration and hence used for cDNA synthesis and RT-qPCR. As negative control, cell-free GelMA/HA-based hydrogels cultured in parallel were used. The mRNA level was normalised to the house keeping gene 18S and compared to OV-MZ-6 cells cultured as monolayer (2D) and within PEG-based hydrogels (3D). Interestingly, cells cultured within GelMA/HA-based hydrogels showed an increased integrin β1 level. Thereby integrin β1 level (was 3.5 times higher compared to monolayer cultures (2D) and 5.8 times higher compared to cells cultured within PEG-based hydrogels (3D) (Fig. 24A). In cell-free hydrogels, as expected, no integrin β1 signal was detected. The level of integrin β1 mRNA expression varied between 2D and 3D cell cultures and also between different 3D cell culture systems (Fig. 24A). This indicates that integrin β1 expression is correlated with properties of the microenvironment.

To extract proteins of cells encapsulated within hydrogels, several protocols have been used. However up to now, no protocol is available for GelMA/HA-based hydrogels. Previous applied protocols using the flow through from the RNA extraction method for protein isolation (Loessner *et al*. 2013), failed in extracting proteins from OV-MZ-6 cells grown within GelMA/HA-based hydrogels. Therefore a protein extraction protocol for cells grown within these hydrogels had to be established and optimised. Hydrogels were enzymatically digested with collagenase II to generate cell lysates for Western Blotting. Glycerinaldedhyde-3-phosphate-dehydrogenase (GAPDH), a glycolysis enzyme with a molecular mass of 37 kDA, a general expressed cellular protein was chosen as protein of interest. Cell lysates from OV-MZ-6 cultured in monolayers (2D) served as positive and cell-free GelMA/HA-based hydrogels cultured in parallel served as negative control. GAPDH was detected in all cell-laden hydrogels. In cell-free samples, no GAPDH signal was detectable (Fig. 24B). This finding demonstrates that proteins were successfully isolated from cells encapsulated within GelMA/HA-based hydrogels after hydrogel digestion. Additionally, after hydrogel digestion no unspecific signals originated from the hydrogel-material itself were detectable (Fig. 24B). In conclusion, the mRNA expression pattern and protein levels of ovarian cancer spheroids grown within GelMA-based hydrogels can be analysed using RT-qPCR and Western Blotting, which was shown here for the first time.

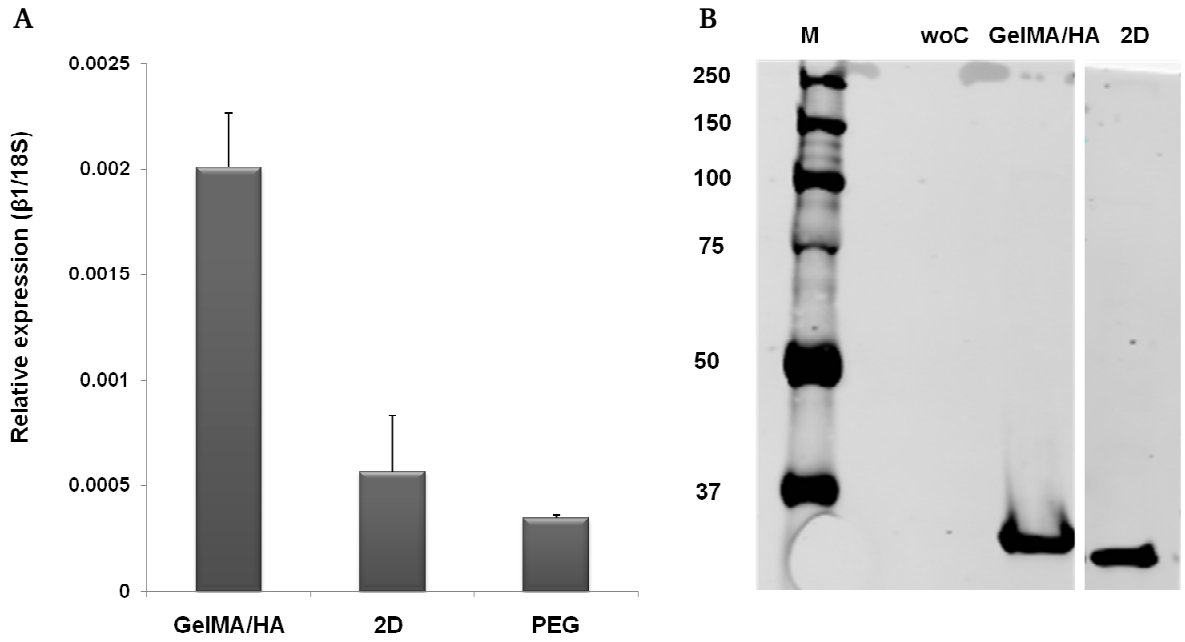

Figure 24: Results of mRNA and protein extraction of OV-MZ-6 cells, embedded in GelMA/HA-based hydrogels. Cell-laden GelMA/HA-based hydrogels cultured for 14 days were analysed. Cell-free GelMA/HA-based hydrogels (woC) served as negative control, OV-MZ-6 cultured as monolayer (2D) and within a PEG-based hydrogel system as positive control (A). All RNA levels were normalised to 18S level (denoted SD (β1/18S, A). Cells cultured within GelMA/HA-based hydrogels showed an increased expression level of integrin β1 compared to 2D and 3D control sample, no specific integrin β1-signal was detected in cell-free control (A). Western blotting revealed GAPDH detection in cell lysate extracted from OV-MZ-6 cells embedded in GelMA/HA-based hydrogels after protein extraction using a method based on collagenase II digestion. GAPDH band from cell-laden GelMA/HA-based hydrogels (GelMA/HA) was at similar height as in positive monolayer control (2D), no band was detected in negative, cell-free control (woC) (B).

3.1.3 Tumour growth and effect of anti-cancer treatment *in vivo*

3.1.3.1 Tumour formation was induced by pre-cultured GelMA-based hydrogels *in vivo* – successfully used for *in vivo* testing of chemo-therapeutics

To investigate whether spheroid-containing hydrogels can induce tumour formation and growth *in vivo*, spheroids were grown for 2 weeks within GelMA-based hydrogels (5%, 3.4 kPa) prior to implantation into mice, adjacent to each ovary (Fig. 25A). Spheroid-containing hydrogels induced tumour formation and peritoneal spread over 8 weeks detected by bioluminescence imaging (Sup. Fig. 3). To study the responsiveness of tumour-bearing mice towards paclitaxel, ATN-161 and the combination of both, treatment started 4 weeks after implantation of the hydrogels. DMSO and/or water served as control treatment. Animals

of the control group developed tumours on the right and left implantation site next to the ovary, with evidence of tumour fluid (ascites) and metastatic spread to the omentum, liver and colon (Fig. 25B-D, Sup. Fig. 3). Paclitaxel treatment decreased tumour growth by 33% and prevented the development of tumour fluid (ascites) and metastatic outgrowth (Fig. 25B, 25D). The combined treatment of paclitaxel and ATN-161 reduced tumour growth by 37.8% compared to controls, while ATN-161 alone had no effect on tumour growth (Fig. 25C-D). These findings suggest that intraperitoneal implantation of spheroid-containing hydrogels promoted tumour formation, growth and metastasis, which were reduced upon paclitaxel but not ATN-161 treatment.

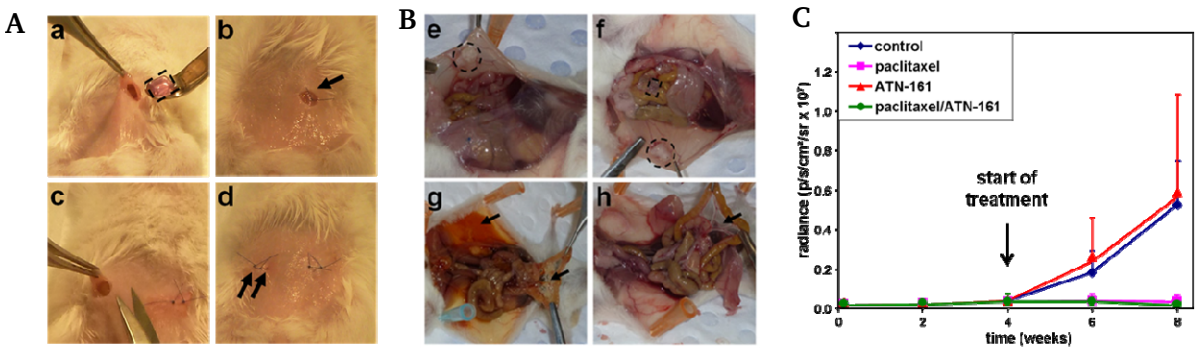

D

	no treatment	Paclitaxel	ATN-161	Paclitaxel/ ATN-161
animals per group	6	6	6	6
tumour fluid (ascites)	3/6	0/6	4/6	0/6
tumour width (mm)	4.7 ± 1.0	5.7 ± 1.0	4.9 ± 1.1	4.0 ± 1.2
tumour length (mm)	6.2 ± 2.0	7.1 ± 0.8	6.5 ± 1.4	4.8 ± 1.8
tumour volume (mm^3)	122.6 ± 66.2	82.1 ± 41.8	138.6 ± 83.6	76.3 ± 36.7
treatment response (%)		33	no response; increased tumour growth by 13.1	37.8
radiance ($p/s/cm^2/sr$)	$5.3x10^6 \pm 2.2x10^6$	$3.4x10^5 \pm 2.8x10^5$	$5.6x10^6 \pm 5.0x10^6$	$1.5x10^5 \pm 1.1x10^5$
Evidence of metastasis (intestine, liver, spleen)	6/6	0/6	6/6	0/6

Figure 25: Spheroid-based implants resulted in tumour formation and peritoneal spread that were reduced by paclitaxel treatment. The surgical procedure was carried out by a left incision to implant the rectangular-shaped, spheroid-containing hydrogel adjacent to the ovary (a) (A). After implantation, the abdominal wall and skin were closed (b) (A). Then, a right incision was made to implant a second hydrogel (c), and the abdominal wall and skin sutured (d) (A). Animals were sacrificed 8 weeks after implantation and tumours developed on the right (e) and left (f) implantation site (B). Evidence of tumour fluid (ascites; arrow) and metastatic spread (arrow) was visible without paclitaxel treatment (g) (B). Upon paclitaxel treatment, neither

tumour fluid (ascites) nor metastatic outgrowth was detected (h) (B). Tumour growth, indicated as radiance, was reduced upon paclitaxel and combined paclitaxel/ATN-161 treatment starting in week 4 after implantation compared to ATN-161 treatment alone and controls (DMSO and/or water) (C). ATN-161 had no effect on tumour growth compared to controls (C). A significant reduction in tumour growth was observed upon paclitaxel alone ($p = 0.003$) and combined paclitaxel/ATN-161 ($p = 0.002$) treatment compared to non-treated controls. There was no significant difference in tumour growth upon ATN-161 treatment alone compared to non-treated controls ($p = 0.95$) and between paclitaxel alone and its combination treatment with ATN-161 ($p = 0.99$) (C). Luciferase-transfected ovarian cancer spheroids (bioluminescence $9.1x10^5 \pm 1.6x10^5$) were implanted into mice and caused formation of tumours over the monitored time frame (D). Paclitaxel and ATN-161 responsiveness was calculated as percentage of change in tumour volume compared to non-treated conditions (D). While paclitaxel and its combination with ATN-161 resulted in a treatment response of 33-37.8%, ATN-161 alone had no effect on tumour growth and peritoneal spread (D).

3.2 Collagen-based hydrogels – a bioengineered 3D cell culture system suitable for high resolution microscopy

To gain insights into native spatio-temporal molecular dynamics of the plasma membrane within a living cell in a physiological context, also high resolution microscopy, i.e. single molecule detection (SMD) has to be performed within a 3D microenvironment. The following chapter introduces a small volume collagen-based hydrogel system for single molecule microscopy, including characterisation of basic hydrogel and cellular parameters, improvement of image acquisition and the final application in an experimental approach for single molecule detection in the plasma membrane of hydrogel-embedded cells.

3.2.1 Preparation of small volume collagen-based hydrogels

3.2.1.1 Stable attachment of collagen-based hydrogels on coverslips resulted in suitable samples for high resolution microscopy

Collagen-based hydrogels were prepared by pipetting a collagen precursor solution on top of a coverslip within a 6 well plate (Fig. 26A). Hydrogels were polymerised for 30 - 45 min, complete polymerisation was indicated by opacity of the hydrogel (Fig. 26A) and reaction was stopped by addition of media. This preparation resulted in round, small volume collagen-based hydrogels of reproducible diameter and shape, controllable by volume of collagen precursor solution used (Fig. 26A). The so prepared hydrogels were very fragile and not stably attached onto non-treated coverslips. During transferring samples, media change and imaging, hydrogels became loose. This resulted most often in hydrogels with high drift rate

during imaging and deformed shapes (Fig. 26B). This highly affected imaging quality of fibrillar architecture, especially seen during imaging over longer time frames and tile scanning (Fig. 26B). Not only the imaging quality over time was influenced, also a drifting sample does not allow single molecule detection with high position accuracy. To overcome these limitations, coated coverslips were tested. The best results were achieved using a coverslip surface coating based on aminosilane. This aminosilane coating resulted in an adhesive surface for collagen-based hydrogels (Fig. 27A), which allowed robust immobilisation over time and drift free imaging of hydrogels (Fig. 27B,C). Hydrogel immobilisation was stable for several weeks, in media/PBS at 37 °C/ 5% CO_2 and non-affected by sample transfer or media change. Hydrogels after 4 weeks were still stable attached and drift free imaging of hydrogel network was possible (Fig. 27B,C).

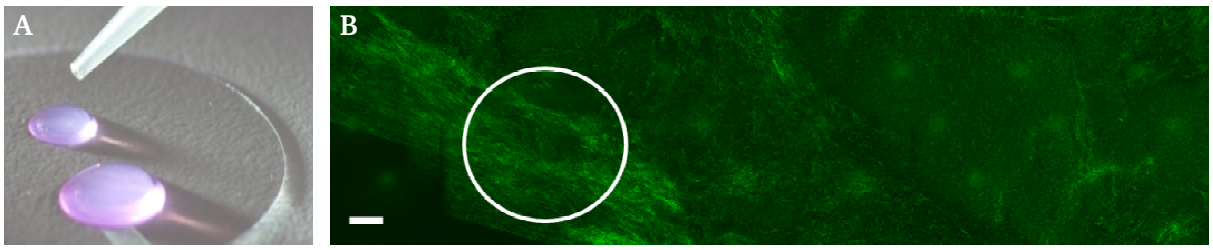

Figure 26: Collagen-based hydrogels on non-treated coverslips. Collagen-based hydrogels polymerised on a non-treated coverslip resulted in small round shaped hydrogels, with controllable size, but not stably attached onto coverslip surface (A). A representative CRM image, of such a hydrogel (2.8 mg/mL collagen; 2 h after preparation; fully immersed in PBS during imaging) showed a deformed hydrogel network, as indicated by white circle (B). The image was generated using the Leica tile scan module; assembling multiple images into a larger overview image (B). Scale bar: 100 μm.

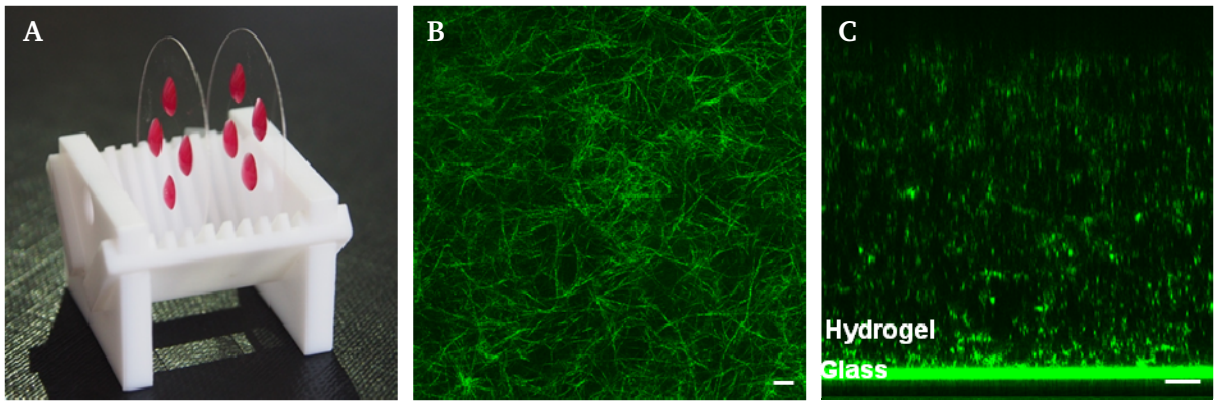

Figure 27: Collagen-based hydrogels on aminosilane coated, adhesive coverslips. Collagen-based hydrogels polymerised on aminosilane coated coverslip surface resulted in round hydrogels, with controllable size, stably attached to the coverslip surface (A). This stable attachment allowed transferring of the sample (A) and drift free imaging (B,C). Shown is a representative

CRM image of a stably attached collagen-based hydrogel (2 mg/mL collagen, 4 weeks after preparation, fully immersed in PBS during imaging) scanned in lateral, xy (B) and axial, xz direction (C). Scale bar: 10 μm.

3.2.2 Characterisation of hydrogel properties

3.2.2.1 E133 and Sirius Red – Fluorescent dyes for imaging of hydrogel structure

CRM allowed detection of fibrillar structures such as collagen fibres on a single photon microscope. However, major disadvantages commonly referred to CRM are that collagen fibres are only detected if they are in a certain angle to the detector and CRM is only possible within certain distances to the coverslip (Artym 2010; Jawerth *et al.* 2010). Fluorescently pre-labelled tropocollagen on the other hand is commercially available, but cost- intensive, the perfect ratio of labelled tropocollagen has to be found and labelling might interfere with hydrogel polymerisation (Franke *et al*. 2014). An alternative, low-cost, simple, post-polymerisation staining method is needed. The performances of two dyes, E133 (Fig. 28) and Sirius Red (Fig. 29) were tested as staining method for collagen-based hydrogels. Both dyes are commercially available and low-cost articles; however not tested for fluorescence microscopically approaches yet.

E133 showed the best fluorescent properties, using excitation at 633 nm and emission detection between 650-750 nm. Collagen-based hydrogels (2.8 mg/mL) were imaged after incubation in E133 solution (100 μg/mL, 10-30 min), washed with PBS and fully immersed in PBS during imaging with CRM (Fig. 28A) and CFM (Fig. 28B) simultaneously. The overlay image, generated from the CRM image and the CFM image, showed that both methods were able to detect collagen fibres (Fig. 28C). However, CFM showed a higher detection rate of collagen fibres (Fig. 28C). CFM allowed detection of discrete fibres better and fibre detection independent from fibre angle (Fig. 28D-F). Achieved contrast in the CFM image (Fig. 28E) was higher, compared to CRM images (Fig. 28D). Single collagen fibres were resolved more accurately using CFM and the overall fibre network was represented better, compared to CRM images (Fig. 28C, F). Next to collagen-based hydrogels, labelling performance of E133 on GelMA-based hydrogels (Fig. 28G) was tested, using the protocol described earlier. E133 was successfully applied as post-polymerisation fluorescence labelling of GelMA-based hydrogels (Fig. 28H). The CFM image showed a homogenous, dense non-fibrillar hydrogel structure (Fig. 28I). In contrary to collagen-based hydrogels, no further structural details using CFM and E133 were attained in GelMA-based hydrogels (Fig. 28I).

Sirius Red showed best fluorescence properties using emission of 514 nm and excitation of 580-660 nm. For imaging, collagen-based hydrogels were incubated in Sirius Red solution (1mg/mL, 60 min) washed and imaged with CRM and CFM simultaneously. To test if Sirius Red detects specifically collagen fibres, cell-laden hydrogels were used (2 mg/mL, with U2OS cells, Fig. 29). Compared to the CRM image (Fig. 29A), again CFM image gained with Sirius Red (Fig. 29B) showed a higher detection rate of collagen fibres (Fig. 29C). CFM allowed a better detection of discrete fibres and fibre detection independent from fibre position to the detector (Fig. 29D-F). Using CRM no differentiation between structures of different origin, was possible (Fig. 29D). This was achieved using Sirius Red, which allowed specific detection of collagen fibres (Fig. 29E).

Overall, the usage of E133 showed a higher detection rate of collagen fibres than CRM and good photo-emission properties, which allowed using low dye-concentration, less incubation time and low laser intensity, compatible with live cell imaging. The emission in the far red spectra is not interfering with widely used cellular labelling in green and red. In contrast to CRM, CFM with E133 is not restricted to fibrillar structures. This allowed labelling of non-fibrillar hydrogels, such as GelMA-based hydrogels. Although, applying of Sirius Red resulted in a collagen specific labelling, this dye had a very low photo-emission. To compensate this, a high dye concentration, long incubation time (60 min) and usage of high laser intensities was needed. This reduced the cell viability dramatically, as recognised in cellular blebbing, shown in the bright field image (Fig. 29G). Therefore for all further experiments, in regards to imaging of collagen fibres, CRM and/or CFM (E133) were used.

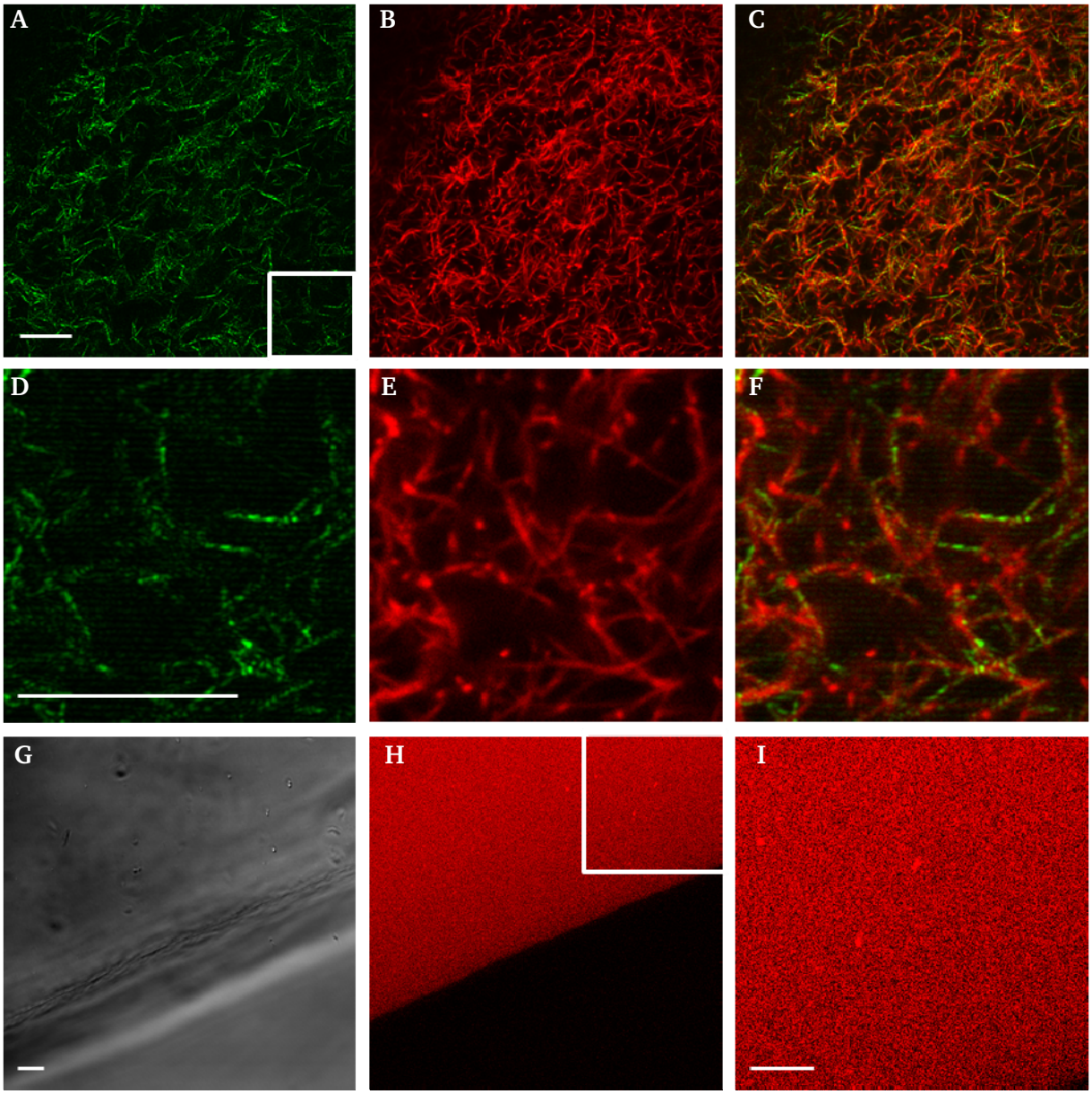

Figure 28: Hydrogel structures imaged with CRM and CFM (E133). The architecture of a collagen-based hydrogel (2.8 mg/mL, 2 hours after preparation, fully immersed in PBS) was imaged using CRM (A) and CFM (B) simultaneously. The overlay of both channels is shown in (C) and a higher magnification (area indicated with white square) in (D-F). The overlay showed that within the CFM image more fibres were detected and a higher contrast between fibres and background was achieved (C, F). GelMA-based hydrogels (10%, 7 days after preparation, fully immersed in PBS) (G) have been successfully labelled with E133 (H); however no further structural information, were observed, as shown in the higher magnified image (white square) (I). Scale bars: 10 μm.

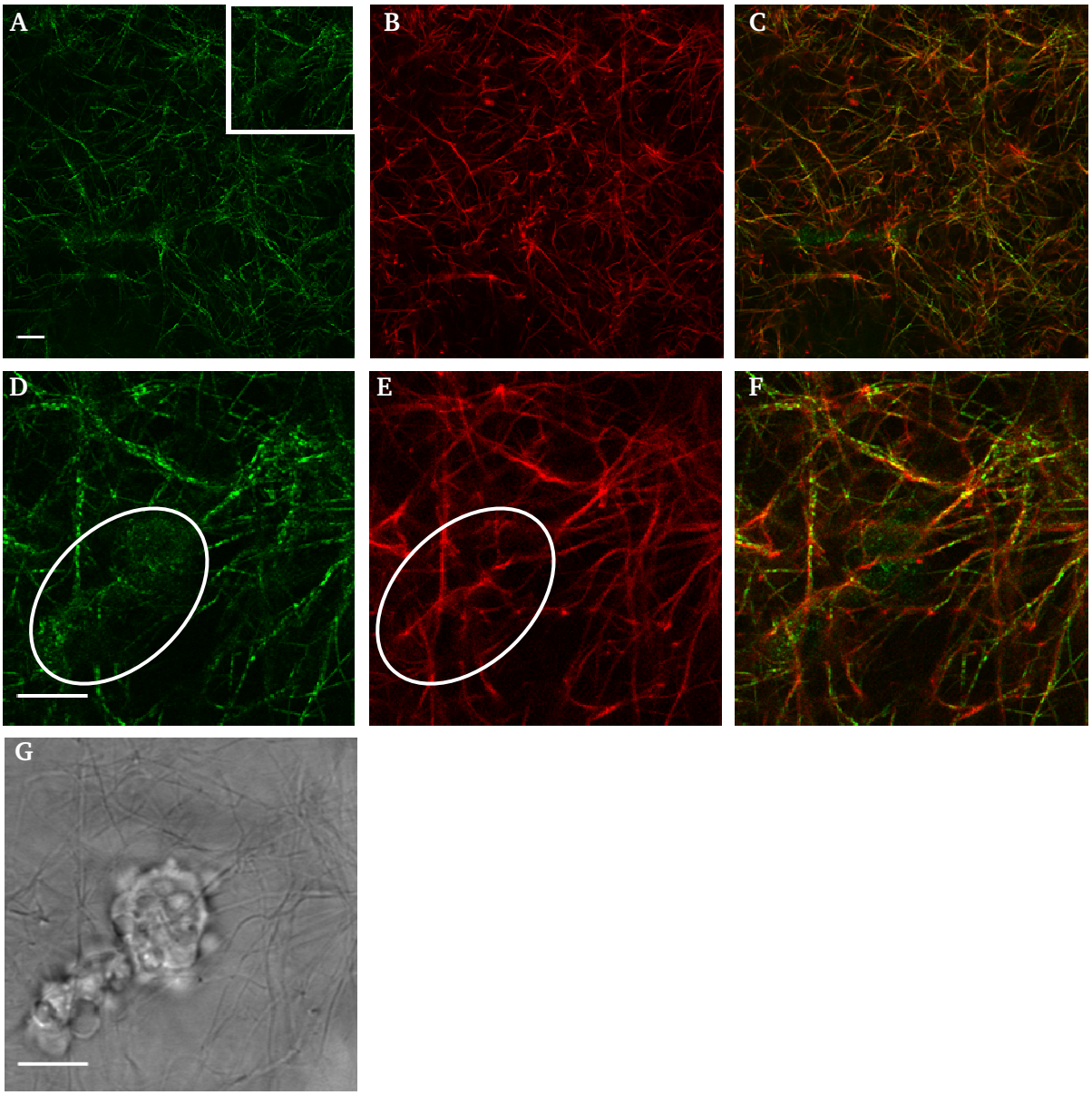

Figure 29: Hydrogel structures imaged with CRM and CFM (Sirius Red). The architecture of a collagen-based hydrogel (2 mg/mL, 2 hours after preparation, fully immersed in PBS) was imaged using CRM (A) and CFM (B) simultaneously. The overlay of both channels is shown in (C) and a higher magnification (area, indicated with white square) in (D-F). The overlay showed that within the CFM image more fibres were detected and a higher contrast between fibres and background was achieved (C, F). A higher magnification (indicated with white square) showed that CRM did not differentiate between structures of different origin (D). In a cell-laden hydrogel, signals from collagen network and cells (indicated with white circle) were detected (D). In contrary, in the CFM image, only collagen fibres were detected (E).The bright field image of this area showed that labelling with Sirius Red affected cellular viability, indicated by cellular blebbing (G). Scale bars: 10 μm.

3.2.2.2 Probing hydrogel pores – Diffusion properties were a function of particle and matrix surface characteristics

Diffusion within a hydrogel is dependent on size exclusion; furthermore it is known that also properties of the hydrogel and the diffusing particle have an effect (Lieleg and Ribbeck 2011). To mimic realistic protein diffusion within a collagen-based hydrogel, carboxylated microspheres (Ø 20 nm) were chosen as model particles. A single-microspheres-suspension was prepared and added from one side to the hydrogel (on non-treated coverslip surface, to avoid binding of carboxylated particles to glass surface). The hydrogel was covered with a metal grid to keep it in position and imaged with CRM (Fig. 30, left column) and CFM (Fig. 30, mid column). In addition the overlay of both channels is shown (Fig. 30, right column). Diffusion was observed over 30 min, then the hydrogel was incubated over 72 h within the microsphere solution and imaged again (Fig. 30J-O). The solution contained single mircospheres (Fig. 30B). By reaching the collagen-based hydrogel, the hydrogel acted as physical barrier and slowed down the particles (Fig. 30C). Moreover microspheres bound to the collagen fibres, till the outer hydrogel area was saturated (Fig. 30C). When more microspheres from the solution reached the already saturated hydrogel edge (Fig. 30C), this yielded into an expanded microsphere diffusion front along the collagen fibres, reaching regions deeper within the hydrogel (Fig. 30F). Particle diffusion along collagen fibres was thereby a very homogenous process over time, forced by a defined diffusion front (Fig. 30B,F,I). However, a fast permeation through hydrogel pores and within the hydrogel centre was not observed (Fig. 30A-I). After 30 min, particles were only found in the outer hydrogel area within the first 20 μm away from the hydrogel-edge (Fig. 30I). After 72 h, particles were also found in the hydrogel centre (Fig. 30L); however, a particle gradient from outer to inner parts of the hydrogel was still present (Fig. 30O). Microspheres bound stable to collagen fibres and showed diffusion along collagen fibres and not through collagen pores (Fig. 30O). These results indicate that within a more physiological 3D hydrogel-based cell culture system more than size-selective filtering occurs and surface properties directly affect diffusion properties.

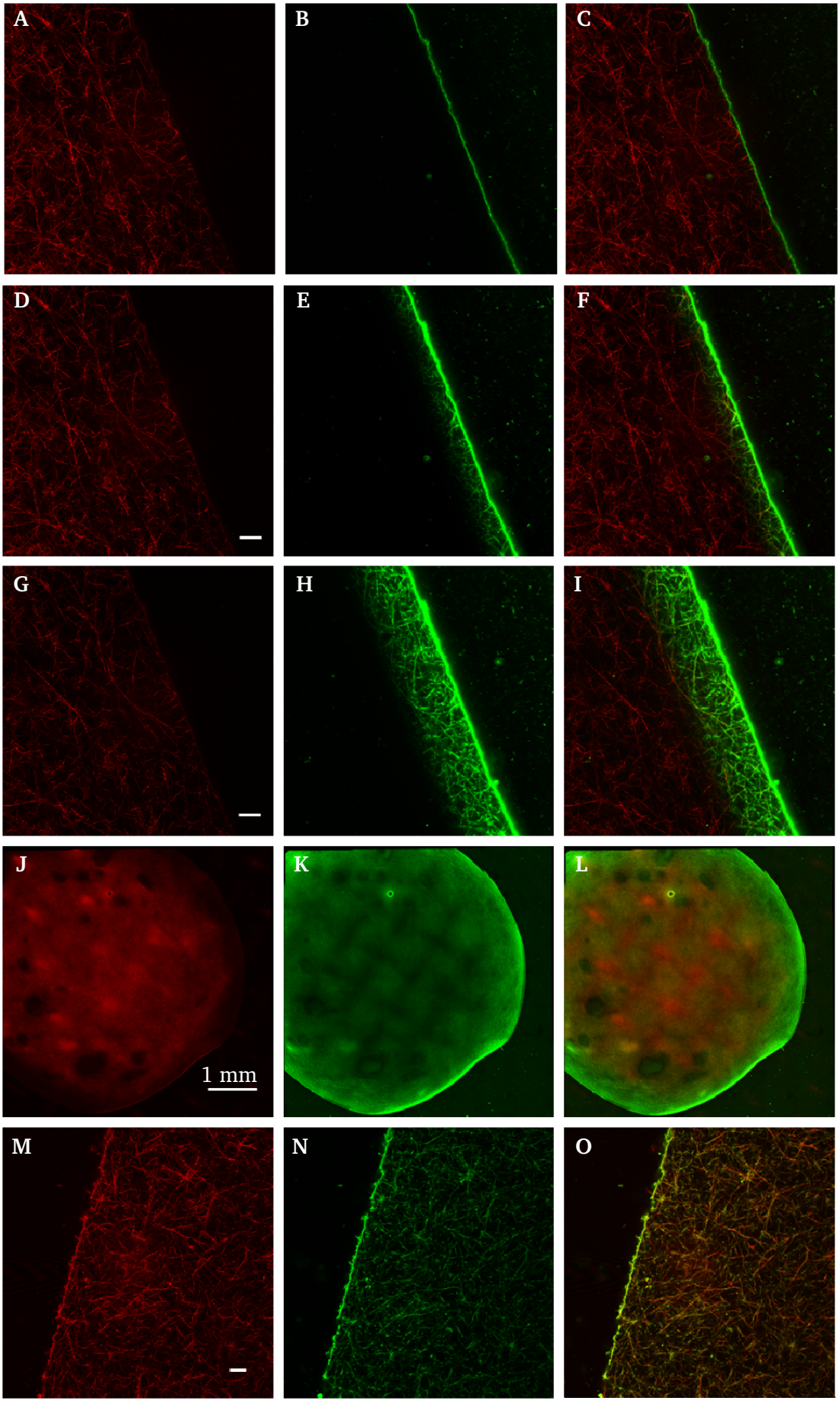
A
B
C
D
E
F
G
H
I
J
K
L
1 mm
M
N
O

Figure 30: Diffusion of microspheres into a collagen-based hydrogel. Diffusion measurements were performed using CRM (collagen fibres) and CFM (Ø20 nm, fluorescent microspheres). Shown is the CRM signal of collagen fibres in red (left column), the CFM signal of particles in green (middle column) and overlay of both channels in yellow (right column). Hydrogel was imaged at the start of the experiment (A-C), after 12:30 min (D-F) and after 30 min (G-I) at the same position. The hydrogel was imaged again after 72 h (J-O). Particles did not diffuse through hydrogel pores; they bound to the collagen fibres and showed motion along collagen fibres. Scale bar: 10 μm, unless noted otherwise.

3.2.3 Characterisation of single cells and multi-cellular aggregates

3.2.3.1 Small volume collagen-based hydrogels were successfully utilised for short and long-term cell cultures

The next step during the optimisation of this small volume collagen-based hydrogel system was the application for cell culture and investigations of its effect on cellular morphology. Therefore 3 widely used cell lines of different tissue origin, COS7 (fibroblast cells), LNCaPs (epithelial cells) and a non-adherent cell line, K562 (lymphoblast cells) were encapsulated in collagen-based hydrogels (2.8 mg/mL) and imaged after 3-5 days of culture (Fig. 31). Cells grown in 2D conditions on glass and in suspension served as control (Fig. 31).

COS7 cells showed an elongated, very flat cell shape, when cultured on glass (Fig. 31A). This morphology changed dramatically within a collagen-based hydrogel. Cells increased their surface and formed large multi-directional filopodia, which resulted in a highly branched cellular shape (Fig. 31D).

LNCaPs showed a polygonal shape on glass, fully attached to substrate in discrete multi-cellular patches (Fig. 31B). When cells were cultured within a collagen-based hydrogel, cells showed a round shape and formed large irregular-shaped multi-cellular aggregates (Fig. 31E).

K562 were cultured in suspension and imaged after cells settled down onto the glass surface (Fig. 31C). Cells showed a spherical shape and did not adhere to the surface (Fig. 31C). When these cells were cultured within a soft collagen-based hydrogel, no morphological change was observed (Fig. 31F).

Small volume hydrogels were successfully used for culture of 3 different cell types. This first experiment indicated that cell morphology of attached, adherent cells is highly influenced by the local microenvironment and changed when cells were cultured on a stiff, 2D substrate or within a soft, 3D substrate. In contrary, no effect of 2D or 3D culture conditions on the morphology of non-adherent, K562 cells was observed.

Next, small volume collagen-based hydrogels were used for long term cell cultures and the effect on imaging properties was analysed afterwards. LNCaPs, which form large irregular shaped cell aggregates when cultured in 3D, were encapsulated within collagen-based hydrogels (2.8 mg/mL) and imaged after 3 weeks of culture (Fig 31G-I). The plasma membrane of LNCaPs was labelled with CellMask™Orange and collagen fibres were stained with E133 (Fig. 31G-I). This approach showed that small volume collagen-based hydrogels were suitable for long term cultures. Also imaging of matrix and cell properties in hydrogels, containing large dense cell aggregates, was possible. Collagen fibres (E133) and cells (CellMask™Orange) were detectable (Fig. 31H,I); however, the overall imaging quality was decreased. In addition, it was observed that dead cells showed an accumulation of CellMask™Orange and E133 which had an impact on imaging quality (Fig. 31H,I).

This first experiment showed that small volume collagen-based hydrogels provided a 3D cell culture system suitable for various cell lines and compatible with short and long-term cell culture approaches; however imaging quality was decreased after long-term cultures (Fig. 31G-I). To investigate basic cellular properties, i.e. morphology and cellular organisation further, COS7 cells and earlier time-points were chosen.

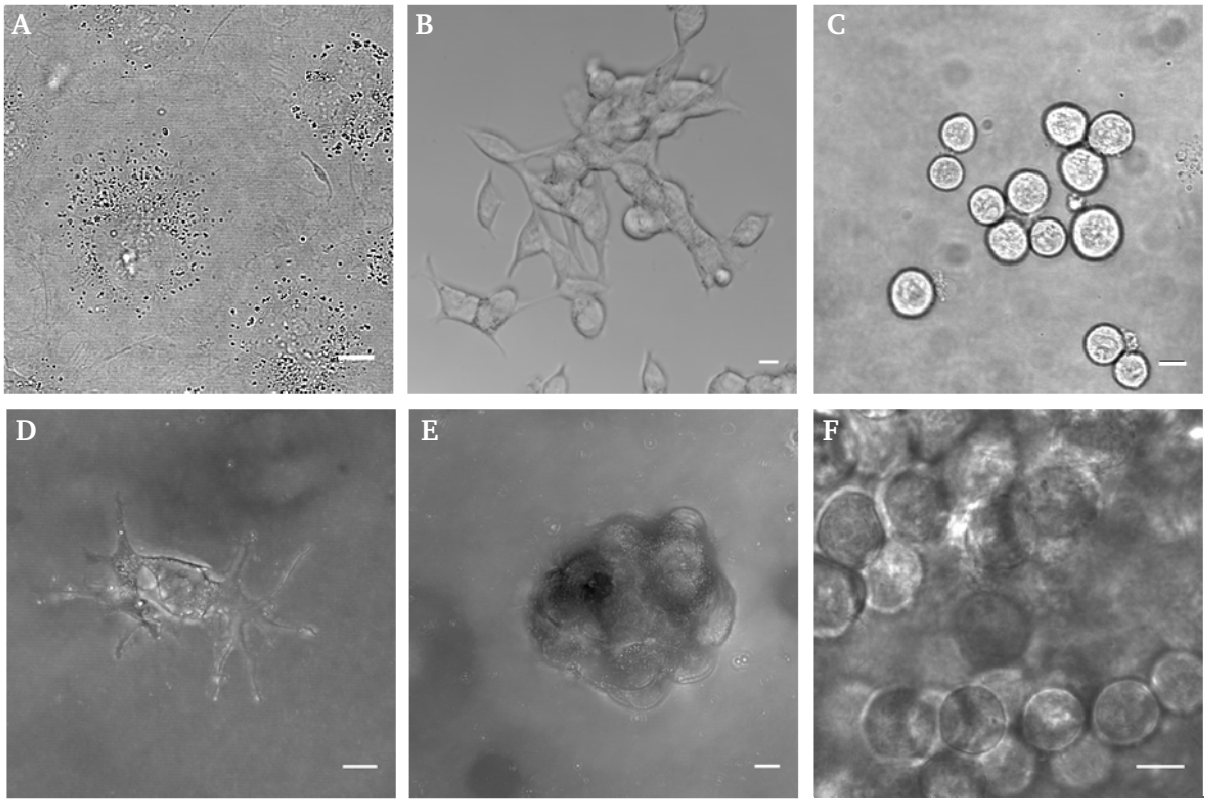

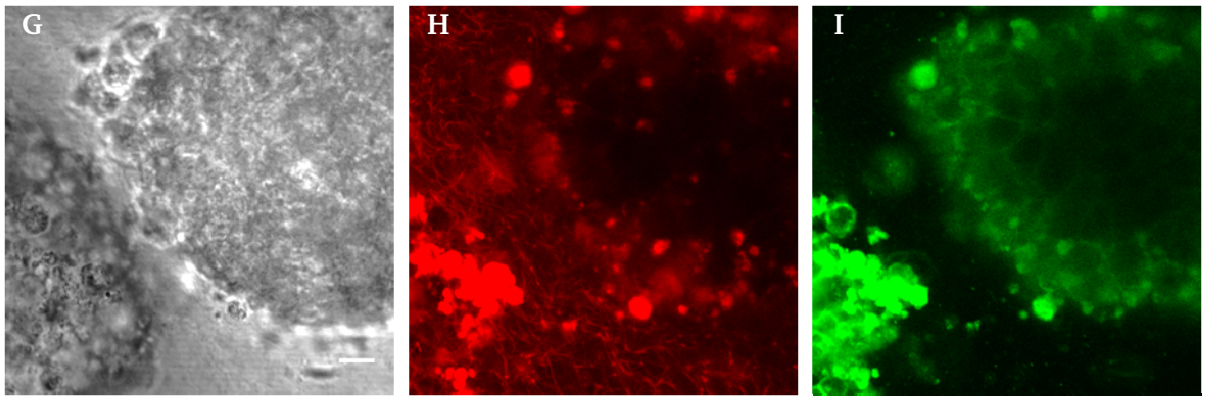

Figure 31: Small volume collagen-based hydrogels were successfully applied as 3D cell culture system for 3 cell lines of different origin. Shown are cells on a stiff substrate, glass (A-C) and within a soft collagen-based hydrogel (2.8 mg/mL) 3-5 days (D-F) and 21 days (G-I) after seeding. COS7 cells showed a typical widely spread, flat, fibroblast morphology in 2D (A) and a highly branched shape, with an increased surface in 3D (D). LNCaPs, when cultured in 2D showed an elongated shape and formed distinct multi-cellular patches (B). In 3D, multi-cellular aggregation of small round cells occurred (E). Non-adherent K562 cells showed a round, non-adhesive morphology when cultured in 2D (C) and in 3D (F). This small volume hydrogel system was successfully used for long term cultures of LNCaP cells (G), collagen fibres stained with E133 (H) and cells stained using the plasma membrane probe, CellMask™Orange (I), 3 weeks after seeding. Scale bars: 10 μm.

3.2.3.2 Cell viability was not a function of microenvironment

To analyse if the microenvironment has an effect on cell viability, COS7 cells were cultured in 2D (glass), in 2.5D (on top culture onto 4 mg/mL collagen-based hydrogels) and in 3D (2.8 mg/mL collagen) conditions for 1 day and viability was analysed using a fluorescent-based live/dead assay. A 2.5D substrate was chosen to analyse transitions of cellular behaviour in a microenvironment with properties of a 2D and 3D microenvironment, using an on top culture on a soft substrate which can be remodelled and allowed cellular invasion. To probe cell viability, a CalceinAM/Propidium iodide-based assay was applied (Fig. 32). Representative images of COS7 cells cultured in different conditions indicate that cell viability was very high in all tested conditions (Fig. 32, green channel). The majority of cells were alive (Fig. 32 green channel, mid column) and nearly no dead cells were detectable (Fig. 32, red channel, right column). No differences in regards to cell viability were observed between the different cell culture methods. This provided evidence that all 3 conditions can be applied to investigate microenvironmental effects on cellular behaviour, without affecting cell viability.

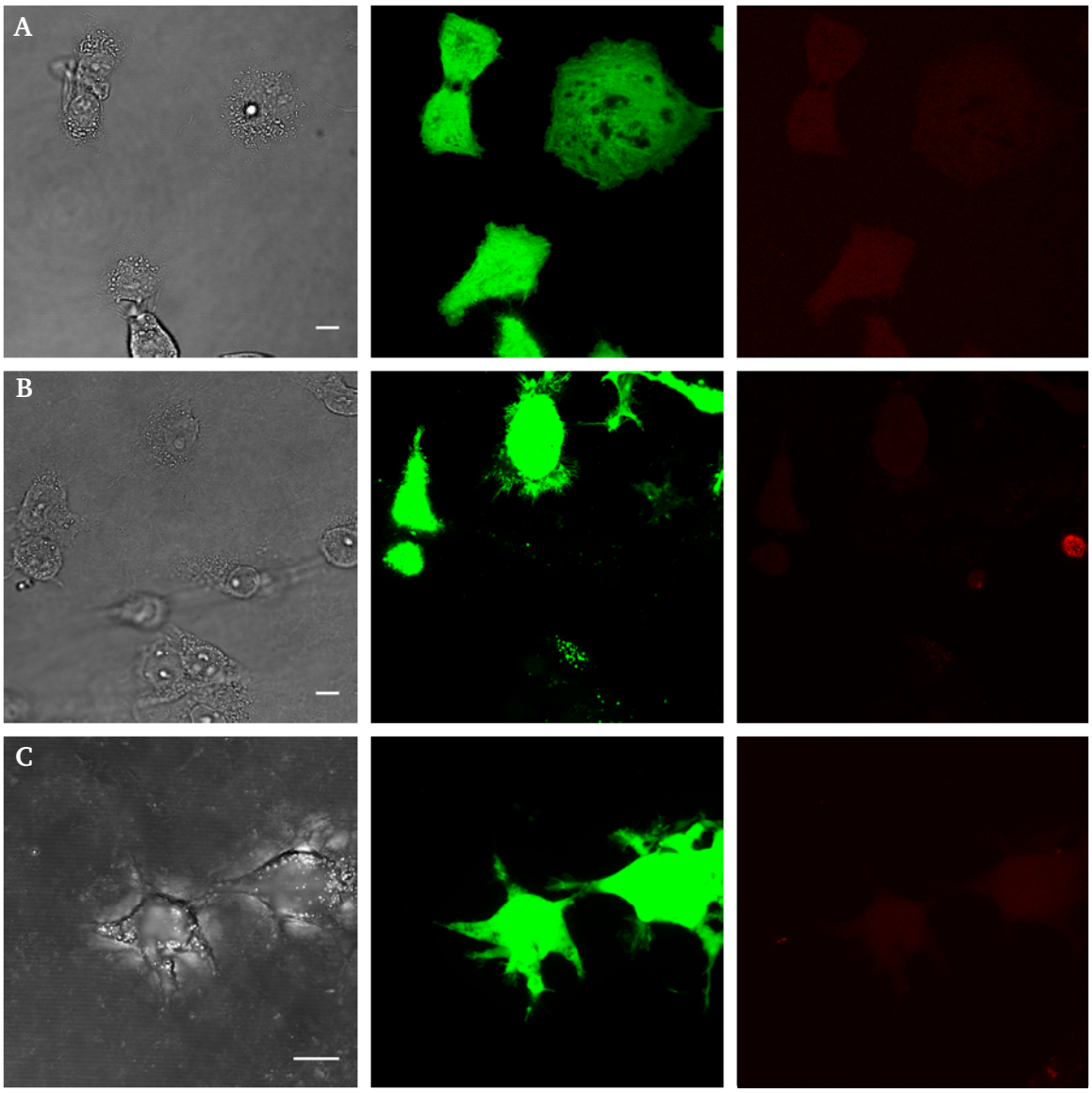

Figure 32: Viability of COS7 cells was not a function of microenvironment. COS7 cells were cultured in 2D (A), in 2.5D (B) and 3D (C). A Calcein AM/Propidium iodide live/dead assay was performed 1 day after seeding. Cell viability is indicated by green fluorescence (mid column) and dead cells by red fluorescence (right column). High cell viability was observed in all conditions tested, without differences, as shown in representative images. Scale bars: 10 μm.

3.2.3.3 Cell morphology and actin cytoskeleton organisation of COS7 cells were a function of the microenvironment

To allow further investigations on cell morphology in dependency of the microenvironment, a COS7 cell line, stably expressing a genetically encoded plasma membrane marker (GFP::CAAX), was generated. Cells were seeded on glass, on top of a collagen-based hydrogel (4 mg/mL) and within a collagen-based hydrogel (2.8 mg/mL). COS7 cells showed a very flat, widely spread morphology in 2D, on a stiff, non-deformable substrate (Fig. 33A). COS7

cells cultured on top of a soft, deformable substrate (2.5D) showed still a flat and widely spread morphology. However, a slightly increased surface and filopodia formation into the substrate were visible (Fig. 33B). Cells fully embedded within a soft substrate were less compact, showed an increased surface and highly branched cell morphology (Fig. 33C).

Next to the morphology, the effect on cytoskeleton organisation in dependency of the local microenvironment was analysed. A COS7 cell line, stably expressing a genetically encoded F-actin marker (Lifeact::GFP2) was generated and cells were cultured in 2D conditions (glass) or embedded in a collagen-based hydrogel (2.8 mg/mL) (Fig. 33D,E). In 2D, COS7 cells showed large F-actin stress fibres, starting from the cell centre to the cell periphery (Fig. 33D). However, in 3D nearly no stress fibres were detected (Fig. 33E).

The usage of these genetically encoded membrane and actin cytoskeleton marker allowed detailed imaging of cellular morphology and actin cytoskeleton organisation in living cells. Furthermore the usage of genetically encoded markers resulted in a specific and high labelling efficiency of cellular components from the intracellular side (Fig. 33). These results showed that morphology and actin cytoskeleton organisation was highly affected by the extracellular microenvironment. In addition it was shown, that cells grown in 2.5D showed a morphological transition with morphological features known from 2D and 3D cell cultures, but the 2D morphology was predominant.

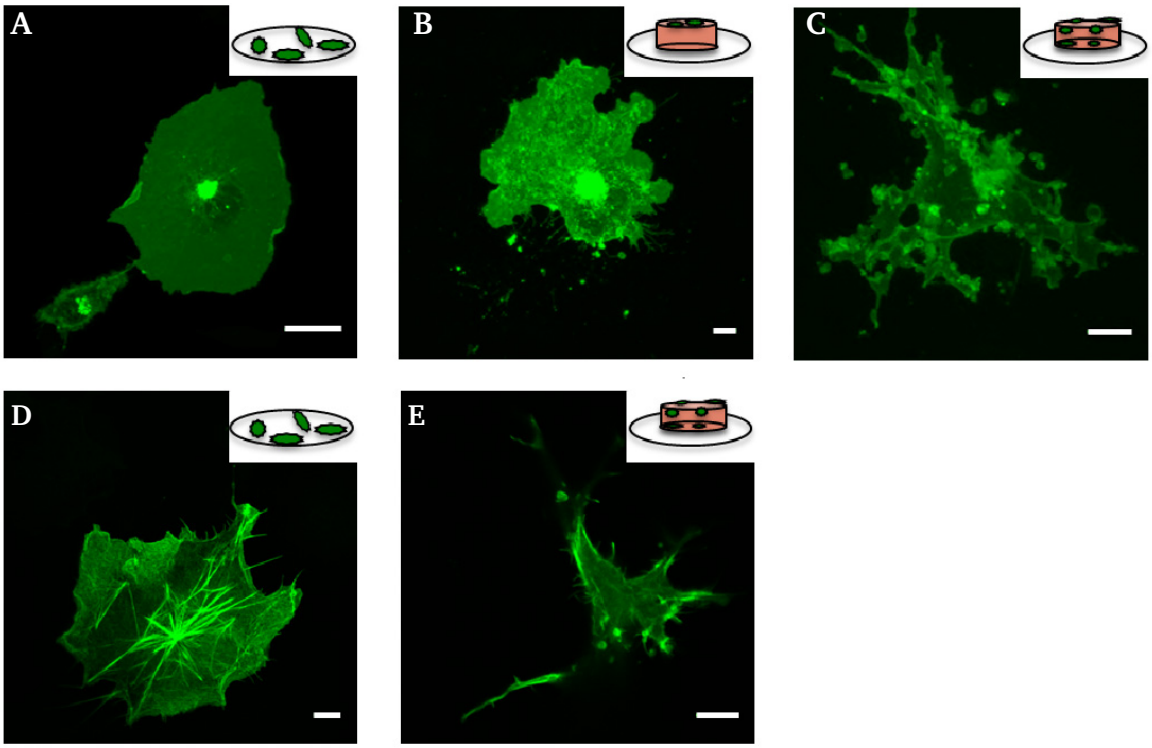

Figure 33: Cell morphology and actin cytoskeleton organisation of COS7 cells was depended on cellular microenvironment. COS7 cells stably expressing GFP::CAAX were cultured in 2D (A), 2.5D (B)

and 3D (C). Shown are maximal projections of multi-z-stacks images. Cells cultured in 2D showed a spread, flat morphology (A). In 2.5D cellular surface was increased and small, thin filopodia were formed, permeating into the hydrogel (B). In 3D, cells showed a highly branched morphology together with an increased surface (C). COS7 cells stably expressing Lifeact::GFP2 were cultured in 2D (D), and 3D (E). In 2D, cells showed many large stress fibres from the cell centre to the cell periphery (D). In contrary in 3D, nearly no stress fibres were detectable (E). Images (A)-(C) were processed using the ImageJ plugin: PureDenoise. Scale bars: 10 μm.

3.2.3.4 Intracellular organelle organisation of COS7 cells was not a function of local microenvironment

TEM was used to gain insights into intracellular organisation in more details than achieved by light-microscope approaches. COS7 cells were cultured on a 2D substrate and detached for TEM analysis before fixation (Fig. 34, top panel) or cultured within a 3D microenvironment (collagen-based hydrogel, 2.8 mg/mL) and fixed after 2 hours (Fig. 34, bottom panel). Cell morphology and intracellular organelle organisation was analysed with TEM. COS7 cells cultured in a 2D microenvironment showed a compactcell shape, with many small, thin filopodia around the whole cell body (Fig. 34, top panel). Cells cultured in 3D conditions showed the same, compact cell morphology. However, in 3D conditions, nearly no filopodia around the cell body, were visible (Fig. 34 bottom pannel). In regards to the intracellular organelle organisation, no differences between cells cultured in 2D and in 3D were observed (Fig. 34). Cells were influenced by the microenvironment in regards to their morphology. The intracellular organelle organisation, as resolved with TEM, was not influenced. TEM allowed very detailed imaging of cell-cell contacts and cellular organelles with high resolution in fixed cells. Further information of cellular dynamics or protein distribution on a more detailed level with high resolution in space and time however, cannot be achieved using this technique.

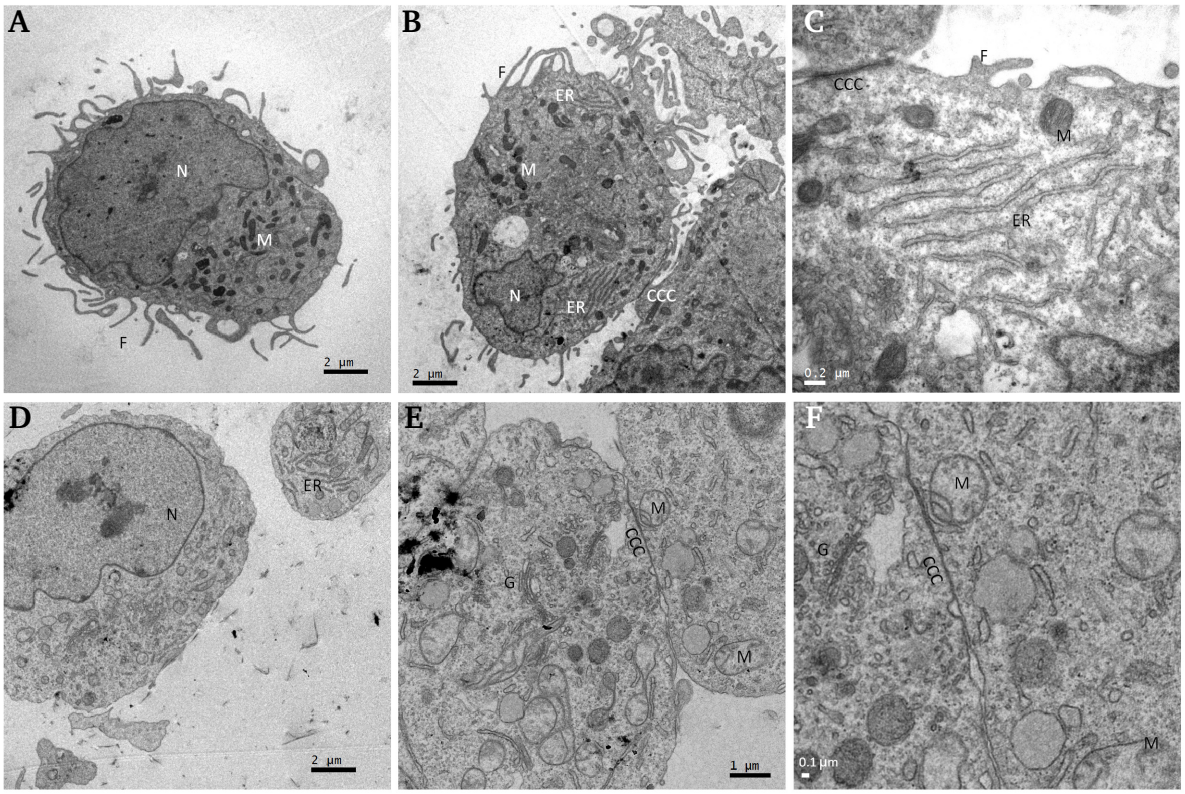

Figure 34: Intracellular organisation of COS7 cells was not a function of microenvironment. TEM images of COS7 cells cultured on a stiff, 2D substrate (tissue culture plastic) and within a soft, 3D microenvironment (collagen-based hydrogel, 2.8 mg/mL). Cells were cultured as monolayers, detached from the surface and fixed before imaging with TEM (A-C). Cells in 3D were fixed 2 hours after hydrogel polymerisation, before imaging with TEM (D-F). Cells cultured in 2D showed many long, thin filopodia around the whole cell body (A, B). These structures were not detected when COS7 cells were cultured in 3D conditions (D, E). A higher magnification showed cell-cell contacts and organelle organisation in more details for cells cultured in both conditions (C, F). In contrast to cell morphology, intracellular organelle organisation was not influenced by cell culture method. Thereby stands F for filopodia, N for nuclei, M for mitochondria, G for Golgi, CCC for cell-cell contact and ER for endoplasmic reticulum.

3.2.4 Small volume collagen-based hydrogels for Single molecule approaches

In earlier chapters, hydrogel properties and optimisations required for imaging were described. It was shown, that this hydrogel system on one hand fulfils essential parameters needed for 3D cell culture and analysis of cell/hydrogel properties and on the other hand meets necessary criteria for high resolution imaging. Next to sample optimisation also imaging acquisition had to be optimised regarding needs for high resolution imaging of cells within a 3D microenvironment. This chapter presents the results of successful sample design and

adaption of microscopy approaches, SMD detection within the plasma membrane of cells fully embedded in a collagen-based hydrogel.

First of all, to directly compare cellular parameters in this small volume hydrogel system later on, conditions used by other groups before were chosen and cellular morphology was compared (Fraley *et al*. 2010; Kubow and Horwitz 2011). Therefore low concentration of U2OS cells were embedded in collagen-based hydrogels (2 mg/mL) and imaged using CLSM, with CFM and CRM. Cells were cultured either on top of a coverslip (Fig. 35A,B) or within a collagen-based hydrogel (Fig. 35C-E) and stained with the plasma membrane maker CellMask™Orange (1 μg/mL). On the 2D substrate, cells were spread, showing a fibroblast-like morphology (Fig. 35A,B). In contrast, in 3D, cells were more elongated and spindle shaped (Fig. 35C,D). CRM images provided proof that cells were fully embedded within the hydrogel (Fig. 35E). Thereby in 2D and 3D conditions majority of CellMask™Orange signals were detected from the plasma membrane and not from solution or molecules bound to hydrogel fibres (Fig. 35). No differences regarding staining efficiency in 2D and 3D were observed and CellMask™Orange staining was consistent over the whole plasma membrane (Fig. 35B,D).

Next to sample preparation also imaging acquisition had to be adapted for SMD in 3D samples. Therefore CellMask™Orange was used to probe the plasma membrane. CellMask™Orange is a small amphipathic molecule, with optimal properties in plasma membrane loading, as indicated by CLSM in 2D and 3D conditions before (Fig. 35). As CellMask™Orange does not have a biological function; it is an ideal tracer molecule to test the suitability of SMD on cells embedded in a hydrogel system. To demonstrate the effect of the different illumination schemes cells cultured on a coverslip and small volume hydrogels, stably attached to the coverslip were used but with dye concentrations (5 ng/mL) higher than optimal for SMD and tracking analyses (Fig. 36). To achieve the needed contrast for SMD, selective excitation and a low fluorophore concentration was applied (Fig. 36). Using, selective TIRF excitation, a high contrast, needed for SMD was achieved within the first nanometres above the coverslip, at the interface between plasma membrane and glass surface (Fig. 36A). Thereby CellMask™Orange molecules bound to the plasma membrane of cells were in focus and molecules in solution were out focus (Fig. 36A). This allowed detection of single lipid-like tracer molecules within the plasma membrane (Fig. 36A). When TIRF illumination was applied to hydrogel samples, again only molecules close to the surface were excited, whereas CellMask™Orange labelled cells fully embedded within the collagen-based hydrogel were outside of the illuminated volume (Fig. 36B). To overcome this limitation

another selective illumination, namely HILO illumination was used, (Fig. 36C). This allowed selective excitation deeper within in the hydrogel, by providing a higher contrast within a light sheet, which permeates deeper into the hydrogel (Fig. 36C). This excitation technique allowed SMD at 10-50 μm within the hydrogel and CellMask™Orange molecules bound to the plasma membrane of cells fully embedded in the hydrogel were observable (Fig. 36C).

To perform true single particle tracking analysis, much lower dye concentrations are required to arrive at sparse labelling conditions. U2OS cells fully embedded within a collagen-based hydrogel (2 mg/mL) were stained with CellMask™Orange (0.1 ng/mL). By illuminating each frame of an imaging sequence recorded at a frame rate of 20 Hz (i.e. 50 ms per frame) for only 5 ms using HILO illumination, individual molecules were successfully detected in the plasma membrane of cells embedded in the hydrogel (Fig. 37A). The short illumination in combination with the frame rate then allowed to track individual CellMask™Orange molecules diffusing within the plane of the plasma membrane. HILO beam angles and focal planes were chosen to ensure that the majority of signals were detected in a plasma membrane horizontal to the detection plane, in order to record lateral movements (coloured tracks, 37B). Due to the 3D distribution of cells, however, also molecules in membranes vertical to the focal plane were detected (arrows, Fig. 37B). In a SMD experiment, imaging sequences of 200 frames were recorded. To represent the dynamic video sequence in still images, maximum (Fig. 37C) as well as average projections (Fig. 37D) were generated. The maximum projection gives an overview of all molecules visible throughout the sequence (Fig. 37C). This visualises the position of the individual plasma membranes within the 3D sample. The average projection gives an impression of the imaging contrast a long illumination would yield (Fig. 37D). Thereby also contributions of fluorescent signals which cannot be detected as individual spots, become apparent. These can be caused by fluorescent molecules in the cell culture media, out of focus dye molecules, and contributions from light scattering.

In conclusion, the detection of single fluorescent molecules in living cells embedded in 3D cultures became possible, by combining low dye concentrations with selective and short illumination. Subsequently, a detection procedure, which is robust against high noise is required to detect and track the signals.

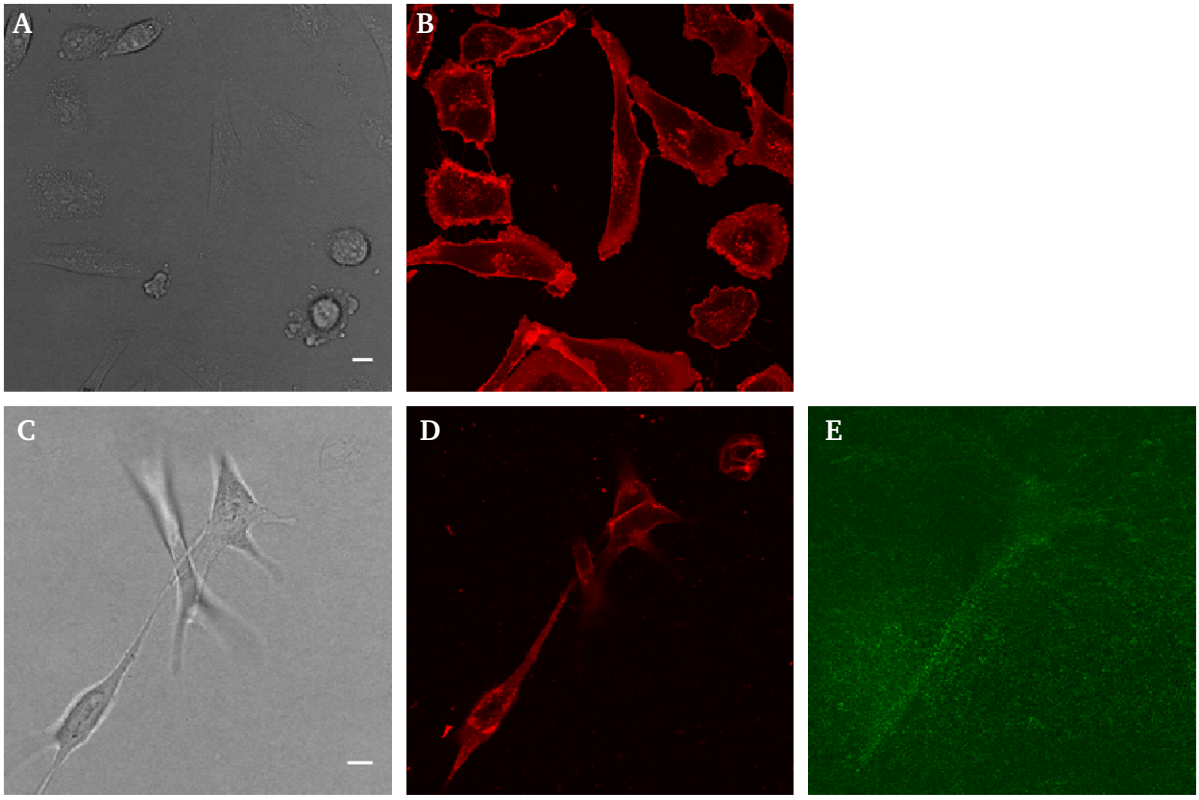

Figure 35: U2OS cells showed different morphology in 2D and 3D. Imaged were U2OS cells cultured on a stiff, 2D substrate (glass) (A, B) and within a soft collagen-based hydrogel (2 mg/mL) (C, D), 1 day after seeding. Shown are bright field images (A,C), CFM images of cells stained with CellMask™Orange (B,D) and CRM image of collagen fibres in (E). Cells were widely spread on stiff 2D substrate and elongated within a soft 3D substrate. CellMask™Orange staining was consistent over the whole plasma membrane and no differences in staining efficiency were observed between cells cultured in 2D and 3D conditions. Scale bars: 10 μm.

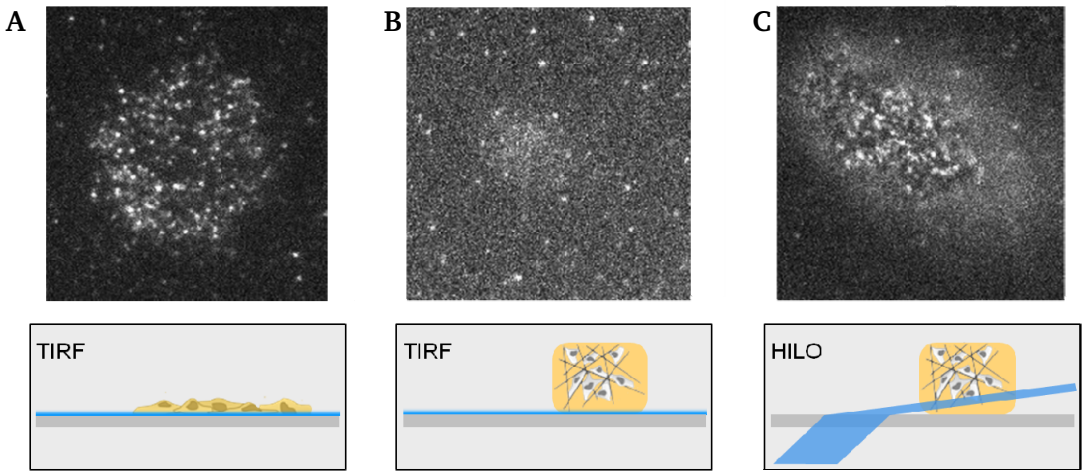

Figure 36: Selective illumination techniques (TIRF, HILO) in principle and applied to cells cultured on 2D or within a 3D substrates. Using TIRF excitation, selective excitation of the first 100 nm above the coverslip was gained. This allowed detection of single signals of

CellMask™Orange (5 ng/ml) bound to the plasma membrane of cells cultured on 2D substrates (A). Using TIRF excitation in hydrogels, only molecules within the evanescent field were excited; here on the coverslip or the hydrogel bottom (B). Selective excitation deeper within the hydrogel was not possible (B). HILO illumination allowed generation of a light sheet and selective excitation deeper within in the hydrogel, this allowed detection of single CellMask™Orange molecules (5 ng/mL) in cells embedded in the hydrogel (C).

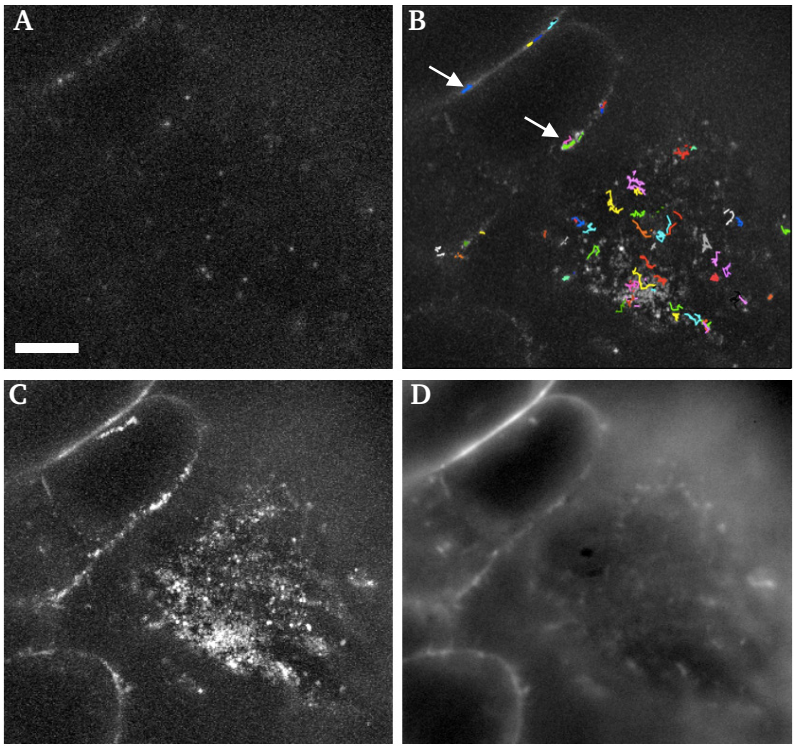

Figure 37: SMD in 3D cell cultures. SMD images of cells stained with CellMask™Orange. U2OS cultured fully embedded in collagen-based hydrogel (2 mg/mL), stained with 0.1 ng/mL CellMask™Orange. Molecules were tracked over duration of 200 frames. A single frame with few signals of individual fluorescent CellMask™Orange molecules showed the achieved imaging contrast (A). Tracks of molecules are shown, which were successfully tracked for a minimum of5 frames (B, coloured tracks). Single molecule tracks were mainly found for molecules diffusing within the plane of a membrane, which is oriented parallel to the detection focal plane, whereas molecules, which diffuse in vertically oriented membranes are able to leave the detection plane (B, arrows). Consequently, far less tracks with a minimum length were detected in these areas (B). As dynamic video sequences are difficult to be visualised by individual still images, maximum (C) as well as average projections (D) of the entire sequence were presented. The maximum projection gives an overview of all molecules visible throughout the sequence. This visualised the position of the individual plasma membranes within the 3D sample (C). The average projection gives an impression of the imaging contrast, under long illumination. Scale bar: 10 μm.

4 Discussion

4.1 GelMA- based hydrogels – a bioengineered 3D cell culture system suitable for cancer research

New biomaterials for 3D cell culture systems are designed in the field of biomedical engineering to provide an experimental model which mimics natural occurring conditions and the clinical picture seen in patients much closer, which can e.g. improve medical-orientated research. In this study, an alternative biomaterial platform for the *in vitro* and *in vivo* analysis of ovarian cancer spheroid growth was presented. The optimisation and validation protocol developed herein resulted in GelMA-based hydrogels with reproducible and tailorable properties. Increasing polymer concentrations resulted in stiffer hydrogels and indicated that spheroid formation, size and shape was highly dependent on hydrogel stiffness. The degradable features of the hydrogels were also linked to spheroid growth. The modification of hydrogels by addition of the ECM components LN-411 and HA enhanced spheroid growth. Optimisation of RNA and protein extraction from spheroids grown within these hydrogels allowed the analyses of mRNA and protein levels. An *in vivo* experiment using female NOD/SCID mice showed tumour formation and metastasis that was induced by spheroid-seeded hydrogels, which were sensitive to paclitaxel, but not to the integrin antagonist ATN-161. Hence, the semi-synthetic biomaterial GelMA combines relevant natural cues with tuneable properties to provide a suitable 3D cancer model.

Cell cultures using 3D techniques are a promising tool for cancer research as they more closely mimic the *in vivo* microenvironment. However, 3D models are still not routinely used (Hutmacher 2010). A potential reason for the slow acceptance in comparison to cell monolayer cultures might be the demand for a complex ECM with defined structure and composition, as this introduces challenges regarding the reproducibility and complexity of such 3D systems. While the use of non-synthetic matrices is associated with a high variability due to their natural origin, synthetic biomaterials generally fail to provide a replica of the natural microenvironment, as cell binding and cleavage sites are missing or composed incorrectly (Cushing and Anseth 2007). To overcome these limitations, this problem was approached by employing a semi-synthetic hydrogel. Its naturally-derived component, gelatine, provides cell binding and cleavage sites, while its chemical modification via introduction of methacrylamide side groups allows the control of its mechanical properties through a chemical crosslinking reaction, in contrast to a physical polymerisation which cannot be precisely controlled and modified (Van Den Bulcke *et al*. 2000). GelMA harbours

optimal properties in representing natural ECM components combined with mechanical robustness as *in vitro* 3D culture model for ovarian cancer by allowing long-term cultures and acting as cancer cell delivery vehicle for *in vivo* applications.

According to a previously reported empirical model (Schuurman *et al*. 2013), hydrogel stiffness increased proportionally with polymer concentration in a quantitatively predictable manner. A high variability was only observed for the softest hydrogels with a low polymer concentration (2.5% GelMA, 0.5 ± 0.2 kPa), and these preparations had the highest discrepancy to the empirical model. As the compression testing was performed using a micro-tester system equipped with a 5N load cell, the sensitivity of the measurements decreased towards low biomaterial stiffness. Despite this systematic error, the compression moduli were robust throughout all hydrogel conditions tested, within one batch and also between two different batches. Hence, GelMA-based hydrogel preparations allow the stiffness to be precisely controlled over the physiological range of most tissues (Buxboim *et al*. 2010).

Next to the molecular composition and stiffness of a matrix, its diffusive properties play an important role in the effort to reproduce a physiological 3D microenvironment. Diffusion into and within a hydrogel directly influences the local cell microenvironment that supplies cells with nutrients, oxygen, growth factors, as well as the effectiveness of drug treatment (Fischbach *et al*. 2009; Lee *et al*. 2008; Lieleg *et al* 2009; Lieleg and Ribbeck 2011; Magzoub *et al*. 2008). This is mainly determined by the pore size and affinity of the diffusing species to the matrix of the hydrogel polymer. In order to assess the diffusive properties of GelMA-based hydrogel preparations, FD70 was used as a tracer molecule, and its diffusion quantified using a robust FRAP protocol (Hendrik Deschout *et al*. 2010). A negative linear relationship between diffusion coefficients of FD70 and polymer concentrations was observed. This is caused by a decreasing mesh size as a result of the higher crosslink density, as well as increased obstruction by the higher volume fraction of polymer chains (Masaro and Zhu 1999). Nevertheless diffusion of FD70 into GelMA-based hydrogels was fast in all conditions tested and diffusion properties were only slightly affected by polymer concentration. Diffusion of FD70 in 7% GelMA-based hydrogels was only retarded by a factor of 2.3 compared to water, indicating that large molecules can still diffuse freely and relatively rapidly through the densest GelMA-based hydrogels. For smaller molecules, the retardation factor will be smaller, and thus, diffusion rates of oxygen, most nutrients and metabolites will be close to those in media in the absence of the hydrogel (Amsden 1998). Long term assessment of diffusion properties in medium concentrated hydrogels (5% GelMA, 3.7 ± 0.5 kPa) showed robust values over 21 days, indicating a stable polymer structure. The direct comparison of cell-free

and cell-laden hydrogels showed nearly constant diffusion coefficients over the complete sample period of 21 days in both conditions, indicating that the overall hydrogel properties are minimally affected by hydrolytic and cell-mediated degradation or compression. Thus, modification of the hydrogel structure is spatially limited to the pericellular microenvironment, enabling cell proliferation and spheroid growth. It can be assumed that due to cellular matrix modification, local structural changes result in a changing diffusion coefficient. However, it was difficult to detect these because the variability of the diffusion coefficient in cell-free hydrogels is increasing over time. Furthermore, FD70 is a very small molecule (radius of 5.25-5.83 nm), so its diffusion coefficient might be less affected by cellular compression or degradation, compared to those of larger molecules. Altogether, even in hydrogels with the highest GelMA-concentration, diffusion of essential components within the hydrogel is possible, and occurs at acceptable rates. Hence, GelMA-based hydrogels provide promising properties as a platform for long term 3D cultures.

Stiffness of the local microenvironment directly affects cell behaviours (Buxboim *et al*. 2010; Loessner *et al*. 2010). The variation of the hydrogel stiffness changed spheroid morphology and size: low stiffness caused loose cell aggregation, medium stiffness led to distinctive, round-shaped spheroids and high stiffness resulted in smaller spheroids. Spheroid morphology and size formed in medium stiff (3.7 ± 0.5 kPa) GelMA-based hydrogels were similar to spheroids formed in PEG-based hydrogels without integrin binding sites (Loessner *et al*. 2010). An increase in metabolic activity and proliferation rate were determined in low (0.5 ± 0.2 kPa) and medium stiff (3.7 ± 0.5 kPa) hydrogels compared to stiff (8.9 ± 1.8 kPa) hydrogels. Distinctive spheroid formation, similar to those formed in the tumour fluid (ascites) that accumulates in the peritoneal cavity of patients with ovarian cancer at the advanced stage of this disease (Shield *et al*. 2009), was observed exclusively in medium stiff (3.7 ± 0.5 kPa) GelMA-based hydrogels. Notably, a high variation in metabolic activity and DNA content was observed, in particular after 14 and 21 days of 3D culture. This phenomenon might be the result of an infrequent observation that cell monolayers were formed on the surface of the plastic culture dishes that were used for 3D cultures upon cell migration out of the hydrogels. As OV-MZ-6 cell monolayers have a higher proliferation rate than cells cultured in 3D over 5 days (Loessner *et al*. 2010), this effect might influence the measurements of spheroid growth.

Enzymatic degradation of the local microenvironment through MMPs plays a key role in spheroid formation, growth and migration (Hirschhaeuser *et al.* 2010; Loessner *et al*. 2010). MMPs are frequently expressed in ovarian cancer and contribute to disease progression by

degradation and remodelling of the ECM (Kenny and Lengyel 2009). MMP-2, MMP-9, and MMP-14 are upregulated in advanced ovarian cancer, tumour fluid (ascites) and abdominal metastasis and associated with shorter survival times (Karam and Dorigo 2012; Kenny and Lengyel 2009). There is a complex crosstalk between MMPs, growth factors and growth factor receptors (Cowden Dahl *et a*l. 2008; Do *et al*. 2008; Karam and Dorigo 2012; Kenny and Lengyel 2009). MMP-9 levels are linked to a loss of E-cadherin and adherens junctions, thereby promoting a more invasive phenotype (Dahl *et al*. 2008). The ovarian cancer spheroids used in this study express MMP-9 but not E-cadherin (Loessner *et al*. 2010). As previously reported OV-MZ-6 cell spheroid growth was reduced by 73% using MMP-sensitive PEG-based hydrogels (Loessner *et al*. 2010). Using the same MMP-inhibitor, spheroid proliferation within GelMA-based hydrogels was reduced, further indicating a regulatory role of MMPs in OV-MZ-6 cell spheroid formation and growth and underlining the importance of the biodegradability of the 3D culture model used. Immunostaining of MMP-9, one of the up-regulated MMPs in ovarian cancer (Schmalfeldt *et al*. 2001), confirmed its expression with and without MMP inhibition over 14 days. Immunostaining of cytokeratin-8 and integrin α6 confirmed that the spheroid morphology and cell adhesive properties were not altered upon MMP inhibition.

Bioengineered, semi-synthetic matrices with close to nature properties become more and more important tools for investigation of cells in approximately native conditions (Hutmacher *et al*. 2010). GelMA offers the possibility of including native ECM components into the precursor hydrogel solution. It was shown that a progressive tumour growth of ovarian cancer occurs along with increased levels of stromal hyaluronan, and that HA promotes metastasis and invasiveness of tumours (Anttila *et al*. 2000; Gardner *et al*. 1996; Toole 2002). Increased levels of LN were also found in the tumour fluid (ascites) of ovarian cancer patients (Byers *et al*. 1995). Therefore, LN-411 and HA were used as additional ECM components within GelMA-based hydrogels. An increased stiffness in hydrogels, but similar diffusive properties, that contained LN-411, HA or a combination of both was observed. Interestingly, there was a positive correlation of these additional ECM components on spheroid growth in GelMA-based 3D cultures, despite their stiffness being higher compared to 5% control hydrogels. It was shown that within PEG-based hydrogels, the elastic modulus was slightly enhanced compared to hydrogels containing low levels of HA (Kutty *et al*. 2007). The incorporation of HA resulted in only small changes regarding the physical and chemical properties of the hydrogel, but increasing fibroblast proliferation activity and cell spreading. Due to the high molecular weight of HA leaching from the hydrogel is unlikely (Kutty *et al*. 2007). Microscopic phase

separation of HA and PEG is a more probable cause, as this might result in a modified microstructure, facilitating cell activity and proliferation. This effect is further increased by the fast degradation of HA, both hydrolytically and through enzymes, such as hyaluronase (Kutty *et al*. 2007). Similar effects were observed in the GelMA-based hydrogels containing HA-methacrylate (Levett *et al*. 2014). The incorporation of HA caused heterogeneous hydrogel formation, containing larger macro-pores and pockets that might support spheroid formation.

Hydrogel systems can also be used to determine changes of gene expression and protein levels upon 3D culture in comparison to 2D cultures (Loessner *et al*. 2010). Therefore, a protocol is needed, which allows harvesting of mRNA and proteins in adequate concentration and purity. The applied micro-column extraction method showed that mRNA was successfully isolated from GelMA/HA-based hydrogel cultures, which were of high purity and concentration. Integrins play a crucial role in metastasis and progression of ovarian cancer (Desgrosellier and Cheresh 2010; Shield *et al*. 2007). Some aspects of expression level of integrins in ovarian cancer spheroids and their role in spheroid formation are still unclear (Loessner *et al*. 2010; Shield *et al*. 2007). Cells cultured in GelMA/HA-based hydrogels showed an increased level of integrin β1mRNA compared to cells cultured in 2D. Interestingly a difference between cells cultured in PEG-based hydrogels and cells cultured within GelMA-based hydrogels was observed. PEG hydrogels were of a lower stiffness range of 0.241-1.201 kPa than, GelMA/HA-based hydrogels, which were of greater stiffness. Integrin distribution and cellular adhesions to the ECM are altered dependent on ECM properties, whereas integrins function as mechanosensors and –regulators in affecting e.g. signalling pathways and cellular fate (Geiger *et al*. 2009; Yamada and Cukierman 2007). These findings indicate that the mRNA expression of integrin β1 is linked to the mechanical properties of the microenvironment.

Furthermore, cell lysates were successfully extracted from cell-laden GelMA/HA-based hydrogels using a collagenase II digestion method. A previous protocol for protein extraction from ovarian cancer spheroids within PEG-based hydrogels using the flow through from the mRNA extraction (Loessner *et al*. 2013), applied to cell-laden GelMA/HA-based hydrogels, resulted in unspecific protein staining for GAPDH. The development and establishment of the shown protocol allowed specific GAPDH detection and showed successful protein extraction of GelMA/HA-based hydrogels for the first time.

Mimicking experimentally the metastasis pattern seen in ovarian cancer patients is an ongoing challenge. In these patients, the primary tumour releases multi-cellular spheroids into the abdomen which then accumulate in the tumour fluid (ascites) mediating secondary tumour

outgrowth and metastasis. This leads to significant morbidity and is a characteristic of the end stage of the disease. Metastatic spread is therefore seen mainly in adjacent organs or tissues, such as the omentum, liver and colon (Shield *et al*. 2009). Implantation of spheroid-containing GelMA-base hydrogels into female NOD/SCID mice showed that this model is able to exactly replicate the tumour growth pattern and route of metastatic spread as it is seen in the clinic. This study provided proof of the application of GelMA-based hydrogels as an ovarian cancer cell carrier. In all mice, tumour formation, growth and metastasis were detected, which was in accordance with the clinical sequence of this disease. Tumour-bearing mice showed sensitivity to paclitaxel treatment, a clinically used anti-cancer drug (Agarwal and Kaye 2003) resulting in reduced tumour growth and a lack of metastasis. Previous studies showed promising effects of the anti-cancer drug ATN-161, a non-RGD-based integrin antagonist on breast and prostate cancer progression and metastasis *in vivo* (Khalili *et al*. 2006). A phase I trial evaluating patients with advanced solid tumours, including prostate cancer, showed a prolonged stable disease upon ATN-161 administration (Cianfrocca *et al*. 2006). However, ATN-161 in this study had no effect on tumour growth and establishment of metastatic lesions and did not enhance the effect of paclitaxel *in vivo*. So far, anti-tumour effects of ATN-161 treatment have been shown for tumours that metastasise via the bloodstream (Cianfrocca *et a*l. 2006; Khalili *et al*. 2006). However, ovarian cancer is predominantly confined within the abdominal cavity and, unlike breast or lung cancer, rarely metastasises hematogenously. In the reported animal studies, ATN-161 was injected intravascularly (Khalili *et al*. 2006). In order to compare the anti-cancer effect of ATN-161 to paclitaxel treatment, both drugs were applied intraperitoneally. This might have impacted on the treatment outcome because drugs reach vascularised metastatic outgrowth faster via the vascular system than intraperitoneally applied drugs that are distributed within the peritoneal fluid.

4.2 Collagen-based hydrogels – a bioengineered 3D cell culture system suitable for high resolution microscopy

Detection and manipulation techniques of single molecules, have improved the understanding of biological processes in its complexity, at the molecular level in time and space, within living cells, tissue and even whole organisms (Biermann *et al*. 2014; Moerner 2007; Neuman and Nagy 2008; Schaaf *et al*. 2009; Shibata *et al*. 2012; Walter *et al.* 2008). To arrive at conditions required for optical SMD a basic principle for optical single molecule detection methods is to achieve a high contrast between signal and noise during acquisition and analysis (Moerner 2007). For that, selective illumination is essential, as it results in a minimised background

fluorescence, especially at high fluorophore concentrations (Ritter *et al*. 2008). This can be achieved also in more complex, heterogeneous multi-cellular systems, by (i) choosing the appropriate acquisition and analyses techniques (Walter *et al*. 2008) and (ii) choosing appropriate model system (Biermann *et al*. 2014, Robin *et al*. 2014). However, to image these samples with high resolution microscopy is still challenging, due to their heterogeneity and sample thickness and is by far not applied routinely (Langhans and Meckel 2014).

In this study, a small volume collagen-based hydrogel has been introduced as a physiological 3D cell culture system utilised for short and long-term cultures of cells from various origins, showing high cell viability and being compatible with high resolution microscopy. E133 and Sirius Red have been used as fluorescent hydrogel staining after polymerisation, to examine the native hydrogel structure. Diffusion properties within collagen-based hydrogels were found to be mainly affected by surface properties of the diffusive particles, rather than size exclusion. Cell culture within a 3D collagen-based hydrogel system had a major effect on cell morphology and cytoskeleton organisation of adherent cell lines compared to traditional 2D cell cultures. However no effect was observed using non-adherent cells. In contrast to cell morphology and cytoskeleton organisation, the intracellular organelle organisation has not been affected by the cell culture method. SMD measurements were carried out within this hydrogel system, using confined HILO excitation and a customised SMD tracking algorithm, which allowed detection of a lipid-like plasma membrane probe in cells embedded in collagen-based hydrogels.

Conventionally collagen-based hydrogels were prepared by pouring a precursor collagen solution into moulds (Walters and Stegemann 2013) or multi-well plates (Fraley *et al*. 2010), resulting in non-attached samples or samples consisting of a thick collagen layer. For quantitative SMD measurements, a high localisation accuracy of signals is imperative (Deschout *et al*. 2014). This requires drift free samples and a stable attachment of the hydrogel onto the coverslip, which can be achieved by coated coverslips. Several coverslip coating products and application protocols are available to allow immobilisation of biological samples such as cells or biopolymers (Metwalli *et al*. 2006; Schaaf *et al*. 2009). An aminosilane-based coating showed the best properties in stable immobilisation of small volume collagen-based hydrogels onto coverslips; thereby being resistant to media change, sample transfer, and compatible with high cell viability and high resolution microscopy. The so prepared collagen-based hydrogels were low in thickness, which made them accessible within the working distance of high NA objectives and confined HILO excitation. Most importantly, however this preparation protocol minimised the impact of light scattering

impact on imaging quality, which often occurs through thick and heterogeneous samples (Graf and Boppart 2010; Ntziachristos 2010).

E133 and Sirius Red were used to stain collagen fibres in polymerised hydrogels, although E133 showed better photo-physical properties than Sirius Red. Hence a lower concentration and laser intensity can be used, which ensures high cell viability. Both CFM approaches were able to overcome limitations of CRM imaging (Artym and Matsumoto 2010; Jawerth *et al*. 2010). Thereby, the quality of generated CFM images using E133 was comparable with images obtained using either fluorescent microscopy, e.g. with TAMRA-labelled tropocollagen (Geraldo *et al*. 2012) or SHG with non-stained hydrogels (Artym and Matsumoto 2010; Wolf *et al*. 2009). Moreover E133 provided a cost and time-effective method for hydrogel staining and was compatible for single-photon CSLM. CFM images of E133-stained collagen-based hydrogels allowed imaging of the fibrillar architecture; however, gained no further structural insights into the organisation of GelMA-based hydrogels. SEM-images indicated that GelMA-based hydrogels consists of a dense and connected pocket-like structure, based on SEM images (Chen *et al*. 2012; Pedron and Harley 2013). Hence, fluorescently labeled GelMA-based hydrogels using E133 solution most probably resulted in a very high staining density within this compact hydrogel and by that in an overlapping of structural features which in turn prevented further insights into hydrogel organisation. However fluorescent hydrogel staining and CFM of hydrated hydrogels might represent the hydrogel structure better, compared to SEM images of dehydrated, fixed hydrogels, which may not represent native, hydrated conditions.

Diffusion within the ECM is a key parameter, e.g. in transport of nutrients, or in context of therapeutics reaching the inside of a tumour (Griffith and Swartz 2006; Magzoub *et al*. 2008). Experiments *in vivo* showed that diffusional slowdown was correlated with increased levels of collagen type-I and its fibrillar organisation (Magzoub *et al*. 2008; Pluen *et al*. 2001). To probe collagen-based hydrogels, carboxylated fluorescent microspheres (Ø 20 nm) were chosen, to match hydrodynamic radii of growth factors (Erickson 2009). In addition the carboxylated surface enabled more realistic, i.e. natural occurring interaction with the ECM. Referring to SEM images, of collagen-based hydrogels within a concentration range of 1-4 mg/mL collagen, the average pore diameter is ranging from 2.2 to 1.1 μm (Miron-Mendoza *et al*. 2010). It was observed that microspheres did not diffuse through the pores; on the contrary, they showed high binding affinities to collagen fibres and motion along these fibres. This effect can be explained by assuming the negatively charged particle, interacting and binding to the collagen fibres. Similar results have been observed using PEG-based

hydrogels probed with charged polystyrene microspheres (Lieleg, *et al.* 2009). These experiments showed that diffusion within the ECM is not only size dependent, but also the presence of other selective filters can directly affect the diffusion parameters, e.g. surface charge of the diffusing particle (Lieleg *et al.* 2009; Lieleg and Ribbeck 2011). Hence, hydrogel probing of charged particles might be a better representative of the natural occurring situation in regards to protein presentation and release, e.g. growth factors (Taipale and Keski-Oja 1997).

Comparing 2D cultured cells to cells in 3D cultures, where cells are fully embedded in an ECM, reveals major differences regarding cell-morphology and actin cytoskeleton organisation (Berrier and Yamada 2007). Thereby 3D cell culture systems mimic closer the *in vivo* situation found in tissue and organs, where cells are fully surrounded by matrix and tension is equally distributed over the complete cell surface and ligands are accessible in every direction (Berrier and Yamada 2007; Griffith and Swartz 2006; Schwarz and Bischofs 2005). A marked polarity of cell morphology is not observed in 3D systems; much in contrast to what is observed in cells in artificial 2D cultures (Beningo *et al*. 2004; Larsen *et al*. 2006). The effect on morphological changes has been already described in various studies, e.g. for prostate cancer cells and fibroblasts (Frederick Grinnell 2003; Rhee 2009; Sieh et al. 2012). Also, in small collagen-based hydrogels this effect was reproduced. COS7 cells showed a widely spread, flat morphology on glass surfaces, typically for fibroblasts on stiff substrates (Grinnell and Bennett 1981). In soft 3D collagen-based hydrogels, however, a highly branched cell shape was observed (Grinnell and Bennett 1981; Grinnell 2003). Fibroblast are highly engaged in biosynthesis, organisation and remodelling of fibrous connective tissue, an effect also seen in collagen-based hydrogels (Grinnell and Petroll 2010). Stiffness and tension of the surrounding influenced fibroblast behaviour (Grinnell 2003; Miron-Mendoza *et al*. 2010). In collagen-based hydrogels tractional force and matrix stiffness are very similar and promote a branched non-polar cell shape compared to 2D cultures (Grinnell and Petroll 2010). Although, LNCaP cells showed a flat, elongated morphology in 2D. In soft 3D collagen-based hydrogels multi-cellular aggregates were formed, consistent with earlier studies using other 3D matrices (Sieh *et al*. 2012). This multi-cellular aggregation has more correlation to the conditions observed in tumours *in vivo*. Additionally a 3D cell culture system better represents physiological parameters, such as compact cell-cell adhesion and gradients of nutrients/oxygen inside the colony better, as shown in studies with tumourigenic cell lines cultured in a soft 3D microenvironment (Loessner *et al*. 2010; Sieh *et al*. 2012). Conversely, the morphology of non-adherent cells was not affected by the microenvironment. K562 cells

showed a round, non-adhesive morphology in 2D and soft 3D collagen-based hydrogels. A reason for this can be found in the integrin expression and integrin activity level in cells of different origin, as integrins are key switches in modulating cell-ECM interactions, e.g. embryonic development, apoptosis and tumour progression and metastasis (Desgrosellier and Cheresh 2010; Kim *et al*. 2003). In adherent cells, cell-ECM interactions are mediated via active integrins (Hynes 2002). Integrin surface expression and activity is highly regulated, especially during the life cycle of circulating cells (Hynes 2002; Springer 1994). Morphology changes and increased cell-substrate adhesion can be induced externally, as shown in using non-adherent, chronic myelogenic leukemic, K562, cells when exposed to phorbol or fibronectin (Burger *et al*. 1992; Dutta *et al*. 2010). This resulted in changes of integrin surface expression pattern, along with morphological and adhesion profile changes and (Burger *et al*. 1992; Dutta *et al*. 2010). However, in collagen-based hydrogels, no morphological change of K562 cells was observed. Hence, as collagen type-I is the main component of the connective tissue but not present in the basal lamina at the vascular endothelium, integrin surface expression and activation might not be triggered in K562 via non-basal lamina ECM components.

Parallel to bright field microscopy, morphology and cytoskeleton organisation were analysed in more details using COS7 cells, expressing genetically encoded fluorescent marker proteins and fluorescence microscopy. Fusion of the anchor domain of human H-Ras (CAAX) to a fluorescent protein, e.g. GFP results in labelling of the inner plasma membrane leaflet from the cytosolic side (Schaaf *et al*. 2009) and allows investigation of cellular morphology in more details than bright field images. The morphology of COS7 cells was observed in 2D (glass), 2.5D (on top of a collagen-based hydrogel) and 3D (embedded in a collagen-based hydrogel) microenvironment. Thereby morphology in 2D and 3D was in line with previous discussed results. Interestingly cells cultured in 2.5D conditions, approached a morphology with aspects from 2D and 3D cell cultures (Beningo *et al*. 2004). In 2.5D and even more so in 3D, cells can penetrate into the matrix and become interweaved within the collagen-based hydrogel (Jiang and Grinnell 2005). Morphological differences in 2D and 3D are the result of different tension on the cell membrane induced via the ECM (Griffith and Swartz 2006). In a 2D microenvironment, cells experience contact to the ECM via ECM-receptors, i.e. integrins, only on the ventral cellular side. This resulted in different stress applied to the top- and the bottom membrane, as seen in widely spread cells. On a soft 2.5D substrate and even more so on a 3D substrate, cells can interact with the ECM over the whole cell body (Larsen *et al*. 2006). Morphological changes in general were regulated via cytoskeleton organisation. Thereby the

actin- and intermediary filament interact with integrins via adaptor proteins. This actin cytoskeleton-plasma membrane continuum can be reorganised during extracellular changes and result in morphological adaption to the microenvironment (Kim *et al*. 2011; Lock *et al*. 2008). COS7 cells showed actin stress fibres when cultured in 2D, as known from earlier studies on fixed samples (Xu *et al*. 2012). In contrast, within a 3D microenvironment only a few and much less pronounced bundles of actin fibres were observed in 3D, in line with previous experiments of embedded fibroblasts in collagen-based hydrogels (Hakkinen *et al*. 2011). Thereby fibroblast actin organisation in 3D cell culture systems, such as collagen-based hydrogels is much closer to cells *in vivo*, where only fibroblasts in tissue with mechanical loading such as tendon show many thick stress fibres (Hakkinen *et al*. 2011; Ralphs *et al*. 2002). The cytoskeleton also forms the physical connection between ECM and intracellular structures, e.g. connection to the nucleus (Buxboim *et al*. 2010; Ketema and Sonnenberg 2011). Mechanical translation can so be transmitted from outside, e.g. via intranuclear membrane proteins to the nucleus and affect nuclear organisation and gene expression pattern (Gieni and Hendzel 2008; Starr and Fridolfsson 2010; Wang *et al*. 2009). This indicates the influence of changes in intracellular organisation due to microenvironmental changes. Using TEM, however, no intracellular differences in cells cultured in 2D and 3D were detectable. In contrast to CLSM images, COS7 cells imaged with TEM showed nearly no morphological differences between cells cultured in 2D and 3D. A more compact cell shape was observed for cells cultured in both conditions, in contrast to the highly branched morphology cells observed in 3D imaged with CLSM. This can be a result of physical sectioning for TEM, representing only 50-90 nm of a cell, whereas in CLSM maximal projections of the whole cell are reconstructed from many single optical sections of a z-stack. Interestingly cells in 2D showed multiple thin filopodia around the whole cell body, which were not present in cells cultured in 3D conditions. These might resemble actin derived filopodia as found in live-cell Bessel-beam microscopy analyses on the membrane facing the culture medium resulted from loosing contact to the ECM after detaching from surface before fixation (Planchon *et al*. 2011). Although TEM provides high resolution insights into cellular organisation, it fails in resolving dynamics of cell-ECM interactions. Therefore other, non-invasive methods which are able to detect protein distribution and dynamics at the molecular level have to be applied, e.g. single molecule microscopy.

Whether differences in the spatial organisation and dynamics, such of proteins, such as focal adhesion, in relation to the cell culture conditions are related to a cellular or rather an imaging effect, has been discussed controversially (Fraley *et al*. 2011; Fraley *et al*. 2010;

Kubow and Horwitz 2011). Hence, methods with a much higher sensitivity and accuracy, such as single molecule detection, are likely to gain much better insights into these processes. Moreover to show that SMD is also applicable in these more complex systems, the same conditions were utilised in small volume collagen-based hydrogels. Consistent with earlier results, U2OS on glass were very flat and widely spread in 2D, which changed within collagen-based hydrogels, to a more elongated shape, which was typically observed within 10-250 μm distance from the coverslip (Fraley *et al*. 2011). Knowing that plasma membrane processes, are very complex, for first SMD measurements, a tracer molecule without biological function was chosen for experiments in a 3D microenvironment. A selective plasma membrane probe, with lipid-like properties, CellMask™Orange was applied to hydrogel-embedded cells. CellMask™Orange belongs to binding-activated probes, which shows strong fluorescence only when intercalated into the hydrophobic core of a biological membrane, but is virtually non-fluorescent in aqueous environment, an important fact especially in a 3D microenvironment (Langhans and Meckel 2014; Meckel *et al*. 2004). Its small size, lipid-like properties, and biological inert properties allowed probing of the plasma membrane fluidity. To achieve high resolution imaging a high contrast has to be achieved, by using low level of bright fluorophores and confined excitation. Therefore, a pico/nano-molar concentration of CellMask™Orange was applied in conjunction with different selective illumination techniques. As selective TIRF illumination is limited to the area close to the coverslip, it cannot be used for imaging of cells embedded within the collagen-based hydrogel (Mashanov *et al*. 2003). Therefore confined illumination deeper inside the hydrogel is needed, which can be achieved using HILO illumination (Bhattacharya *et al*. 2012; Lim *et al*. 2011; Tokunaga *et al*. 2008). HILO illumination has the great benefit of being performable on any objective type TIRF system, which makes it simply and broadbandly accessible (Tokunaga *et al*. 2008), compared to approaches where special microscopes set ups were needed (Pampaloni and Stelzer 2010; Testa *et al*. 2012). This resulted in increased application of HILO illumination, e.g. in hydrogels and small living transparent animal models (York *et al*. 2012). The presented experiment provided evidence that this small volume collagen-based hydrogel system, combined with selective illumination and adapted tracking algorithm can achieve single molecule resolution in time (5 ms) and space (30 nm) also within cells in a more complex microenvironment. Thereby HILO illumination and this 3D cell culture system provide a flexibility of imaging position, suitability for various cell types in short and long term cultures, resulting in a representative, reductionistic model system which allows SMD measurements in a more complex, more realistic microenvironment.

5 Conclusion and Outlook

In summary, I provided proof that semi-synthetic GelMA-based hydrogel were suitable for ovarian cancer cell studies in a 3D microenvironment due to their well characterised, reproducible and tuneable properties combined with natural binding and cleavage sites. Compared to other widely used hydrogel systems, such as PEG-based hydrogels, GelMA-based cell cultures can be prepared following an easy step by step protocol with minimal fabrication-costs. The stiffness was adjusted by adapting the polymer concentration, with minor impact on diffusion properties. GelMA-based hydrogels can be modified using ECM components that are incorporated into the precursor solution creating a more complex microenvironment. GelMA allowed modelling of the metastasis pattern seen in ovarian cancer patients with late stage *ex vivo* and within an animal study. Most importantly, these semi-synthetic hydrogels provided also a 3D spheroid-based model to screen chemotherapeutics for intraperitoneal treatment of advanced ovarian cancer. However this hydrogel system has at the moment limitations regarding its usage for high resolution microscopy. The sample preparation needs to be further optimised to provide thinner hydrogels, which can be stably attached to a coverslip in order to improve the contrast of the image and to reduce the light scattering and drifting of the sample during imaging.

Therefore another system was used to investigate processes on the cell-ECM interface and membrane dynamics. A natural origin, collagen-based hydrogel system was established for high resolution microscopy. An aminosilane-based coverslip coating was applied to prepare small volume hydrogels immobilised onto the coverslip. Structural analyses of fibre-alignment have been optimised using alternative fluorescently labelling of the collagen fibres after hydrogel polymerisation. This small volume collagen-based hydrogel was successfully applied for short and long-term cultures of various cell lines and reduced due to its volume experimental costs. As reporter molecule for first single molecule measurements a lipid like plasma membrane probe, CellMask™Orange, was chosen. Confined HILO excitation within these immobilised hydrogels and tracking of single molecules using a customised tracking algorithm enabled probing of the plasma membrane fluidity with CellMask™Orange in a 2D and 3D microenvironment. However, also this system has its limitation, lacking tuneable properties in terms of stiffness and mechanical stability. Furthermore this sample is a minimised 3D cell culture model system for high resolution microscopy and by this of course not representing all key features of ECM complexity and cell behaviour in thick tissue-like samples.

Evidently, the focus of life sciences is on the key role of the local microenvironment and its effects on biological processes; thus, there is a huge demand to mimic those 3D cell-ECM interactions within experimental, pre-clinical and pre-animal model systems. However, so far, there is no “one fits all approach” and finding the appropriate compromise, of representing physiological conditions within reductionist models suitable for answering the biological question is still challenging. Not only the preparation of complex samples is a challenge, but also their analysis becomes more difficult.

Single molecule microscopy is a very sensitive method and has a great potential for capturing cellular processes in time and space. But as described before, these measurements are limited in maximum penetration depth into the sample and low background levels. So far, only a few examples of single molecule microscopy approaches within a more physiological context were applied, including, multi-cellular spheroids, organotype-based-models or small, transparent animal models, all model system based on reduced complexity. Studies that characterise cellular and hydrogel parameters and apply SMD to the same system are very rare. In this thesis, a novel combination incorporation methods originated from the field of tissue engineering, cell biology and microscopy, resulted in bioengineered *ex vivo* and *in vivo* models, to investigate cancer cell behaviour in a system with (i) tailorable ECM properties and (ii) accessible for downstream analysis, such as high resolution microscopy; however so far analysed in two different model systems (Fig. 38).

Future experiments will combine all achievement made with the two model systems in one approach. GelMA-based hydrogels will be prepared with lower thickness and stably immobilised onto a coverslip to image cancer spheroids with HILO excitation. Single emitter signals will be analysed with a custom written algorithm, to detect signals in presence of a higher noise/background level. Preliminary results using thick, non-attached GelMA-based hydrogels with OV-MZ-6 spheroids (Fig. 39A), stained with CellMask™Orange and HILO excitation, did not provide the image quality needed for single molecule detection (Fig. 39B). Therefore GelMA-based hydrogels have to be (i) immobilised onto a coverslip, for high position accuracy and (ii) need to be of a lower thickness, to position spheroids closer to the surface, near the area, where HILO is possible and the scattering background is lower.

This improved approach will allow precise single molecule microscopy analysis on spheroids cultured in a well characterised local tumour microenvironment. Additionally complementary analyses of protein and lipid dynamics within a spheroid upon anti-cancer treatment in near native conditions will be possible.

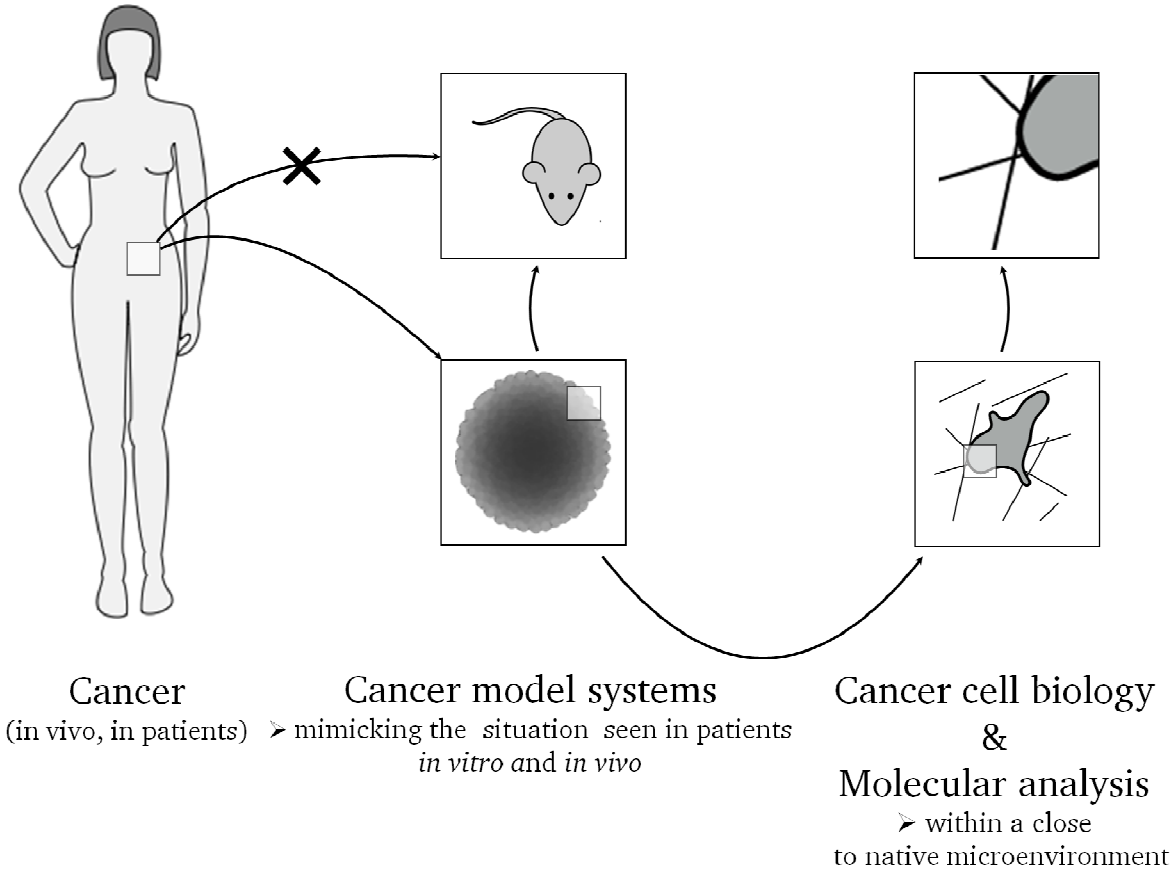

Figure 38: Summary of the project aims and the achieved model systems of this thesis. A close to native microenvironment for cancer cells in an experimental *ex vivo* and *in vivo* GelMA-based model system was developed; providing controlled, but tailorable ECM properties and allowing molecular analysis of cells cultured in this 3D. A collagen-based hydrogel system was optimised to fulfil requirements needed for high resolution microscopy in cells cultured in a physiological relevant 3D cell culture system.

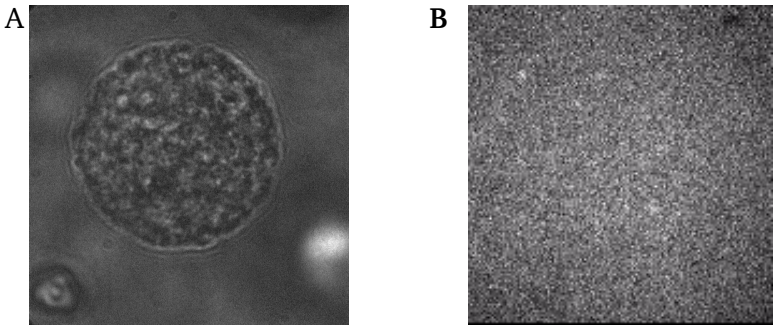

Figure 39: Ovarian cancer spheroid within a GelMA-based hydrogel, labelled with the plasma membrane marker Cellmask™Orange. Cells were imaged using widefield illumination (A) and HILO excitation (B), on the bottom of a spheroid. Cellmask™Orange signals have been recorded (B), as shown in a single frame of a video sequence (bright dots), but the contrast of signal to background and/or noise was not high enough to analyse these images further.

6 Abstract

The aim of this thesis was the application and establishment of a semi-synthetic, bioengineered model system for ovarian cancer and a naturally based, optimised hydrogel system for non-invasive high resolution microscopy analysis of plasma membrane dynamics in a physiological relevant microenvironment.

Providing *ex vivo* models for cancer research with physiologically relevant 3D conditions combined with controllable physical and chemical composition is an ongoing challenge in the field of tissue engineering and cell biology. In this study a semi-synthetic GelMA-based hydrogel system was successfully applied to the study of ovarian cancer cells. Thereby GelMA provided a biomaterial approach combining natural binding and cleavage sites with tuneable properties in an easy to handle and cost-effective hydrogel system. Using this model system, the unique metastatic pattern of ovarian cancer, found in patients with late stage disease, was replicated *in vitro* and *in vivo*. The polymer concentration (2.5-7% w/v) did directly impact the hydrogel stiffness (0.5± 0.2 kPa – 8.9 kPa ± 1.8 kPa) but had only minor impact on solute diffusion. Diffusion of FITC labelled 70 kDa dextran was in all tested hydrogels (2.5-7% w/v; 29.9±3.3 till 16.9 $\mu m^2/s$) close to the diffusion coefficient measured in water (39.2 ± 2.8 $\mu m^2/s$). In the stiffest tested hydrogel the diffusion coefficient was decreased by only 2.3 times. Spheroid formation, occurring in the tumour fluid (ascites) of ovarian cancer patients with late stage disease, combined with the highest metabolic and proliferation rates was reflected in medium stiff hydrogels (5%, 3.4 kPa). Inhibition of hydrogel degradation, with a MMP inhibitor, reduced spheroid growth and metabolic activity. Additional ECM components, Laminin-411 and hyaluronic acid increased spheroid growth, metabolic and proliferation activity significantly. Furthermore this hydrogel system allowed bio-molecular analysis of mRNA and protein levels. Ovarian cancer cells showed an increased mRNA level of integrin β1 compared to monolayer or other 3D cultures. Next to the *ex vivo* experiments it was shown that GelMA-based hydrogels can be successfully used as spheroid-based cancer cell carrier system for *in vivo* studies. Spheroid-seeded hydrogels were intraperioteneally implanted into female NOD/SCID mice, resulting in tumour development and metastasis, known from the clinical sequence of the disease. The developed tumours showed a response rate of 33% to the anti-cancer drug paclitaxel, but not the integrin antagonist ATN-161. Combined treatment using both therapeutics resulted in 37.8% treatment response, while treatment with ATN-161 alone had no effect.

Collagen-based hydrogel systems are widely used for investigations of cell-ECM crosstalk; however, they often lack reproducible, well characterised properties and are mostly not suitable for high resolution microscopy. A small volume collagen-based hydrogel system provided a 3D cell culture model utilised for high resolution microscopy approaches with optimised sample properties, such as sample immobilisation and minimised sample thickness. This study provided evidence of an alternative fluorescent labelling of collagen fibres after hydrogel polymerisation with E133 and Sirius Red. In particular E133 was a cost and time-effective staining method, compatible with single photon CLSM and simultaneous cell-ECM imaging. Diffusion through collagen-based hydrogels was affected by surface properties of the diffusive particles rather than a size exclusive filtering. Carboxylated mircospheres (Ø 20 nm) did not diffuse through the hydrogel pores; they showed a high binding affinity towards collagen fibres. Also after 72 h, a gradient from the outer hydrogel parts to the centre was observable. This small volume collagen-based hydrogel system allowed culture of 4 different cell lines, showing high cell viability and being suitable for short and long term cultures. Compared to 2D cultures, adherent cell lines showed a different morphology in 3D, while non-adherent K562 cells did not show a morphological change. Studies on COS7 cells showed that next to morphology also cytoskeleton organisation was a function of the local microenvironment. In contrast, no differences in the intracellular organelle organisation between cells cultured in 2D or 3D was observed. Additionally this small volume collagen-based hydrogel system was suitable for single molecule microscopy measurements using the lipid like tracer molecule CellMask™Orange; a specific probe for plasma membrane labelling without biological function. This model system, combined with confined HILO excitation and a customised algorithm allowed single molecule microscopy also in a more complex, 3D microenvironment.

Overall it was shown that mimicking a more natural, bioengineered microenvironment in a realistic experimental model can deepen the understanding of cancer cell behaviour and reaction to anti-cancer treatment. Moreover a 3D microenvironment does not exclude quantitative molecular assessment using single molecule microscopy, but therefore model system and analysis methods had to be adapted to this more complex situation.

7 Zusammenfassung

Ziel dieser Arbeit war zum einen die Optimierung und Etablierung eines semi-synthetischen hydrogelbasierten 3D Zellkultursystems als experimentelles Modell für Eierstockkrebs und zum anderen die Optimierung eines natürlichen Hydrogelsystems für Untersuchungen der Membrandynamik an Zellen in einer möglichst natürlichen (3D) Umgebung.

Die Entwicklung und Anwendung von Modellsystemen, die zellbiologische Untersuchungen in einer physiologischeren, 3D Umgebung ermöglichen, werden immer wichtiger, besonders in der Krebsforschung. In dieser Arbeit konnte gezeigt werden, dass ein Gelatine-methacrylamidbasiertes (GelMA)-basiertes Hydrogelsystem erfolgreich als *ex vivo* und *in vivo* Modellsystem für Eierstockkrebs verwendet werden konnte. GelMA bietet dabei eine Kombination aus natürlichen Bindungs- und Degradierungsstellen mit einstellbaren physikalisch-chemischen Eigenschaften, beispielsweise Steifigkeit. GelMA-basierte Hydrogele wurden mit verschiedenen Polymerkonzentrationen (2.5%-7%) hergestellt, dabei stieg die Steifigkeit mit steigender Polymerkonzentration an (0.5± 0.2 kPa – 9.0 kPa ± 1.8 kPa). Überraschenderweise hatte die Polymerkonzentration dabei fast keinen Einfluss auf die Diffusionseigenschaften. Der Diffusionskoeffizient von FITC markiertem 70 kDA Dextran war bei allen Proben (2.5-7% w/v; 29.9±3.3 bis 16.9 $\mu m^2/s$) in der gleichen Größenordnung wie der in Wasser (39.2 ± 2.8 $\mu m^2/s$). Sphäroidbildung, wie sie in der Aszitesflüssigkeit bei Patientinnen mit Eierstockkrebs im fortgeschrittenen Stadium auftritt, zusammen mit einer hohen metabolischen Aktivität und Proliferationsrate wurde am besten in Hydrogelen mittlerer Steifigkeit (5%, 3.4 kPa) wiedergegeben. Eine Inhibierung der Hydrogel-Degradierung durch einen MMP-Inhibitor, reduzierte sowohl Sphäroidwachstum als auch Proliferation und die metabolische Aktivität. Das Einbringen zusätzlicher ECM-Komponenten, wie Laminin-411 und Hyaluronsäure resultierte des Weiteren in einem gesteigerten Sphäroidwachstum, einer höheren metabolischen Aktivität und einer angestiegenen Proliferationsrate. Für weitere molekularbiologische und biochemische Untersuchungen konnten erfolgreich mRNA und Proteinextrakt aus vorkultivierten GelMA-HA/-basierten Hydrogelen gewonnen werden. Dabei zeigte sich eine deutlich erhöhte integrin β1 Expression im Vergleich zu Zellen in 2D oder Zellen die in einem anderen 3D, PEG-basierten, Hydrogel kultiviert wurden. Neben den *in vitro* Experimenten konnte gezeigt werden, dass vorkultivierte GelMA-Hydrogele, implantiert in weibliche NOD/SCID Mäuse, zur Tumorentwicklung führen und das gleiche Metastasierungsmuster zeigten, wie Patientinnen im fortgeschrittenen Krankheitsstadium. Eine Behandlung mit Paclitaxel resultierte in einem

Tumorrückgang von 33% und die Kombination mit dem Integrin Antagonist ATN-161 in einem Rückgang von 37.8%. Die Behandlung mit ATN-161 alleine zeigte keinen Effekt.

Kollagenbasierte Hydrogele werden häufig für Untersuchungen von Zellinteraktionen mit der extrazellulären Matrix (ECM) eingesetzt, dabei sind die Hydrogeleigenschaften meist unvollständig charakterisiert, wenig reproduzierbar, und es gibt kaum Systeme die mit hochauflösenden Mikroskopiemethoden kompatibel sind. In dieser Arbeit wurde ein kleinvolumiges Hydrogelsystem etabliert, welches stabil an der Deckglasoberfläche anhaftete und so driftfreie Mikroskopie und reproduzierbare Eigenschaften ermöglichte. Um die Architektur dieser fibrillären Hydrogele genauer zu untersuchen, wurden alternative fluoreszierenden Farbstoffe, E133 und *Sirus Red* eingesetzt. Die Diffusionseigenschaften eines Hydrogels sind nicht nur abhängig von der Porengröße, vielmehr spielen Oberflächeneigenschaften eine wichtige Rolle. Es konnte gezeigt werden, dass carboxilierte *micropsheres* (Ø 20 nm) nicht ungehindert durch das kollagenbasierte Hydrogel diffundierten, sondern an Kollagenfasern binden und entlang dieser diffundieren. Diffusion durch Hydrogelporen wurde nicht beobachtet und auch nach 72 h war ein *microspheres*-Gradient vom äußeren Gelrand zur Gelmitte sichtbar. Das kleinvolumige kollagenbasierte Hydrogelsystem wurde erfolgreich für die Kultivierung von vier verschiedenen Zelllinien eingesetzt. Adhärente Zelllinien zeigten dabei eine unterschiedliche Morphologie und Organisation des Aktincytoskelets unter 2D und 3D Zellkulturbedingungen. Nicht-adhärente K562 Zellen zeigten keinerlei morphologische Unterschiede in 2D und 3D Kulturbedingungen. Unterschiede bezüglich der intrazellulären Organisation der Organellen in COS7-Zellen zwischen Zellen die unter 2D und 3D Bedingungen kultiviert wurden, wurden nicht beobachtet. Dieses kleinvolumige, kollagenbasierte Hydrogelsystem wurde dann für erste Einzelmolekülmessungen eingesetzt. Hierfür wurde *Cellmask™Orange*, ein lipophiler, plasmamembran-spezifischer Farbstoff, als *Tracer*-Molekül, eingesetzt um basale Parameter der Plasmamembranfluidität in Zellen in einer 3D Umgebung zu untersuchen. Mit Hilfe des optimierten Hydrogelsystems, selektiver Beleuchtung (HILO) und einem angepassten *Tracking*-Algorithmus waren erste Messungen von einzelnen *Cellmask™Orange* Molekülen in der Plasmamembran von lebenden Zellen in einer 3D Umgebung möglich.

Zusammenfassend konnte gezeigt werden, dass ein experimentelles Modell mit physiologischeren Eigenschaften das Wissen über Krebszellen, ihr Verhalten und Reaktion auf Therapeutika vertieft werden kann. Des Weiteren, wurde gezeigt, dass quantitative Analysen mittels Einzelmikroskopie auch in einer komplexeren, 3D Umgebung durchgeführt werden können, wenn Modellsystem und Analysemethoden aneinander angepasst werden.

8 References

Abbe, E. 1873.“Beitraege zur Theorie des Mikroskops und der mikroskopischen Wahrnehmung.”

Agarwal, R and Kaye, SB. 2003. “Ovarian Cancer: Strategies for Overcoming Resistance to Chemotherapy.” *Nat Rev Cancer* 3(7): 502–16.

Ahmed, N; Pansino, F; Riley, C; Murthi, P; Quinn, MA; Rice, GE; Agrez, MV; Mok, S and Baker, MS. 2002. “Overexpression of alpha(v)beta6 integrin in serous epithelial ovarian cancer regulates extracellular matrix degradation via the plasminogen activation cascade.” *Carcinogenesis* 23(2): 237–44.

Ahmed, N; Riley, C; Rice, G and Quinn, M. 2005. “Role of integrin receptors for fibronectin, collagen and laminin in the fegulation of ovarian carcinoma functions in response to a matrix microenvironment.” *Clin Exp Metastasis* 22(5): 391–402.

Amsden, B. 1998. “Solute Diffusion in Hydrogels . An examination of the retardation effect.” *Polym Gels Networks* 6: 13–43.

Anttila, MA; Tammi, RH; Tammi, MI; Syrjänen, KJ; Saarikoski, SV and Kosma V-M. 2000. “High Levels of Stromal Hyaluronan Predict Poor Disease Outcome in Epithelial Ovarian Cancer High Levels of Stromal Hyaluronan Predict Poor Disease Outcome in Epithelial Ovarian Cancer 1.” *Cancer Res* 60: 150–55.

Artym, VV and Matsumoto K. 2010. "Imaging Cells in Three-Dimensional Collagen Matrix". *Curr Protoc Cell Biol* Chapter: Unit10.1820.

Auersperg, N. 2013. “The Origin of Ovarian Cancers- hypotheses and controversies.” *Front Biosci* 5: 709–19.

Axelrod, D. 1981. “Cell-Substrate Contacts Illuminated by Total Internal Reflection Fluorescence.” *J Cell Biol* 89(1): 141–45.

Axelrod, D. 1984. “Total Internal Reflection Fluorescence.” *Annu Rev Biophys Bioeng* 13: 247–68.

De Belder, AN, and Granath, K. 1973. “Preparation and properties of fluorescein-labelled dextrans.” *Carbohydr Res* 30: 375–78.

Beningo, KA; Dembo, M and Wang Y. 2004. “Responses of fibroblasts to anchorage of dorsal extracellular matrix receptors.” *PNAS* 101(52): 18024–29.

Berrier, AL and Yamada, KM. 2007. “Cell – Matrix Adhesion.” *J Cell Physiol* 213(3): 565–73.

Bhattacharya, D; Singh VR; Zhi, C; So, PTC; Matsudaira, P and Barbastathis, G. 2012. “Three Dimensional HiLo-based structured illumination for a digital scanned laser sheet microscopy (DSLM) in thick tissue imaging.” *Opt Express* 20(25): 27337–47.

Biermann, B; Sokoll, S; Klueva, J; Missler, M; Wiegert,JS; Sibarita,J-B and Heine, M. 2014. “Imaging of molecular surface dynamics in brain slices using single-particle tracking.” *Nat Commun* 5: 3024.

Booth, BW; Park, JP and Burg KJL. 2013. “Evaluation of normal and metastatic mammary cells grown in different biomaterial matrices: establishing potential tissue test systems.” *J Biomater Sci Polym Ed* 24(6): 758–68.

Braeckmans, K; Peeters, L; Sanders, NN; De Smedt, SC and Demeester, J. 2003. “Three-Dimensional Fluorescence Recovery after Photobleaching with the Confocal Scanning Laser Microscope.” *Biophys J* 85(4): 2240–52.

Van den Bulcke, AI; Bogdanov,B; De Rooze, N; Schacht, EH; Cornelissen, M and Berghmans, H. 2000. “Structural and Rheological Properties of Methacrylamide Modified Gelatin Hydrogels.” *Biomacromolecules* 1(1): 31–38.

Buxboim, Amnon; Ivanovska, IL and Discher, DE. 2010. “Matrix elasticity, cytoskeletal forces and physics of the nucleus: how deeply do cells ‘feel’ outside and in?” *J Cell Sci* 123(3): 297–308.

Byers, LJ; Osborne, JL; Carson, LF; Carter, JR; Haney, AF; Weinberg, B and Ramakrishnan, S. 1995. “Increased levels of laminin in ascitic fluid of patients with ovarian cancer.” *Cancer Lett* 88(1): 67–72.

Chandler, EM; Seo, BR; Califano, JP; Andresen Eguiluz,RC; Lee, JS; Yoon,CJ; Tims, DT; Wang, JX; Cheng, L; Mohanan, S; Buckley, MR; Cohen, I; Yu, A; Williams, RM; Gourdon D; Reinhart-King, CA and Fischbach, C. 2012. “Implanted adipose progenitor cells as physicochemical regulators of breast cancer.” *PNAS* 109(25): 9786–91.

Chen, Y-C; Lin, R-Z; Qi, H; Yang, Y; Bae, H; Melero-Martin, JM and Khademhosseini, A. 2012. “Functional Human Vascular Network Generated in Photocrosslinkable Gelatin Methacrylate Hydrogels.” *Adv Funct Mater* 22(10): 2027–39.

Chudakov, DM; Matz, MV and Lukyanov, KA. 2010. “Fluorescent Proteins and Their Applications in Imaging Living Cells and Tissues.” *Physiol Rev* 90(3): 1103–63.

Cianfrocca, ME; Kimmel,KA; Gallo, J; Cardoso, T; Brown, MM; Hudes,G; Lewis, N; Weiner, L; Lam, GN; Brown, SC; Shaw,DE; Mazar, AP and Cohen, RB. 2006. “Phase 1 trial of the antiangiogenic peptide ATN-161 (Ac-PHSCN-NH(2)), a beta integrin antagonist, in patients with solid tumours.” *Bri J Cancer* 94(11): 1621–26.

Cicchi, R; Vogler, N; Kapsokalyvas,D; Dietzek, B; Popp, J and Pavone, FS. 2013. “From molecular structure to tissue architecture: collagen organization probed by SHG microscopy.” *J BIOPHOTONICS* 6(2): 129–42.

Cordes, N and Park, CC. 2007. “β1 integrin as a molecular therapeutic target.” *Int J Radiat Biol* 83(11-12): 753–60.

Cowden KD; Symowicz, J; Ning,Y; Gutierrez,E; Fishman,DA; Adley, BP; Stack, MS and Hudson, LG. 2008. “Matrix Metalloproteinase 9 Is a Mediator of Epidermal Growth

Factor-Dependent E-Cadherin Loss in Ovarian Carcinoma Cells." *Cancer Res* 68(12): 4606–13.

Cushing, MC and Anseth, KS. 2007. "Materials Science. Hydrogel Cell Cultures." *Science* 316(5828): 1133–34.

Deschout, H; Shivanandan, A; Annibale, P; Scarselli,M and Radenovic, A. 2014. "Progress in quantitative single-molecule localization microscopy." *Histochem Cell Biol*.

Deschout, H; Hagman,J; Fransson, S; Jonasson, J; Rudemo, M; Lorén, N and Braeckmans, K. 2010. "Straightforward FRAP for quantitative diffusion measurements with a laser scanning microscope." *Opt Express* 18(22): 22886–905.

Desgrosellier, JS and Cheresh, DA. 2010. "Integrins in cancer: biological implications and therapeutic opportunities." *Nat Rev Cancer* 10(1): 9–22.

Do, TV; Kubba, LA; Hongyan, D; Sturgis, CD and Woodruff., TK. 2008. "Transforming Growth Factor-β1, Transforming Growth Factor- β 2, and Transforming Growth Factor- β 3 Enhance Ovarian Cancer Metastatic Potential by Inducing a Smad3-Dependent Epithelial-to-Mesenchymal Transition." *Mol Cancer Res* 6(5): 695–705.

Domogatskaya, A; Rodin,S and Tryggvason, K. 2012. "Functional Diversity of Laminins." *Annu Rev Cell Dev Biol* 28: 523–53.

Dutta, A; Sen, T and Chatterjee, A. 2010. Culture of K562 human myeloid leukemia cells in presence of fibronectin expresses and secretes MMP-9 in serum free culture medium. Int *J Clin Exp Pathol* 3 (3): 288-302.

Eke, I and Cordes, N. 2011. "Radiobiology goes 3D: How ECM and cell morphology impact on cell survival after irradiation." *Radiother Oncol* 99(3): 271–78.

Erickson, HP. 2009. "Size and Shape of Protein Molecules at the Nanometer Level Determined by Sedimentation, Gel Filtration, and Electron Microscopy." *Biol Proced Online* 11(1): 32–51.

Even-Ram, S and Yamada, KM. 2005. "Cell migration in 3D matrix." *Curr Opin Chem Biol* 17(5): 524–32.

Farsiu, S; Robinson,D; Elad, M and Milanfar, P. 2004. "Advances and Challenges in Super-Resolution." *Int J Imaging Syst Technol* 14(2): 47–57.

Fischbach, C; Kong, HJ; Hsiong, SX; Evangelista,MB; Yuen, W and Mooney, DJ. 2009. "Cancer cell angiogenic capability is regulated by 3D culture and integrin engagement." *PNAS* 106(2): 399–404.

Fraley, SI; Yunfeng, F; Krishnamurthy,R; Hwee Kim, D; Celedon, A; Longmore, GD and and Wirtz, D. 2010. "A Distinctive role for focal adhesion proteins in three-dimensional cell motility." *Nat Cell Biol* 12(6): 598–604.

Fraley, SI; Feng,Y; Wirtz, D and Longmore GD. 2011. “Reply: reducing background fluorescence reveals adhesions in 3D matrices.” *Nat Cell Biol* 13(1): 3–5; author reply 5–7.

Franke, K; Sapudom, J; Kalbitzer, L; Anderegg, U and Pompe, T. 2014. “Topologically defined composites of collagen types I and V as in vitro cell culture scaffolds.” *Acta Biomater* 10(6): 2693-702.

Frantz, C; Stewart,KM and Weaver, VM. 2010. “The extracellular matrix at a glance.” *J Cell Sci* 123(24): 4195–200.

Gardner, MJ; Catterall, JB; Jones, LM and Turner, GA. 1996. “Human ovarian tumour cells can bind hyaluronic acid via membrane CD44: A possible step in peritoneal metastasis.” *Clin Exp Metastasis* 14(4): 325–34.

Gattazzo, F; Urciuolo, A and Bonaldo, B. 2014. “Extracellular matrix: A dynamic microenvironment for stem cell miche.” *Biochim Biophys Acta*

Geiger, B; Spatz,JP and Bershadsky, AD. 2009. “Environmental sensing through focal adhesions.” *Nat Rev Mol Cell Biol* 10(1): 21–33.

Geiger, B and Yamada, KM. 2011. “Molecular Architecture and Function of Matrix Adhesions.” *Cold Spring Harb Perspect Biol* 3(5).

Geraldo, S; Simon, A; Elkhatib, N; Louvard, D; Fetler, L and Vignjevic., DM. 2012. “Do cancer cells have distinct adhesions in 3D collagen matrices and in vivo?” *Eur J Cell Biol* 91(11-12):

Gieni, RS, and Hendzel MJ. 2008. “Mechanotransduction From the ECM to the Genome: Are the Pieces now in Place?” *J Cell Bioechem* 104(6): 1964–87.

Gluzman, Y 1981. “SV40-Transformed Simian Cells Support the Replication of Early SV40 Mutants.” *Cell* 23(1): 175–82.

Van Goethem, E; Poincloux,R; Gauffre,F; Maridonneau-Parini,I and Le Cabec, V. 2010. “Matrix Architecture Dictates Three-Dimensional Migration Modes of Human Macrophages: Differential Involvement of Proteases and Podosome-like Structures.” *J Immunol* 184(2): 1049–61.

Goñi, FM. 2014. “The basic structure and dynamics of cell membranes: An Update of the Singer-Nicolson Model.” *Biochim Biophys Acta* 1838(6): 1467–76.

Graf, BW and Boppart, SA. 2010. “Imaging and Analysis of Three-Dimensional Cell Culture Models.” *Methods Mol Biol* 591: 211–27.

Griffith, LG, and Swartz, MA. 2006. “Capturing complex 3D tissue physiology in vitro.” *Nat Rev Mol Cell Biol* 7(3): 211–24.

Grinnell, F and Bennett MH. 1981. “Fibroblast Adhesion on Collagen Substrata in the Presence and Absence of Plasma Fibronectin.” *J Cell Sci* 48: 19–34.

Grinnell, F. 2003. “Fibroblast biology in three-dimensional collagen Matrices.” *Trends Cell Biol* 13(5) 264-69.

Grinnell, F and Petroll, MW. 2010. “Cell Motility and Mechanics in Three-Dimensional Collagen Matrices.” *Annu Rev Cell Dev Biol* 26: 335–61.

Hakkinen, KM; Harunaga, JS; Doyle, AD and Yamada, KM. 2011. “Direct Comparisons of the Morphology, Migration, Cell Adhesions, and Actin Cytoskeleton of Fibroblasts in Four Different Three-Dimensional Extracellular Matrices.” *Tissue Eng* 17(5-6): 713–24.

Helmlinger, G; Netti, PA; Lichtenbeld,HC; Melder, RJ and Jain, RK. 1997. “Solid stress inhibits the growth of multicellular tumor spheroids.” *Nat Biotechnol* 15(8): 778–83.

Hirschhaeuser, F; Menne, H; Dittfeld, C; West, J; Mueller-Klieser, W and Kunz-Schughart, LA. 2010. “Multicellular tumor spheroids: An underestimated tool is catching up again.” *J Biotechnol* 148(1): 3–15.

Horoszewicz, J S; Leong, SS; Chu,TM; Wajsman, ZL; Friedman, M; Papsidero,L; Kim, U; Chai, LS; Kakati, S; Arya SK and Sandberg, AA. 1980. “The LNCaP Cell Line--a New Model for Studies on Human Prostatic Carcinoma.” *Prog Clin Biol Res* 37: 115–32.

Huang, B; Bates, M and Zhuang, X. 2009. “Super resolution fluorescence microscopy.” *Annu Rev Biochem* 78: 993–1016.

Humphries, JD; Byron A and Humphries, MJ. 2006. “Integrin ligands at a glance.” *J Cell Sci* 119(19): 3901–3.

Hutmacher, DW. 2010. “Biomaterials offer cancer research the third dimension.” *Nature Mater* 9(2): 90–93.

Hutmacher, DW; Loessner, D; Rizzi, S; Kaplan, DL; Mooney, DJ and Clements JA. 2010. “Can Tissue Engineering Concepts Advance Tumor Biology Research?” *Trends Biotechnol* 28(3): 125–33.

Hynes, RO. 2002. “Integrins : Bidirectional , Allosteric Signaling Machines In Their Roles as Major Adhesion Receptors” *Cell* 110: 673–87.

Hynes, RO. 2009. “The Extracellular Matrix: Not Just Pretty Fibrils.” *Science* 326(5957): 1216–19.

Jaqaman, K; Loerke, D; Mettlen, M; Kuwata,H; Grinstein, S; Schmid, SL and Danuser, G. 2008. “Robust Single-Particle Tracking in Live-Cell Time-Lapse Sequences.” *Nat Methods* 5(8): 695–702.

Janmey, PA, and Miller, RT. 2011. “Mechanisms of mechanical signaling in development and disease.” *J Cell Sci* 124(1): 9–18.

Jawerth, LM; Münster, S; Vader, DA; Fabry, B and Weitz, DA. 2010. “A Blind Spot in Confocal Reflection Microscopy: The Dependence of Fiber Brightness on Fiber Orientation in Imaging Biopolymer Networks.” *Biophys J* 98(3): L1–3.

Jayo, A and Parsons, M. 2012. “Imaging of cell adhesion events in 3D matrix environments.” *Eur J Cell Biol* 91(11-12): 824–33.

Jiang, H and Grinnell, F. 2005. “Cell – Matrix Entanglement and Mechanical Anchorage of Fibroblasts in Three-Dimensional Collagen Matrices.” *Mol Biol Cell* 16: 5070 –5076.

Kaemmerer, E; Melchels, FPW; Holzapfel, BM; Meckel, T; Hutmacher, DW and Loessner, D. 2014. “Gelatine methacrylamide-based Hydrogels: An alternative three-dimensional cancer cell culture system.” *Acta Biomater* 10(6): 2551–62.

Kanchanawong, P; Shtengel, G; Pasapera, AM; Ramko,EB; Davidson, MW; Hess, HF and Waterman, CM. 2010. “Nanoscale architecture of integrin-based cell adhesions.” *Nature* 468(7323): 580–84.

Karam, A and Dorigo, O. 2012. “MMPs in Ovarian Cancer as Therapeutic Targets.” *Anti-Cancer Agents Med Chem* 12(7): 764–72.

Kenny, HA; Kaur, S; Coussens, LM and Lengyel, E. 2008. “The initial steps of ovarian cancer cell metastasis are mediated by MMP-2 cleavage of vitronectin and fibronectin.” *J Clin Invest* 118(4): 1367–79.

Kenny, HA, and Lengyel, E. 2009. “MMP-2 functions as an early response protein in ovarian cancer metastasis.” *Cell Cycle* 8(5): 683–88.

Kessenbrock, K, Plaks, V and Werb, Z. 2010. “Matrix Metalloproteinases: Regulators of the Tumor Microenvironment.” *Cell* 141(1): 52–67.

Ketema, M and Sonnenberg, A. 2011. “Nesprin-3: a versatile connector between the nucleus and the cytoskeleton.” *Biochem Soc Trans* 39(6): 1719–24.

Khalili, P; Arakelian, A; Chen, G; Plunkett, ML; Beck, I; Parry, GC; Doñate,F; Shaw, DE; Mazar, AP and Rabbani, SA. 2006. “A non-RGD-based integrin binding peptide (ATN-161) blocks breast cancer growth and metastasis in vivo.” *Mol Cancer Ther* 5(9): 2271–80.

Kim, M; Carman, CV and Springer, TA. 2003. “Bidirectional Transmembrane Signaling by Cytoplasmic Domain Separation in Integrins.” *Science* 301(5640): 1720–25.

Kim, SH; Turnbull, J and Guimond, S. 2011. “Extracellular matrix and cell signalling: the dynamic cooperation of integrin, proteoglycan and growth factor receptor.” *J Endocrinol* 209(2): 139–51.

Kleinman, HK and Martin, GR. 2005. “Matrigel: Basement membrane matrix with biological Activity.” *Semin Cancer Biol*15(5): 378–86.

Knapinska, A and Fields, GB. 2012. “Chemical biology for understanding matrix metalloproteinase function.” *ChemBioChem* 13(14): 2002–20.

Kostourou, V and Papalazarou, V. 2014. “Non-collagenous ECM proteins in blood vessel morphogenesis and cancer.” *Biochim Biophys Acta*.

Kubow, KE, and Horwitz, AR. 2011. “Reducing background fluorescence reveals adhesions in 3D matrices.” *Nat Cell Biol* 13(1): 3–7.

Kusumi, A; Fujiwara,TK; Chadda, R; Xie, M; Tsunoyama, TA; Kalay, Z; Kasai,RS and Kenichi Suzuki, KGN. 2012. “Dynamic Organizing Principles of the Plasma Membrane That Regulate Signal Transduction: Commemorating the Fortieth Anniversary of Singer and Nicolson’s Fluid-Mosaic Model.” *Annu Rev Cell Dev Biol* 28: 215

Kutty, JK; Cho, E; Lee, JS; Vyavahare, NJ and Webb K. 2007. “The effect of hyaluronic acid incorporation on fibroblast spreading and proliferation within PEG-diacrylate based semi-interpenetrating networks.” *Biomaterials* 28(33): 4928–38.

Langhans, M and Meckel, T. 2014. “Single-molecule detection and tracking in plants.” *Protoplasma* 251(2): 277–91.

Larsen, M; Artym, VV; Green, JA and Yamada KM. 2006. “The matrix reorganized: extracellular matrix remodeling and integrin signaling.” *Curr Opin Cell Biol* 18(5): 463–71.

Leblond, CP and Inoue, S. 1989. “Structure, composition, and assembly of basement membrane.” *Am J Anat* 185(4): 367–90..

Lee, J; Cuddihy, MJ and Kotov, NA. 2008. “Three-Dimensional Cell Culture Matrices : State of the Art.” *Tissue Eng Rev* 14(1): 61–86.

Levett, PA; Melchels, FPW; Schrobback, K; Hutmacher,DW; Malda, J and Klein, TJ. 2014. “A biomimetic extracellular matrix for cartilage tissue engineering centered on photocurable gelatin, hyaluronic acid and chondroitin sulfate.” *Acta Biomater* 10(1): 214–23.

Lieleg, O; Baumgärtel, RM and Bausch, AR. 2009. “Selective Filtering of Particles by the Extracellular Matrix: An Electrostatic Bandpass.” *Biophys J* 97(6): 1569–77.

Lieleg, O and Ribbeck, K. 2011. “Biological Hydrogels as Selective Diffusion Barriers.” *Trends Cell Biol* 21(9): 543–51.

Lim, D; Ford, TN; Chu, KK and Mertz, J. 2011. “Optically sectioned in vivo imaging with speckle ollumination HiLo microscopy.” *JBO* 16(1): 016014.

Lock, JG; Wehrle-Haller, B and Strömblad, S. 2008. “Cell-matrix adhesion complexes: master control machinery of cell migration.” *Semin Cancer Biol* 18(1): 65–76.

Loessner, D; Flegg, JA; Byrne, HM; Clements JA; Hutmacher, DW. 2013. “Growth of confined cancer spheroids: a combined experimental and mathematical modelling approach.” *Integrative biology* 5(3): 597–605.

Loessner, D; Rizzi, SC; Stok, KS; Fuehrmann, T; Hollier, B; Magdolen, V; Hutmacher, DW and Clements, JA. 2013. “A Bioengineered 3D ovarian cancer model for the assessment of peptidase-mediated enhancement of spheroid growth and intraperitoneal spread.” *Biomaterials* 34(30): 7389–7400.

Loessner, D; Stok, KS; Lutolf, MP; Hutmacher, DW; Clements, JA and Rizzi, SC. 2010. “Bioengineered 3D Platform to Explore Cell-ECM Interactions and Drug Resistance of Epithelial Ovarian Cancer Cells.” *Biomaterials* 31(32): 8494–8506.

Lozzio, B B, and Lozzio, CB. 1977. “Properties of the K562 cell line derived from a patient with chronic myeloid leukemia.” *Int J Cancer.* 19(1): 136.

Lu, P; Takai,K; Weaver, VM and Werb,Z. 2011. “ExtracellularmMatrix degradation and remodeling in development and disease.” *Cold Spring Harb Perspect Biol* 3(12).

Lu, P; Weaver, VM and Werb, Z. 2012. “The extracellular matrix: a dynamic niche in cancer progression.” *J Cell Biol* 196(4): 395–406.

Luisier, F; Vonesch,C; Thierry, B and Unser, M. 2010. “Fast interscale wavelet denoising of Poisson-corrupted images.” *Signal Processing* 90(2): 415–27.

Magzoub, M; Jin, S and Verkman, AS. 2008. “Enhanced macromolecule diffusion deep in tumors after ezymatic digestion of extracellular matrix collagen and its associated proteoglycan decorin.” *FASEBJ* 22(1): 276–84..

Masaro, L, and Zhu, XX. 1999. “Physical models of diffusion for polymer solutions, gels and solids.” *Prog Polym Sci* 24(5): 731–75.

Mashanov, GI; Tacon, D; Knight, AE; Peckham, M and Molloy, JE. 2003. “Visualizing single molecules inside living cells using total internal reflection fluorescence microscopy.” *Methods* 29(2): 142–52.

Meckel, T; Hurst, AC; Thiel, G and Homann, U. 2004. “Endocytosis against high turgor: intact guard cells of Vicia faba constitutively endocytose fluorescently labelled plasma membrane and GFP-tagged K-channel KAT1.” *Plant J* 39(2): 182–93.

Metwalli, E; Haines, D; Becker, O; Conzone,S and Pantano, CG. 2006. “Surface characterizations of mono-, di-, and tri-aminosilane Ttreated glass substrates.” *J Colloid Interface Sci* 298(2): 825–31.

Miron-Mendoza, M; Seemann, J and Grinnell, F. 2010. “The differential regulation of cell motile activity through matrix stiffness and porosity in three dimensional collagen matrices.” *Biomaterials* 31(25): 6425–35.

Möbus, V; Gerharz, CD; Press, U; Moll, R; Beck,T; Mellin, W; Pollow, K; Knapstein, PG and Kreienberg, R. 1992. “Morphological, immunohistochemical and biochemical characterization of 6 newly established human ovarian carcinoma cell lines.” *Int J Cancer* 52(1): 76–84.

Moerner, WE. 2007. “New directions in single-molecule imaging and analysis.” *PNAS* 104(31): 12596–602.

Nam, JM; Chung, Y; Hsu, HC and Park, CC. 2009. “beta1 integrin targeting to enhance radiation therapy.” *Int J Rad Biol* 85(11): 923–28.

Negi, LM; Talegaonkar, S; Jaggi, M; Ahmad, FJ; Iqbal, Z and Khar, RK. 2012. Role of CD44 in tumour progression and strategies for targeting. *J Drug Target* 20(7): 561-73.

Neuman, KC and Nagy, A. 2008. "Single-molecule force spectroscopy: optical tweezers, magnetic tweezers and atomic force microscopy." *Nat Methods* 5(6): 491–505.

Nguyen-Ngoc, KV; Cheung, KJ; Brenot, A; Shamir, ER; Gray, RS; Hines, WC; Yaswen, P; Werb, Z and Ewald, AJ. 2012. "ECM microenvironment regulates collective migration and local dissemination in normal and malignant mammary epithelium." *PNAS* 109(39): E2595–604.

Nichol, JW; Koshy, ST; Bae, H; Hwang, CM; Yamanlar, S and Khademhosseini, A. 2010. "cell-laden microengineered gelatin methacrylate hydrogels." *Biomaterials* 31(21): 5536–44.

Nicodemus, GD and Bryant, SJ. 2008. "Cell Encapsulation in Biodegradable Hydrogels for Tissue Engineering Applications." *Tissue Eng Rev* 14(2): 149–65.

Ntziachristos, V. 2010. "Going deeper than microscopy: the optical imaging frontier in biology." *Nat Methods* 7(8): 603–14.

Pampaloni, F; Reynaud, EG and Stelzer, EHK. 2007. "The third dimension bridges the gap between cell culture and live tissue." *Nature Rev Mol Cell Biol* 8: 839–45.

Pampaloni, F and Stelzer, EHK. 2010. "Three-dimensional cell cultures in toxicology." *Biotechnol Genet Eng Rev* 26: 117–38.

Pang, Y; Wang, X; Lee, D and Greisler, HP. 2011. "Dynamic quantitative visualization of single cell alignment and migration and matrix remodeling in 3-D collagen hydrogels under mechanical force." *Biomaterials* 32(15): 3776–83.

Park, CC; Bissell, MJ and Barcellos-Hoff, MH. 2000. "The influence of the microenvironment on the malignant phenotype." *Molecular Med Today* 6(8): 324–29.

Pedron, S and Harley, BA. 2013. "Impact of the biophysical features of a 3D gelatin microenvironment on glioblastoma malignancy." *J Biomed Mater Res* 101(12): 3404–15.

Petroll, WM., MA, L and Jester, JV. 2003. "Direct correlation of collagen matrix deformation with focal adhesion dynamics in living corneal fibroblasts." *J Cell Sci* 116(8): 1481–91.

Pickl, M, and Ries, CH. 2009. "Comparison of 3D and 2D Tumor models reveals enhanced HER2 activation in 3D associated with an increased response to trastuzumab." *Oncogene* 28(3): 461–68.

Pizzo, AM; Kokini, K; Vaughn, LC; Waisner, BZ and Voytik-Harbin, SL. 2005. "Extracellular matrix (ECM) microstructural composition regulates local cell-ECM biomechanics and fundamental fibroblast behavior: a multidimensional perspective." *J Appl Phys* 98(5): 1909–

Planchon, TA; Gao, L; Milkie, DE; Davidson, MW; Galbraith, JA; Galbraith, CG and Betzig, E. 2011. "Rapid three-dimensional isotropic imaging of living cells using Bessel beam plane illumination."*Nat Methods* 8 (5): 417-23.

Pluen, A; Boucher, Y; Ramanujan, S; McKee, TD; Gohongi, T; di Tomaso,E; Brown, EB; Izumi, Y; Campbell, RB; Berk, DA and Jain, RK. 2001. “Role of tumor-host interactions in interstitial diffusion of macromolecules: cranial vs. subcutaneous tumors.” *PNAS* 98(8): 4628–33.

Poincloux, R; Collin, O; Lizárraga, F; Romao, M; Debray, M; Piel, M and Chavrier, P. 2011. “Contractility of the cell rear drives invasion of breast tumor cells in 3D Matrigel.” *PNAS* 108(5): 1943–48.

Pupa, SM; Ménard, S; Forti, S and Tagliabue, E. 2002. “New insights into the role of extracellular matrix during tumor onset and progression.” *J Cell Physiol* 192(3): 259–67.

Ralphs, JR; Waggett, AD and Benjamin, M. 2002. “Actin stress fibres and cell–cell adhesion molecules in tendons: organisation in vivo and response to mechanical loading of tendon cells in vitro.” *Matrix Biol* 21(1): 67–74.

Rayleigh, L. 1903. “On the Theory of Optical Images, with special reference to the Microscope.” *Journal of the Royal Microscopical Society* 23(4): 474–82.

Rhee, S. 2009. “Fibroblasts in three dimensional matrices: cell migration and matrix remodeling. *J Exp Med* 41(12): 858–65.

Ricciardelli, C and Rodgers, RJ. 2006. “Extracellular matrix of ovarian tumors.” *Semin Reprod Med* 24(4): 270–82.

Riedl, J; Crevenna, AH; Kessenbrock, K; Yu, JH; Neukirchen, D; Bradke, F; Jenne, D; Holak,TA; Werb,Z; Sixt, M and Wedlich-Soldner, R. 2008. “Lifeact : a versatile marker to visualize F-Actin.” *Nat Methods* 5(7): 605–7.

Ritter, JG; Veith, R; Siebrasse, JP and Kubitscheck, U. 2008. “High-contrast single-particle tracking by selective focal plane illumination microscopy.” *Opt Express* 16(10): 7142–52.

Robin, FB; McFadden, WM; Yao, B and Munro, EM. 2014. “Single-molecule analysis of cell surface dynamics in Caenorhabditis Elegans embryos.” *Nat Methods* 11(6): 677–82.

Roeder, BA; Kokini, K; Sturgis, JE; Robinson, JP and Voytik-Harbin, SL. 2002. “Tensile mechanical properties of three-dimensional type I collagen extracellular matrices with varied microstructure.” *J Biomech Eng* 124(2): 214-22.

Rossignol, JF; La Frazia, S; Chiappa, L; Ciucci, A and Santoro, MG. 2009. “Thiazolides, a new class of anti-influenza molecules targeting viral hemagglutinin at the post-translational level.” *J Biol Chem* 284(43): 29798–808.

Schaaf, MJ; Koopmans, WJ; Meckel, T; van Noort, J; Snaar-Jagalska, BE; Schmidt TS, and Spaink, HP. 2009. “Single-molecule microscopy reveals membrane microdomain organization of cells in a living vertebrate.” *Biophys J* 97(4): 1206–14.

Schermelleh, L; Heintzmann, R and Leonhardt, H. 2010. “A guide to super-resolution fluorescence microscopy.” *J Cell Biol* 190(2): 165–75.

Schindelin, J; Arganda-Carreras, I; Frise, E; Kaynig, V; Longair, M; Pietzsch, T; Preibisch, S; Rueden, C; Saalfeld, S; Schmid, B; Tinevez, JY; White, DJ; Hartenstein, V; Eliceiri, K; Tomancak, P and Cardona, A. 2012. “Fiji: an open-source platform for biological-image analysis.” *Nat Methods* 9(7): 676–82.

Schmalfeldt, B; Prechtel, D; Härting, K; Rutke, S; Konik, E; Fridman, R; Berger, U; Schmitt, M; Kuhn, W and Lengyl, E. 2001. “Increased expression of matrix ,metalloproteinases (MMP) -2 , MMP-9 , and the urokinase-type plasminogen activator is associated with progression from benign to advanced ovarian cancer increased” *Clin Cancer Res* 7: 2396–2404.

Schneider, CA; Rasband, WS and Eliceiri, KW. 2012. “NIH Image to ImageJ: 25 Years of Image Analysis.” *Nat Methods* 9(7): 671–75.

Schuurman, W; Levett, PA; Pot, MW; van Weeren,PR; Dhert, WJ; Hutmacher, DW; Melchels, FPW; Klein, TJ and Malda, J. 2013. “Gelatin-methacrylamide hydrogels as potential biomaterials for fabrication of tissue-engineered cartilage constructs.” *Macromol Biosci* 13(5): 551–61.

Schwarz, US and Bischofs, IB. 2005. “Physical determinants of cell organization in soft media.” *Med Eng Phys* 27(9): 763–72.

Schwarzbauer, J. 1999. “Basement membrane: Putting up the barriers.” *Curr Biol* 9(7): R242–R244.

Shibata, AC; Fujiwara, TK; Chen, L; Suzuki, KG; Ishikawa, Y; Nemoto, YL; Miwa, Y; Kalay, Z; Chadda, R; Naruse,K and Kusumi, A. 2012. “Archipelago architecture of the focal adhesion: membrane molecules freely enter and exit from the focal adhesion zone.” *Cytoskeleton (Hoboken)* 69(6): 380–92.

Shield, K; Ackland, ML; Ahmed, N and Rice, GE. 2009. “Multicellular spheroids in ovarian cancer metastases: Biology and pathology.” *Gynecol Oncol* 113(1): 143–48.

Shield, K; Riley, C; Quinn, MA; Rice, GE; Ackland, ML and Ahmed, N. 2007. “Alpha2beta1 integrin affects metastatic potential of ovarian carcinoma spheroids by supporting disaggregation and proteolysis.” *J Carcinog* 6: 11.

Shoulders, MD and Raines, RT. 2009. “Collagen structure and stability.” *Annu Rev Biochem* 78: 929–58.

Sieh, S; Taubenberger, AV; Rizzi, SC; Sadowski, M; Lehman, ML; Rockstroh, A; An, J; Clements, JA; Nelson, CC and Hutmacher, DW. 2012. “Phenotypic characterization of prostate cancer LNCaP cells cultured within a bioengineered microenvironment.” *PloS one* 7(9): e40217.

Singer, SJ and Nicolson, GL. 1971. “The structure and chemistry of mammalian cell membranes.” *Am J Pathol* 65(2): 427–37.

Singer SJ and Nicolsen GL “The fluid mosaic model of the structure of cell membranes.” *Science* 175(4023): 720–31.

Soofi, SS; Last, JA; Liliensiek, SJ; Nealey,PF and Murphy, CJ. 2009. “The elastic modulus of Matrigel as determined by atomic force microscopy.” *J Struct Biol* 167(3): 216–19.

Springer, TA. 1994. “Traffic signals for lymphocyte recirculation and leukocyte emigration: the multistep paradigm.” *Cell* 76(2): 301–14.

Spurr AR. 1969. A low-viscosity epoxy resin embedding medium for elctron microscopy. *J Ultrastruct Res*. 26(1) 31-43.

Starr, DA and Fridolfsson, HN. 2010. “Interactions between nuclei and the cytoskeleton are mediated by SUN-KASH nuclear-envelope bridges.” *Annu Rev Cell Dev Biol* 26: 421–44.

Szot, CS, Buchanan, CF; Freeman, JW and Rylander, MN. 2011. “3D in vitro bioengineered tumors based on collagen I hydrogels.” *Biomaterials* 32(31): 7905–12.

Tabarin, T; Pageon, SV; Bach, CT; Lu, Y; O’Neill, GM; Gooding, JJ and Gaus, K. 2014. “Insights into adhesion biology using single-molecule localization microscopy.” *Chemphyschem* 15(4): 606–18.

Taipale, J and Keski-Oja J. 1997. “Growth Factors in the Extracellular Matrix.” *FASEBJ* 11: 51–59.

Testa, I; Urban, NT; Jakobs,S; Eggeling, C; Willig,KI and Hell, SW. 2012. “Nanoscopy of living brain slices with low light levels.” *Neuron* 75(6): 992–1000.

Timmins, NE; Dietmair, S and Nielsen, LK. 2004. “Hanging-drop multicellular spheroids as a model of tumour angiogenesis.” *Angiogenesis* 7(2): 97–103.

Tirrell, M; Kokkoli,E and Biesalski, M. 2002. “The role of surface science in bioengineered materials.” *Surface Science* 500(1-3): 61–83.

Tokunaga, M; Imamoto, N and Sakata-Sogawa, K. 2008. “Highly inclined thin illumination enables clear single-molecule imaging in cells.” *Nat Methods* 5(2): 159–61.

Tomayko, Mary M, and C Patrick Reynolds. 1989. “Determination of subcutaneous tumor size in athymic (nude) mice *.” *Cancer Chemother Pharmacol* 24: 148–54.

Toole, BP. 2002. “Hyaluronan promotes the malignant phenotype.” *Glycobiology* 12(3): 37R–42R.

Vasaturo, F; Mallacrino,C; Sallusti, E; Coppotelli, G; Birarelli, P; Giuffrida, A; Albonici, L; Simonelli, L; Modesti, A; Modesti, M and Scarpa, S. 2005. “Role of extracellular matrix in regulation of staurosporine-induced apoptosis in breast cancer cells.” *Oncol Rep* 13(4): 745–50.

Walter, NG; Huang, CY; Manzo, JA and Sobhy, MA. 2008. “Do-it-yourself guide: how to use the modern single-molecule toolkit.” *Nat Methods* 5(6): 475–89.

Walters, BD and Stegemann, JP. 2013. “Strategies for directing the structure and function of three-dimensional collagen biomaterials across length scales.” *Acta Biomater* 10(4): 1488-501..

Wang, N; Tytell, JD and Ingber, DE. 2009. “Mechanotransduction at a distance: mechanically coupling the extracellular matrix with the nucleus.” *Nat Rev Mol Cell Biol* 10(1): 75–82.

Williams, CG; Malik, AN; Kim, TK; Manson, PN and Elisseeff, JH. 2005. “Variable cytocompatibility of six cell lines with photoinitiators used for polymerizing hydrogels and cell encapsulation.” *Biomaterials* 26(11): 1211–18.

Wirtz, D; Konstantopoulos, K and Searson, PC. 2011. “The physics of cancer: the role of physical interactions and mechanical forces in metastasis.” *Nat Rev Cancer* 11(7): 512–22.

Wolf, K; Alexander, S; Schacht, V; Coussens, LM; von Andrian, UH; van Rheenen, J; Deryugina, E and Friedl, P. 2009. “Collagen-based cell migration models in vitro and in vivo.” *Semin Cell Dev Biol* 20(8): 931–41.

Wright, LP and Philips, MR. 2006. “Thematic review series: lipid posttranslational modifications. CAAX modification and membrane targeting of Ras.” *J Lipid Res* 47(5): 883–91.

Xu, K; Babcock, HP and Zhuang, X. 2012. “Dual-objective STORM reveals three-dimensional filament organization in the actin cytoskeleton.” *Nat Methods* 9(2): 185–90.

Yamada, KM and Cukierman, E. 2007. “Modeling tissue morphogenesis and cancer in 3D.” *Cell* 130(4): 601–10.

Yang, Z and Zhao, X. 2011. “A 3D model of ovarian cancer cell lines on peptide nanofiber scaffold to explore the cell-scaffold interaction and chemotherapeutic resistance of anticancer drugs.” *Int J Nanomedicine* 6: 303–10.

York, AG; Parekh, SH; Dalle Nogare, D; Fischer, RS; Temprine, K; Mione,M; Chitnis, AB; Combs, CA and Shroff, H. 2012. “Resolution doubling in live, multicellular organisms via multifocal structured illumination microscopy.” *Nat Methods* 9(7): 749–54.

Zaman, MH. 2013. “The role of engineering approaches in analysing cancer invasion and metastasis.” *Nat Rev Cancer* 13(8): 596–603.

Zamir, E and Geiger, B. 2001. “Molecular complexity and dynamics of cell-matrix adhesions.” *J Cell Sci* 114(20): 3583–90.

Zhang, S; Gelain, F and Zhao, X. 2005. “Designer self-assembling peptide nanofiber scaffolds for 3D tissue cell cultures.” *Semin Cancer Biol* 15(5): 413–20

9 Supplementary Information

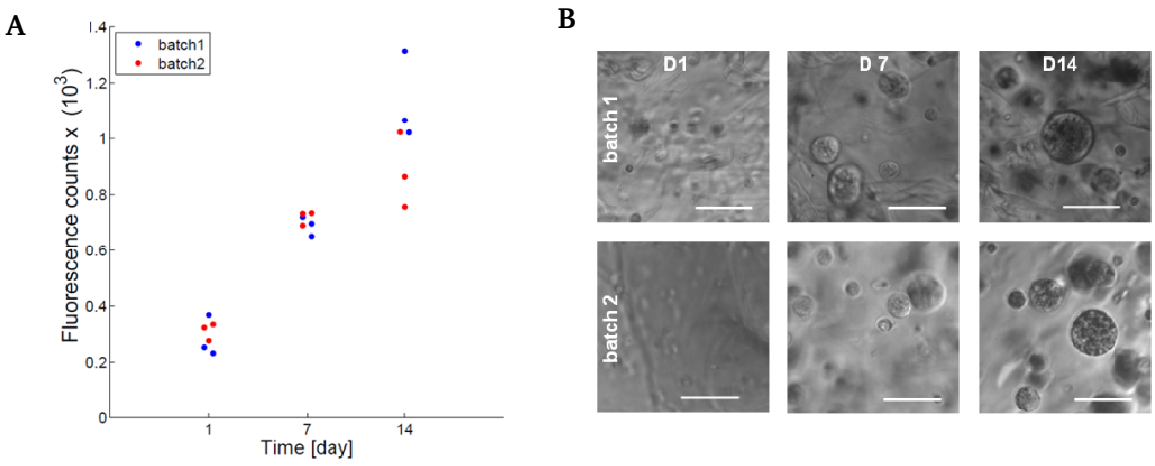

Supplementary Figure 1: Highly reproducible GelMA properties resulted in similar cell behaviour within hydrogels of different batches. Cell-laden hydrogels were prepared from one cell suspension and mixed into precursor solutions of two different GelMA batches (A). The metabolic activity was increased from day 1 over 14 days of 3D culture in both batches tested, indicating highly reproducible results of the two different batches tested (n = 3; *p* values not significant). Spheroid formation out of single cells (day 1) was observed after 7 and 14 days respectively in both batches tested (B). Scale bars, 100 μm.

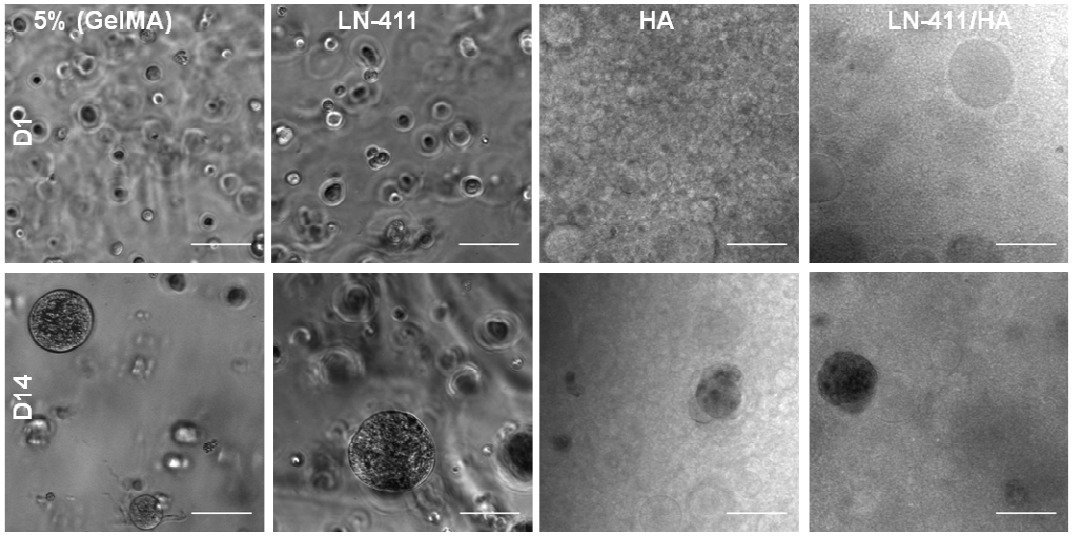

Supplementary Figure 2: HA addition to GelMA-based hydrogels resulted in heterogeneous polymer-network with larger macro-pores; LN did not influence hydrogel structure. Bright field mages indicated spheroid formation upon LN-411 and HA incorporation into hydrogels on day 1 (top panel) and day 14 (bottom panel). Addition of HA resulted in hydrogels with larger macro-pores and pockets. However, LN-411 alone did not affect the hydrogel structure. Scale bars, 100 μm.

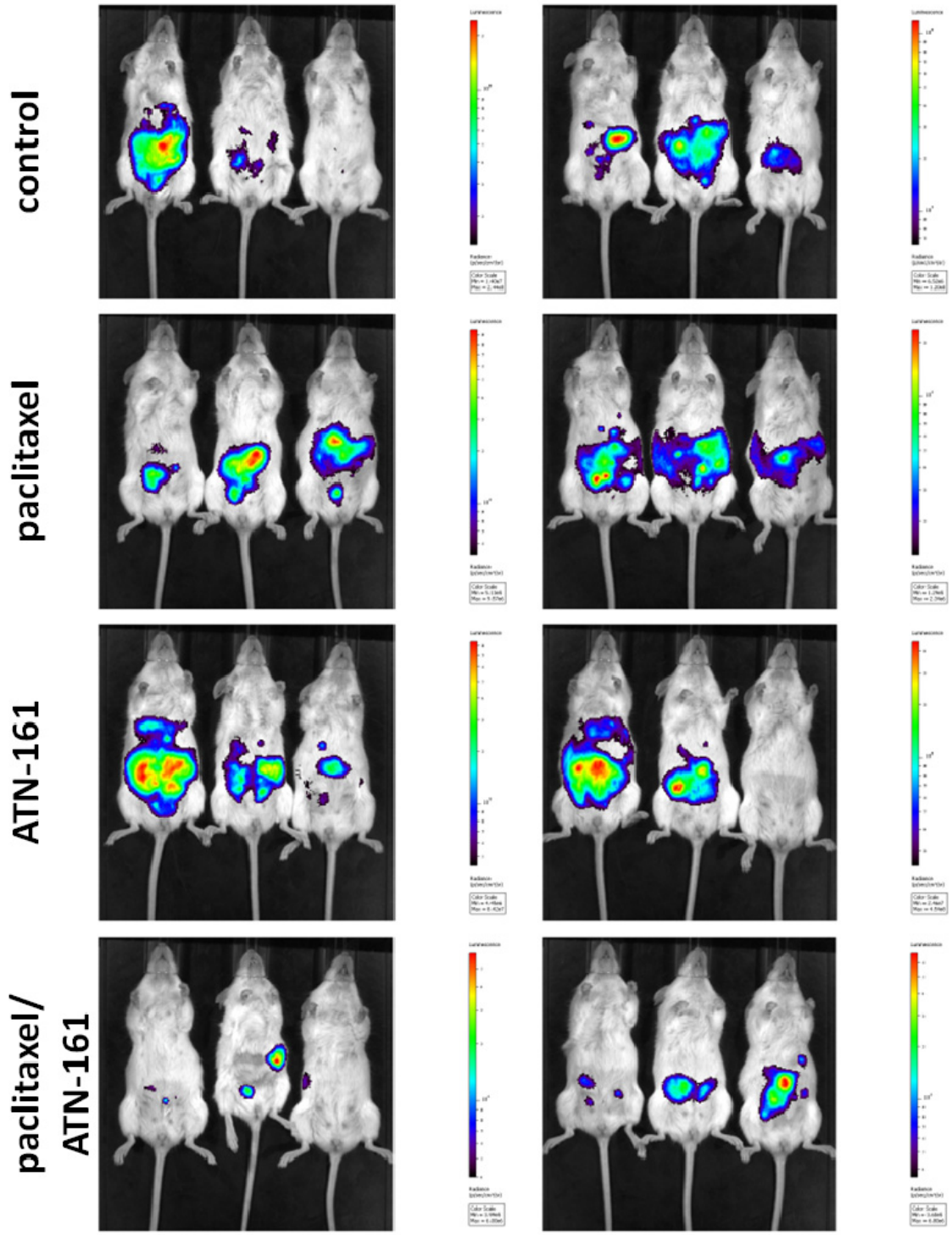

Supplementary Figure 3: Paclitaxel reduced tumour growth *in vivo*. Spheroid-containing GelMA-based hydrogels were implanted into mice adjacent to each ovary and caused tumour formation and growth over 8 weeks as indicated by bioluminescence imaging. While paclitaxel treatment reduced tumour mass and peritoneal spread, treatment with ATN-161 did not affect tumour growth. The combination treatment of paclitaxel with ATN-161 showed the same effect as paclitaxel treatment alone.

10 Acknowledgment

During the time I was working on this PhD thesis, I have received numerous support and guidance from various people, to whom I would like to express my deepest gratitude.

First of all, I want to thank **PD Dr. Tobias Meckel**, my primary supervisor for a very interesting topic and an exciting PhD thesis, for his guidance, patience and support in Germany; and at the back of beyond.

Many thanks go to **Prof. Dr. Gerhard Thiel**, for accepting the *Ko-Referat*, for his interest in this thesis, his ideas and advices and his great sense of humour.

Sincere thanks are given to **Prof. Dr. Dietmar W. Hutmacher**, for the great opportunity to visit his lab and having the chance to experience a great research environment at IHBI. I am grateful for this project what started as a training internship and resulted at the end in a mutual project in Darmstadt and Brisbane and became an important part of this thesis.

Many thanks go to **Dr. Daniela Loessner**, for her guidance into the field of ovarian cancer, introducing me to new methods and being a supportive supervisor.

I appreciate **Prof. Dr. Robert Stark**, for his interest in a biophysical topic and the DFG Cluster of Excellence 259, Center of Smart Interface, for funding my research.

Many thanks are given to **Dr. Boris M. Holzapfel** for performing the animal experiments and **Dr. Christina Theodoropoulus**, **Dr. Brigitte Hertel, Dr. Anna V. Taubenberger**, **Dr. Marek Janko, Dipl.-Phys. Florian Lauer** for their cooperation in (CLSM/EM/AFM/SMD) microscopy approaches and fruitful discussions.

To **Joanne Richardson** and **Barbara Reinhards** go many thanks for their assistance in all administrative tasks.

Furthermore I want to express my gratitude to all the actual and former members of the AG Thiel and Meckel, Regenerative medicine and Physics of Surfaces group and IHBI people, for their support, friendship and a great time during the daily lab work and beyond.

Many thanks also go to all my friends, especially to **Karin**, **Joan**, **Thomas**, **Marie-Luise**, **Laure**, **Jana** and **Joe** for their friendship, support and confidence in me and for making me feel at home, even thousands of miles away.

I am grateful for the unconditional support of my family, my parents, **Hannelore** and **Gernot** and my sister **Kerstin** during all the time and helping me through this journey.

Special thanks go to **Peiman** for his heartfelt support, friendship and love; and being a wonderful partner by my side.

11 Curriculum Vitae

Personal Details

Name	Elke Kämmerer
Date of birth	02nd September 1984, Offenbach Main, Germany

Education

2012-2014	Occupational trainee in Prof. Dr. D.W. Hutmacher's group at Institute of Health and Biomedical Innovation, Science and Engineering Faculty, Queensland University of Technology, Brisbane, Australia.
2010- 2014	PhD student in PD Dr. T. Meckel's group at Department of Biology, Technische Universität Darmstadt, Darmstadt, Germany. Subject: "Influence of the extracellular matrix on cellular behaviour – Development and application of a bioengineered 3D cell culture system for cancer research and high resolution microscopy".
2010	Diploma thesis in Prof. Dr. G. Thiel's group at the Department of Biology, Technische Universität Darmstadt, Darmstadt, Germany. Title: "Functional characterisation of a synthetic Calcium Biosensor based on a modified Potassium channel". Graduation (Diplom) mark: 1.0, with distinction.
2005 - 2010	Study of Biology at Technische Universität Darmstadt, Darmstadt, Germany. Subjects: Plant physiology, Biochemistry, Microbiology.
2004 - 2005	Study of Biomedical Chemistry at Johannes Gutenberg Universität, Mainz, Germany.
2001 - 2004	Secondary school ("Oberstufenschule"), Claus von Stauffenberg Oberstufenschule, Rodgau, Germany. Examination ("Abitur") 2004, mark: 2.7.
1995 - 2001	Secondary school, Georg Büchner Schule, Rodgau, Germany.
1991 - 1995	Primary school, Münchhausen Grundschule, Rodgau, Germany.

Conference participations

2014	Sydney, Australia, Focus on Microscopy conference: Oral presentation. Title: "Impact of the extracellular environment and anti-cancer treatment on spatio-temporal dynamics of the plasma membrane".
2013	Brisbane, Australia, IHBI inspires student conference: Poster presentation
2013	Heidelberg, Germany, Seeing is Believing conference: Poster presentation
2012	Gold Coast, Australia, IHBI inspires student conference: Poster presentation
2012	Brisbane, Australia, Metastasis conference: Participant
2011	Heidelberg, Germany, Seeing is Believing conference: Participant

Scientific publications

- Kaemmerer, Elke; Melchels, Ferry PW; Holzapfel, Boris M; Meckel, Tobias; Hutmacher, Dietmar W and Loessner, Daniela. 2014. "Gelatine methacrylamide-based hydrogels: An alternative three-dimensional cancer cell culture system". *Acta Biomaterialia*. 10(6):2551-2562, 2014.

- Kaemmerer, Elke; Lauer, Florian and Meckel Tobias, "Single molecule microscopy in 3D cell cultures and tissues". *Advanced Drug Delivery Reviews*. Accepted manuscript, 2014.

Additional work experience

2008 – 2012	Mentoring laboratory courses for students and supervising individual bachelor students in the frame of internships at the Department of Biology, Technische Universität Darmstadt, Darmstadt, Germany.
2009	Internship at Paul Ehrlich Institute, Langen, Germany, Department of Immunochemistry.
2008	Internship at Max Planck Institute of Biophysics, Frankfurt a. M., Germany, Department of Molecular Membrane Biology.
2011-2012	Organising the postgraduate seminar at Department of Biology, Technische Universität Darmstadt, Darmstadt, Germany.